eLife

Cell Biology

Atlas of Fshr Expression from Novel Reporter Mice

Reviewed Preprint
v2 • August 7, 2024
Revised by authors

Reviewed Preprint
v1 • March 26, 2024

Hong-Qian Chen, Hui-Qing Fang, Jin-Tao Liu, Shi-Yu Chang, Wen-huan Chai, Li-Ben Cheng, Ming-Xin Sun, Zhi-wei Yang, Jian-Rui Feng, Ze-Min Liu, Xiao-Li Li, Yong-Hong Zhang, Clifford Rosen, Peng Liu

Laboratory of Bone and Adipose Biology Shanxi Medical University Taiyuan, Shanxi, China • Department of Dentistry The 980 • Department of Orthopedic Surgery The Second Hospital University Shanxi Medical University Taiyuan, Shanxi, China • Maine Medical Center Research Institute Scarborough ME 04074, USA

Abstract

The FSH-FSHR signaling pathway has traditionally been considered an essential regulator in reproductive development and fertility. But there has been emerging evidence of FSHR expression in extragonadal tissues/organs. This poses new questions and long-term debates regarding the physiological role of the FSH-FSHR pathway, and underscores the need for reliable, in vivo analysis of FSHR expression in animal models. However, conventional methods have proven insufficient for examining FSHR expression due to limitations, such as the scarcity of 'reliable' antibodies, rapid turnover/degradation of transcripts, and a lack of robust in vivo tools. To address this challenge, we developed Fshr-ZsGreen 'knockin' reporter mice under the control of Fshr endogenous promoter using CRISPR/Cas9 genome-editing technology to append a P2A-ZsGreen targeting vector into a locus between the last exon and the stop codon of Fshr. With this novel genetic tool, we provide a reliable readout of Fshr expression at single-cell resolution level in vivo and in real time. Reporter animals were also subjected to additional analyses, including immunohistochemical staining, ddRT-PCR, and *in situ* hybridization, to define the accurate expression profile of FSHR in gonadal and extragonadal organs/tissues. Our compelling results not only demonstrated Fshr expression in intragonadal tissues but also, strikingly, unveiled notably increased expression in Leydig cells, osteoblast lineage cells, endothelial cells in vascular structures, and epithelial cells in bronchi of the lung and renal tubes. The genetic decoding of the widespread pattern of Fshr expression highlights its physiological relevance beyond reproduction and fertility, and opens new avenues for therapeutic options for age-related disorders of the bones, lungs, kidneys, and hearts, among other tissues/organs. Exploiting the power of the Fshr knockin reporter animals, this report provides the first comprehensive genetic record of the spatial distribution of FSHR expression, correcting a long-term misconception about Fshr expression and offering prospects for extensive exploration of FSH-FSHR biology.

eLife assessment

These **valuable** findings develop a mouse model with trackable fusion Fshr protein, which will be of use to the field. The animal model helps to elucidate the expression and function of the FSH receptor in extra-gonadal tissues. The strength of the evidence is **solid** in most parts, although additional validation of the localization data would strengthen the study considerably.

https://doi.org/10.7554/eLife.93413.2.sa2

Introduction

Follicle-stimulating hormone (FSH), secreted by anterior pituitary gonadotrophs, is recognized as a crucial regulator of male and female gonadal function; indeed, reproductive biology textbooks strongly emphasize its role in normal physiology [1]. FSH exerts its effects via a specific receptor, follicle-stimulating hormone receptor (FSHR), which belongs to the highly conserved family of G-protein-coupled receptors [2]. Traditional views hold that in females, FSHR is expressed in granulosa cells and controls the maturation of Graafian follicles, granulosa cell proliferation, and estrogen production [1], while in males, FSHR is expressed in testicular Sertoli cells and regulates their metabolic functions, which are essential for proper spermatogenesis and germ cell survival [3]. The large FSHR gene is located on chromosome 2p21 and comprises 10 exons [4].

However, accumulating evidence demonstrates that FSHR is also expressed in extragonadal tissues, such as endothelium [5], monocytes [6], developing placenta [7], endometrium [8], malignant tissues [9], bone, adipose and neural cells [10]. Intriguingly, blocking the interaction of Fsh with Fshr mitigates some degenerative disorders in mice, such as low bone mass [11], obesity [12], and neurocognitive decline [13]. Fshr was reported to be expressed in osteoclasts *in vitro*, and global Fsh or Fshr knockout resulted in an increase in bone mass by inhibiting bone resorption [11]. Blocking the Fsh-Fshr interaction with either Fsh polyclonal or monoclonal specific antibodies triggered thermogenesis in adipose tissues, significantly reduced body weights [12], and reduced Alzheimer's symptoms in mice [13]. Fshr expression is also found in the vasculature of tissues [7] and is particularly high in solid tumors [14]. Nevertheless, the relevance of its extragonadal expression and functions have been debated [2,15]. Therefore, precisely defining the localization of Fshr expression remains an imperative challenge in FSH-FSHR biology due to the concern of the 'non-specificity' of available antibodies used to localize FSHR expression and the 'quick turnover' and 'rapid degradation' of Fshr transcripts [2,10,16]. Thus, a suitable genetic approach to resolve this issue is warranted [17].

To address this challenge, we can utilize a GFP reporter driven by the endogenous promoter of Fshr, which enables the visualization of the expression of low-abundance transcripts in more accurate and context-specific ways [18,19], when other approaches, e.g., antibodies and RT-PCR, are limited in their ability to detect Fshr expression. Therefore, in this study, we employed CRISPR/Cas9-mediated technology to create a novel Fshr-ZsGreen reporter mouse model for precisely clarifying Fsh expression. We believe that this powerful approach, as a reliable readout of Fshr expression at the single-cell level, should allow us to accurately capture Fshr expression in real time in a tissue-specific manner. We also used other techniques to ensure the accuracy and reliability of the results. Our results challenge the current understanding of Fshr expression and refine that Fshr has a wider expression profile than previously thought. The findings of Fshr in reproductive and nonreproductive tissues/organs will provide significant insights into new roles

of Fsh and Fshr in physiology and pathology and have implications for the development of new therapies for reproductive and nonreproductive disorders, particularly metabolic diseases and degenerative diseases.

Methods

1. Generation of the CRISPR/Cas9-mediated Fshr-ZsGreen knockin reporter line

Fshr-P2A-ZsGreen knockin reporter mice were generated by a CRISPR/Cas9-based approach. Briefly, one sgRNA was designed by the CRISPR design tool (*http://www.sanger.ac.uk/*) to target the region of the stop codon in the transcript NM_013523.3 exon 10 of mouse Fshr [20], and then was screened for on-target activity using a Universal CRISPR Activity Assay [UCATM, Biocytogen Pharmaceuticals (Beijing) Co., Ltd]. The targeting vector containing P2A-ZsGreen and 2 homology arms of left (1378 bp) and right (1493 bp) each was used as a template to repair the DSBs generated by Cas9/sgRNA. P2A-ZsGreen was precisely inserted before the stop codon of the Fshr locus. The T7 promoter sequence was added to the Cas9 or sgRNA template by PCR amplification in vitro. Cas9 mRNA, sgRNA and the targeting vector were co-injected into the cytoplasm of one-cell-stage fertilized C57BL/6J eggs. The injected zygotes were transferred into oviducts of Kunming pseudopregnant females to generate F0 mice. F0 mice with the expected genotype as confirmed by tail genomic DNA PCR, DNA sequencing and Southern blotting were mated with C57BL/6J mice to establish germline transmitted F1 heterozygous mice. F1 heterozygous mice were further genotyped by tail genomic PCR, DNA sequencing and Southern blotting. Primer sequences for genotyping F0 and F1 are described in Supplementary Material 1.

The produced Fshr-ZsGreen (Fshr-ZsG) knockin mice were maintained as heterozygotes, and homozygotes were used for experiments. For genotyping, genomic DNA was extracted from tail tips and assayed using polymerase chain reaction (PCR) primer sets for the Fshr-ZsGreen allele. The primer sequences for genotyping are described in Supplementary Materials 1. All mice were maintained on a 12 h light/dark cycle with food and water *ad libitum*. The care and treatment of animals in all procedures strictly followed the NIH Guide for the Care and Use of Laboratory Animals. The animal protocols used in this study were approved by the Shanxi Medical University IACUC committee.

2. Tissue harvest and preparation

Mice were terminated by CO_2, and organs were harvested and fixed with 4% paraformaldehyde (PFA) for 12 to 24 hours at 4°C. For bone samples, decalcification was performed with daily changes of EDTA solution (0.5 M, pH 8) for 7 days. After fixation and decalcification processes, samples were transferred to 15% and 30% sucrose overnight, respectively. The tissues were then embedded with optimal cutting temperature (OCT) compound and stored at -80°C. The embedded samples were sectioned into 5- to 25-μm-thick sections using a Leica cryostat CM1950.

3. Immunofluorescence staining

Immunofluorescence staining was performed as described previously [21]. Briefly, air-dried 7- to 25-μm-thick frozen sections were washed with 1×PBS for 10 minutes three to five times, followed by blocking with 10% BSA for 20 minutes at room temperature, and the samples were permeabilized with 0.5% Triton X-100 in 1×PBS for 10 minutes. Then, diluted primary antibodies were added to the slides. After overnight incubation with antibodies at 4°C, the slides were washed with 1×PBS for 15 minutes three to five times and then incubated with secondary antibody conjugated with fluorescence for 30 minutes at room temperature. The slides were washed again thoroughly with 1×PBS for 10 minutes three times. The slides were then stained with DAPI, rinsed with 1×PBS three times for 5 minutes each, and mounted with 50% glycerol for confocal imaging.

Rabbit IgG was used as the negative control. Primary and secondary antibodies were purchased from Servicebio (Wuhan Servicebio Technology Co., Wuhan, China), except when indicated otherwise. The primary antibodies are listed in Supplementary Materials 2. In addition, sections of different tissues/organs derived from C57BL/6J (B6) mice were used as negative controls for Fshr-ZsGreen expression. A donkey anti-rabbit IgG conjugated with Cy3 was employed at a 1:400 dilution as the secondary antibody (Servicebio, Wuhan, China).

4. Single RNA-fluorescence in situ hybridization (RNA-smFISH)

RNA in situ hybridization, the gold standard method for visualizing RNA expression and localization in cells, tissue sections, and whole organs, was performed on tissue sections as described previously [22]. Briefly, frozen tissue sections of the testis from Fshr-ZsGreen mice were washed with 1XPBS three times. The sections were then treated with proteinase K (20 μg/ml) for 5 minutes at 37°C to permeabilize the cells and allow probe penetration, followed by three washes with 1XPBS. Specific oligonucleotide sense and antisense DNA probes for Fshr were designed and synthesized by the manufacturer (GeneCreate Biological Engineering Co., Ltd., Wuhan, China). The probes were labeled with a fluorescent dye (e.g. Cy3) for visualization. RNA-smFISH was performed on tissue sections using a commercially available kit (e.g., SureFISH, Agilent Technologies) at 37 ° C for 2 hours. After hybridization, the sections were washed with SSC solution (2xSSC, 37°C for 10 mins, 1xSSC, 37°C for 5 mins twice, 0.5xSSC for 10 mins) to remove unbound probes, and counterstained with a nuclear stain (e.g., DAPI) to visualize the tissue architecture. The sections were imaged using a fluorescence microscope equipped with appropriate filter sets. A sense probe was used as a negative control to ensure specificity and sensitivity. The sequences of sense and antisense probes are described in Supplementary Materials 2.

6. Imaging

Imaging of the slides was carried out as described before [21]. Briefly, the fluorescence images of the frozen sections were obtained using a Nikon A1 HD25 confocal microscope with a DUVB detector and plan Apo λ 4×, plan Apo VC 20× DIC N2, plan Apo λ 40×, and plan Apo λ 100×C oil objectives, illuminated with a wavelength of 405, 488, or 561 nm to excite DAPI, GFP, or Cy3, respectively; detection was performed with a 425–475, 500–550, or 570–620 nm bandpass filter. To assess the number of cells in each field of view, tissue-cleared images were converted from 3D to MAIP (maximum projection of the Z-stack across the whole section). Data were acquired with NIS-Elements AR 5.20.00 64-bit software. Structured illumination microscope (SIM) images were obtained and processed with N-SIM-S super-resolution model (Nikon) and Image J-Colocalization Finder.

7. Droplet digital RT−PCR (ddRT-PCR)

Tissues were harvested from 10-week-old B6 mice. Samples were dissected free of connective tissue and homogenized with a fast multi-sample tissue cryogenic grinder (LC-FG-96, Lichen Instrument Technology Co., Ltd., Shanghai, China), and total RNA was extracted using NucleoZOL (NucleoZOL; Macherey-Nagel GmbH & Co., KG, Dylan, Germany). mRNA was reverse transcribed using an M5 Super qPCR RT kit with gDNA remover (MF012-T, Mei5bio, Beijing). Droplet digital PCR was performed as described previously [21]. The primers used for ddRT-PCR were as follows: mFshr Fwd-5’ ccgcagggacttcttcgtcc-3’; mFshr Rev-5’-ttggtgactctgggagccga-3’.

8. Cell cultures of Leydig cell line TM3

TM3 cells were purchased from Pricella (Wuhan Pricella Biotechnology Co., Ltd., Wuhan, China) and subcultured with DMEM/F12 +5% HS +2.5% FBS +1% P/S with the company’s instruction in T25 flasks for extraction of total RNA and on coverslips for immunofluorescence staining of Fshr expression.

Results

To precisely define Fshr expression in mice, we utilized several complementary strategies, including Fshr endogenous promoter driving ZsGreen knockin reporter mice, immunofluorescence staining with antibodies against tissue/cell type-specific markers and Fshr, ddRT-PCR and RNA-smFISH, to comprehensively examine Fshr expression.

1. Generation of Fshr-ZsGreen knockin reporter mice

CRISPR/Cas9-mediated homologous recombination was used to generate embryonic stem cell (ESC) clones, in which a P2A-ZsGreen cassette was precisely inserted before the stop codon of the Fshr gene followed by the 3' UTR of the Fshr allele, as described in the Methods (**Fig. 1A**). This P2A-ZsGreen expression cassette under the control of endogenous Fshr regulatory elements ultimately generates ZsGreen proteins without disrupting Fshr expression. The 19 amino acids P2A sequences functions to cause ribosomal " skipping" during translation, resulting in a missing peptide bond and effectively separates the two proteins, e.g. Fshr and ZsGreen [23,24,25]. The injected zygotes were transferred into oviducts of Kunming pseudopregnant females to generate F0 mice. F0 mice with the expected genotype were confirmed by tail genomic DNA PCR, DNA sequencing and Southern blotting (**Fig. 1B and C**) and then mated with C57BL/6J mice to establish F1 heterozygous mice with the germline-transmitted transgene. F1 heterozygous mice were further genotyped by tail genomic PCR, DNA sequencing and Southern blotting (**Fig. 1B and C**). The results from these tail genomic PCR, DNA sequencing and Southern blots in both F0 and F1 pups demonstrated that the targeted P2A-ZsGreen cassette was accurately inserted into the designed site between exon 10 and the stop codon of the Fshr gene before the 3' UTR. We maintained heterogeneous Fshr-ZsGreen mice and used homogeneous mice for experiments. These mice were genotyped using primer sets specific to P2A-ZsGreen, as shown in **Figure 1D**. Fshr and GFP are transcribed in a bicistronic mRNA but subsequently translated into two independent proteins rather than as a fusion protein. This design ensures unaffected Gαi3 transcription and function and simultaneous GFP expression as a reporter protein. All animals were fertile and showed normal behavior and no obvious abnormal phenotypes.

2. Examination of Fshr expression in Fshr-ZsGreen reporter mice

With confirmation that the Fshr-P2A-ZsGreen targeting vector was successfully inserted into the Fshr locus, we investigated Fshr expression by confocal microscopy to detect ZsGreen and immunostaining for tissue/cell markers in frozen sections of tissues/organs of Fshr-ZsGreen reporter mice. To ensure that there was no nonspecific expression of Fshr-ZsGreen in the examined tissues/organs, we took frozen sections derived from wild-type mice (B6) as negative controls. The negative controls were imaged under the conditions used for examining Fshr-ZsGreen expression. The representative results are shown in Supplementary Data 1, showing no nonspecific expression of Fshr-ZsGreen in the negative controls. On this basis, we performed the following imaging to examine Fshr-ZsGreen expression in the major organs and tissues.

1) Reproductive organs

As the reproductive system is well known to express Fshr, we first tested Fshr- ZsGreen expression in the ovary and testis to ensure ZsGreen expression driven by the endogenous Fshr promoter. In the ovary, we observed Fshr-ZsGreen expression in the different stages of follicles from primordial follicles to primary follicles, secondary follicles, and the corpus luteum (**Fig. 2A-b** and e). In the ovarian/Graafian follicles, expression was observed in the oocytes, granulosa cells/follicle cells and theca (interna and externa) (**Fig. 2A-b**, c, e and f). We also found Fshr-ZsGreen expression in the ciliated epithelial cells in the oviduct (**Fig. 2A-d** and h). Furthermore, we employed an antibody

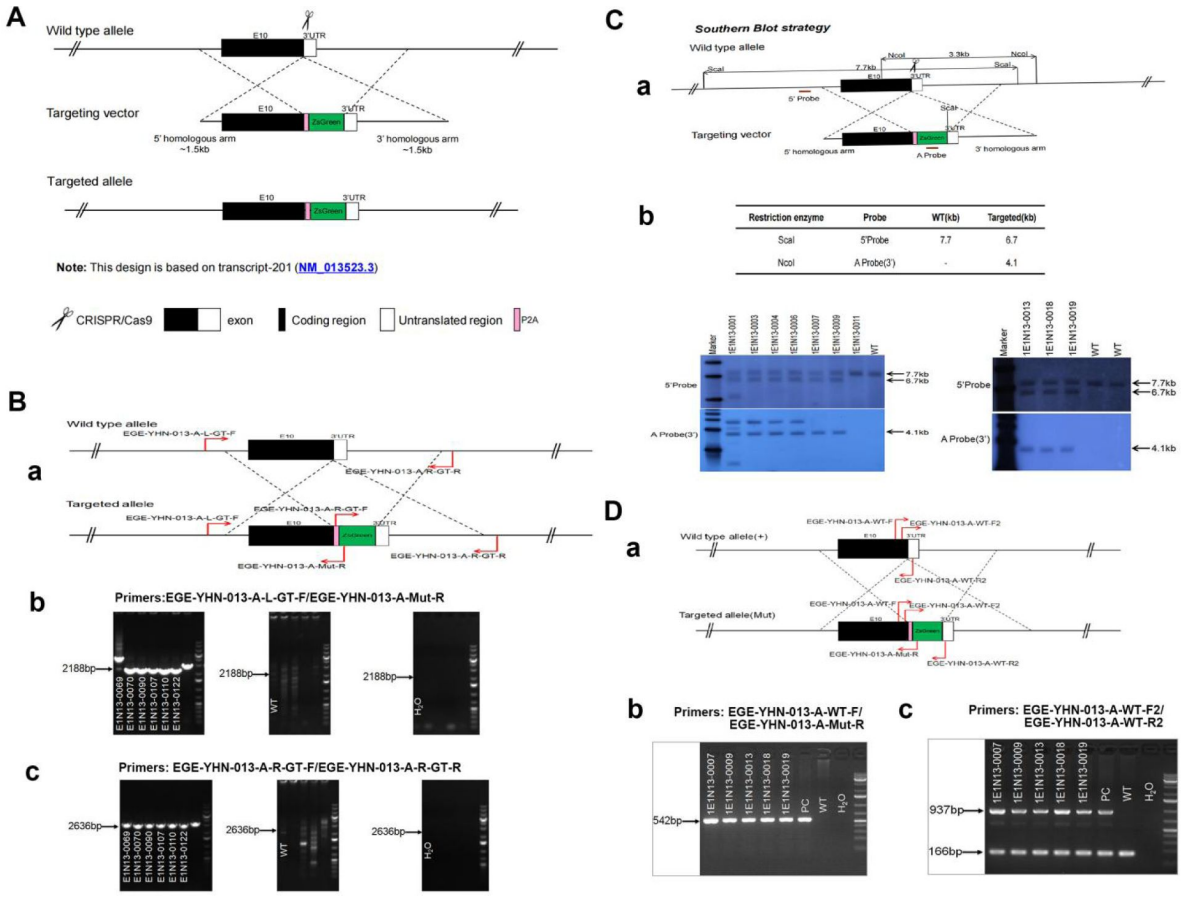

Figure 1.

Generation of CRISPR/Cas9-mediated Fshr-ZsGreen knockin reporter mice.

A. CRISPR/Cas9-mediated targeting strategy to generate Fshr-P2A-ZsGreen knockin mice. **B**. Detection of integration by PCR in F0 and F1 mice: (a) Schematic of PCR primer design specific to Fshr-P2A-ZsGreen and the wild-type allele. The results of genomic DNA PCR genotypes using the primer pair EGE-YHN-013-A-L-GT-F/EGE-YHN- 013-A-Mut-R (b) and another primer pair EGE-YHN-013-A-R-GT-F/EGE-YHN-013-A-R- GT-R (c). **C**. Southern blot confirmation of the correct integration of the P2A-ZsGreen allele in F0 and F1 mice. The Southern blot results demonstrated the successful generation of the targeted P2A-Fshr-ZsGreen allele: (a) Restriction sites in the wild-type sequence and targeted vector; (b) Southern blot analysis probes, expected restriction fragment lengths as indicated and blotted images. **D**. The 2nd PCR genotyping strategy using primers: (a) schematic for the design of PCR primer sets for the Fshr-ZsGreen allele; (b and c) genotyping readout of heterozygous mice;

against Stra8 [26] to perform immunofluorescence staining to identify reproductive cells and observed the colocalization of Fshr-ZsGreen with Stra8 staining as a marker for reproductive cells (**Fig. 2A**).

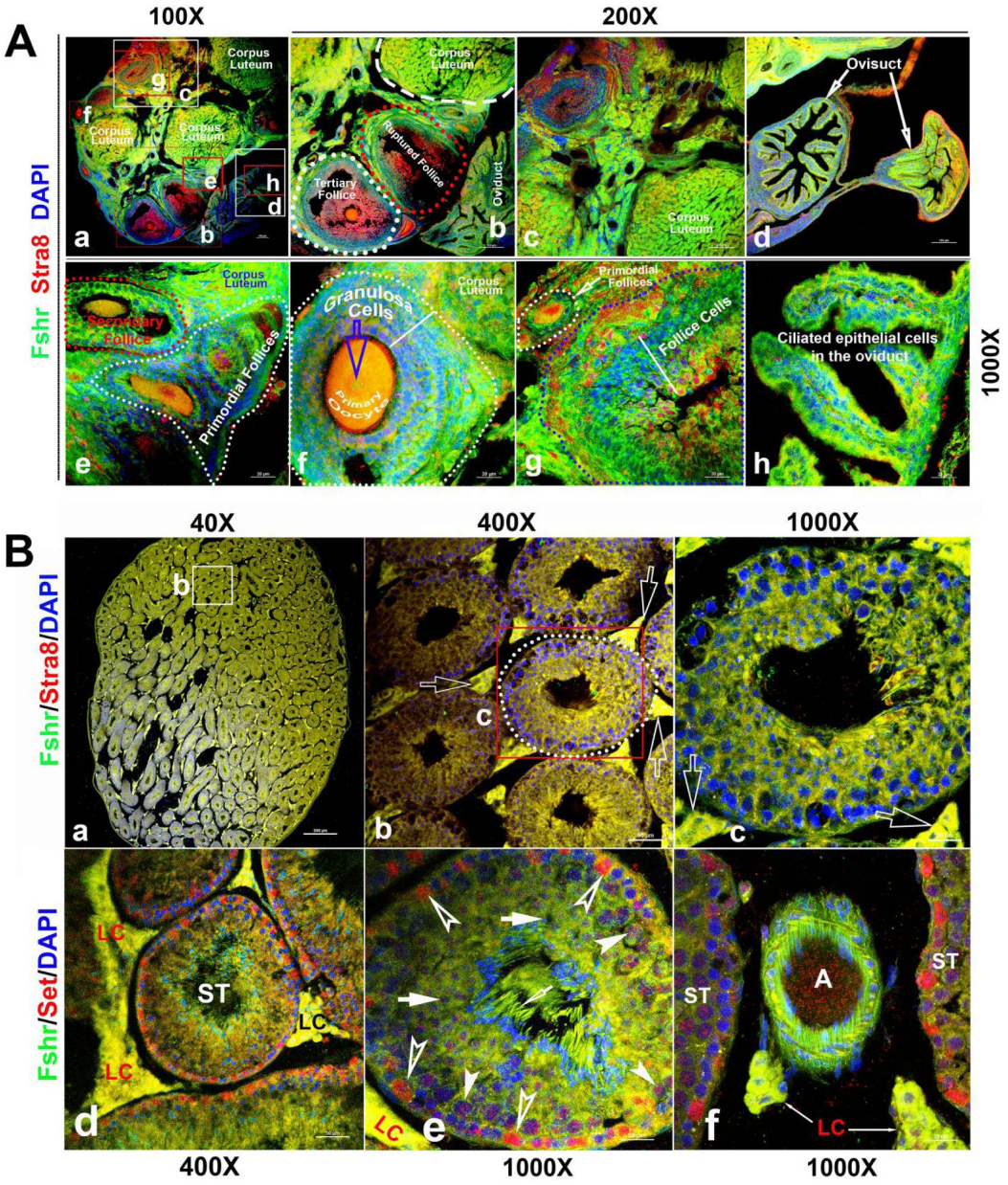

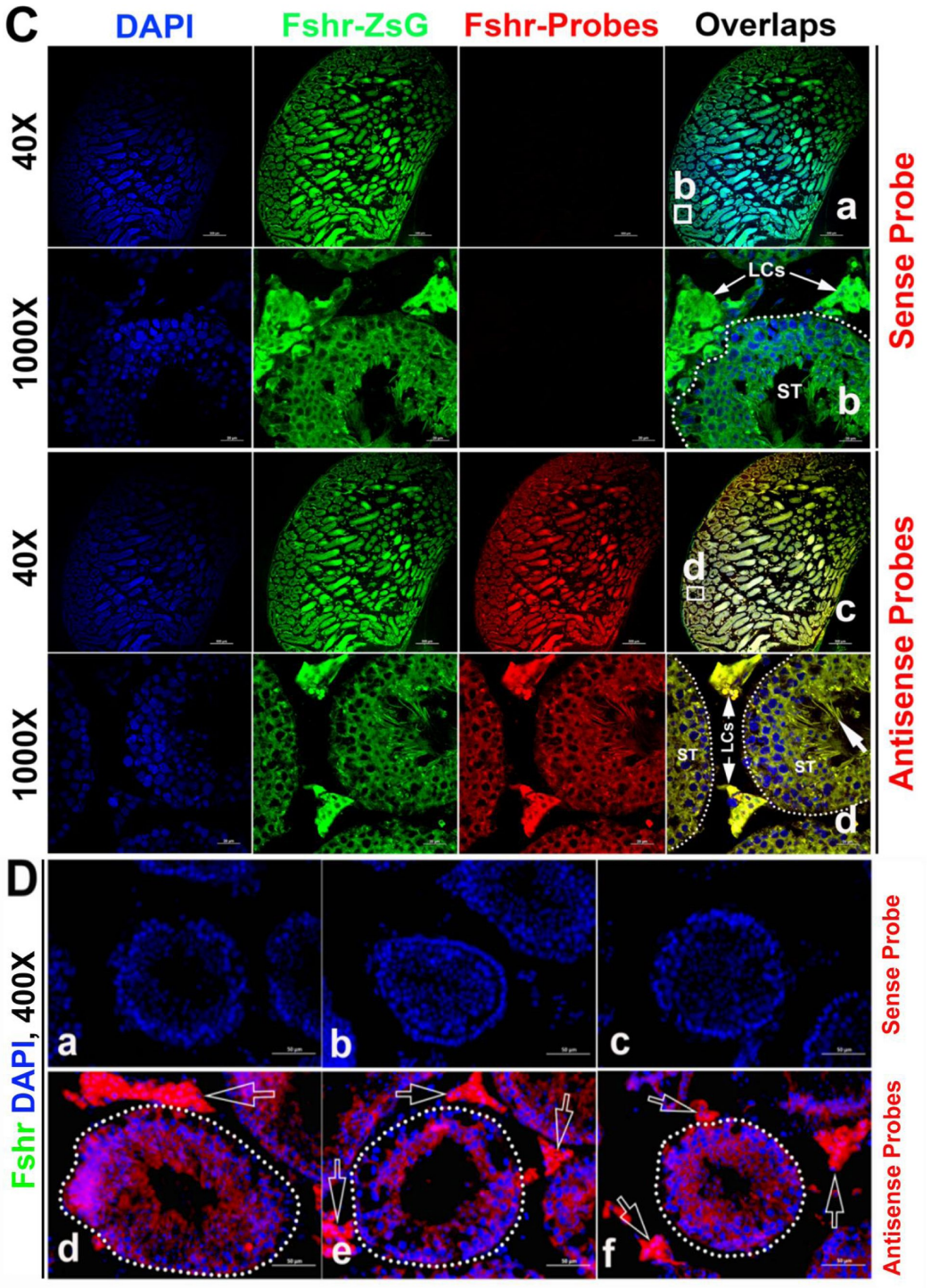
C
DAPI
Fshr-ZsG
Fshr-Probes
Overlaps
40X
1000X
40X
1000X
Sense Probe
Antisense Probes
LCs
ST
ST
LCs
ST
a
b
c
d
D
Fshr DAPI, 400X
a
b
c
d
e
f
Sense Probe
Antisense Probes

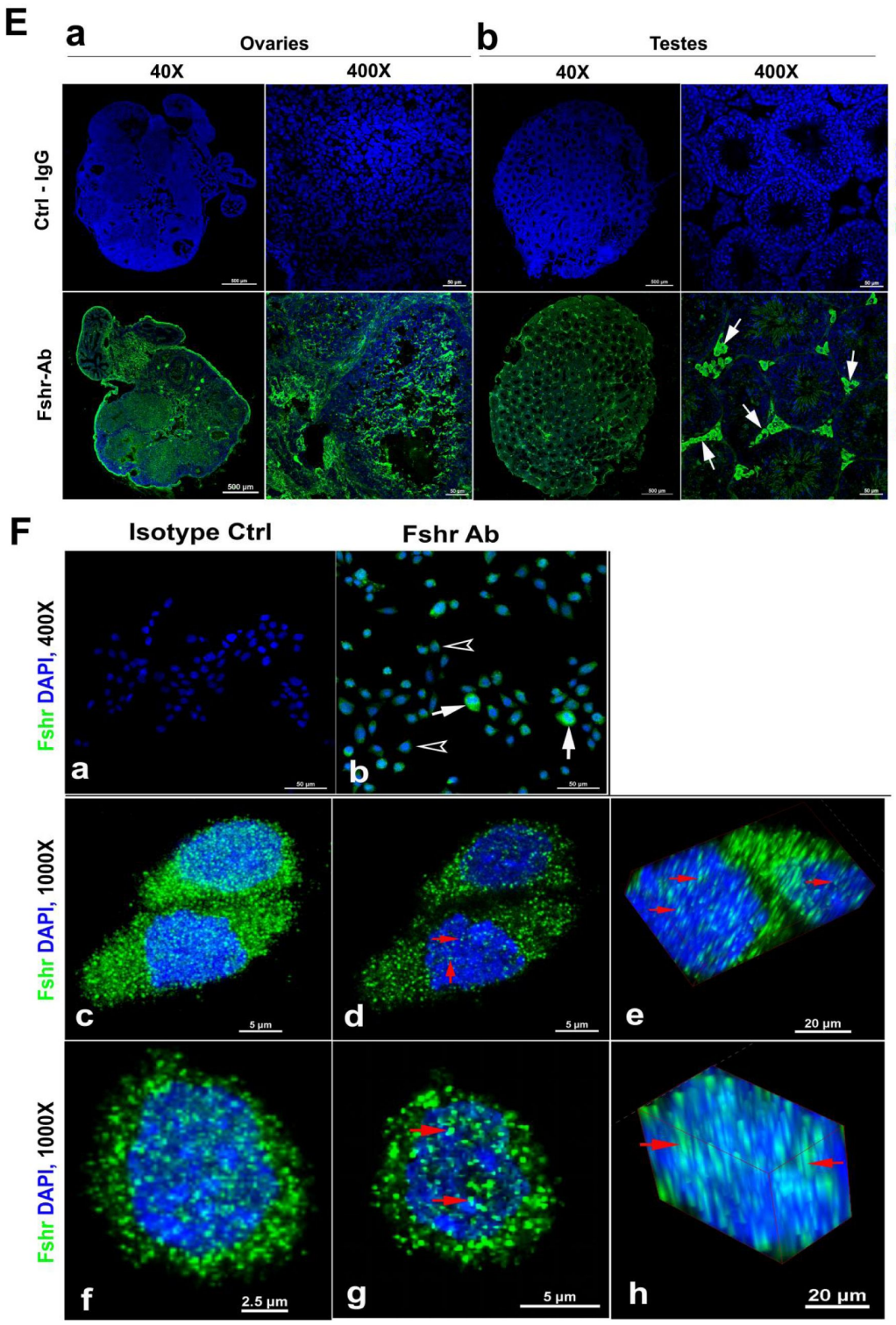
E
a
Ovaries
b
Testes
40X
400X
40X
400X
Ctrl - IgG
Fshr-Ab
Fshr DAPI
Fshr DAPI
500 μm
F
Isotype Ctrl
Fshr Ab
Fshr DAPI, 400X
a
b
Fshr DAPI, 1000X
c
d
e
5 μm
5 μm
20 μm
Fshr DAPI, 1000X
f
g
h
2.5 μm
5 μm
20 μm

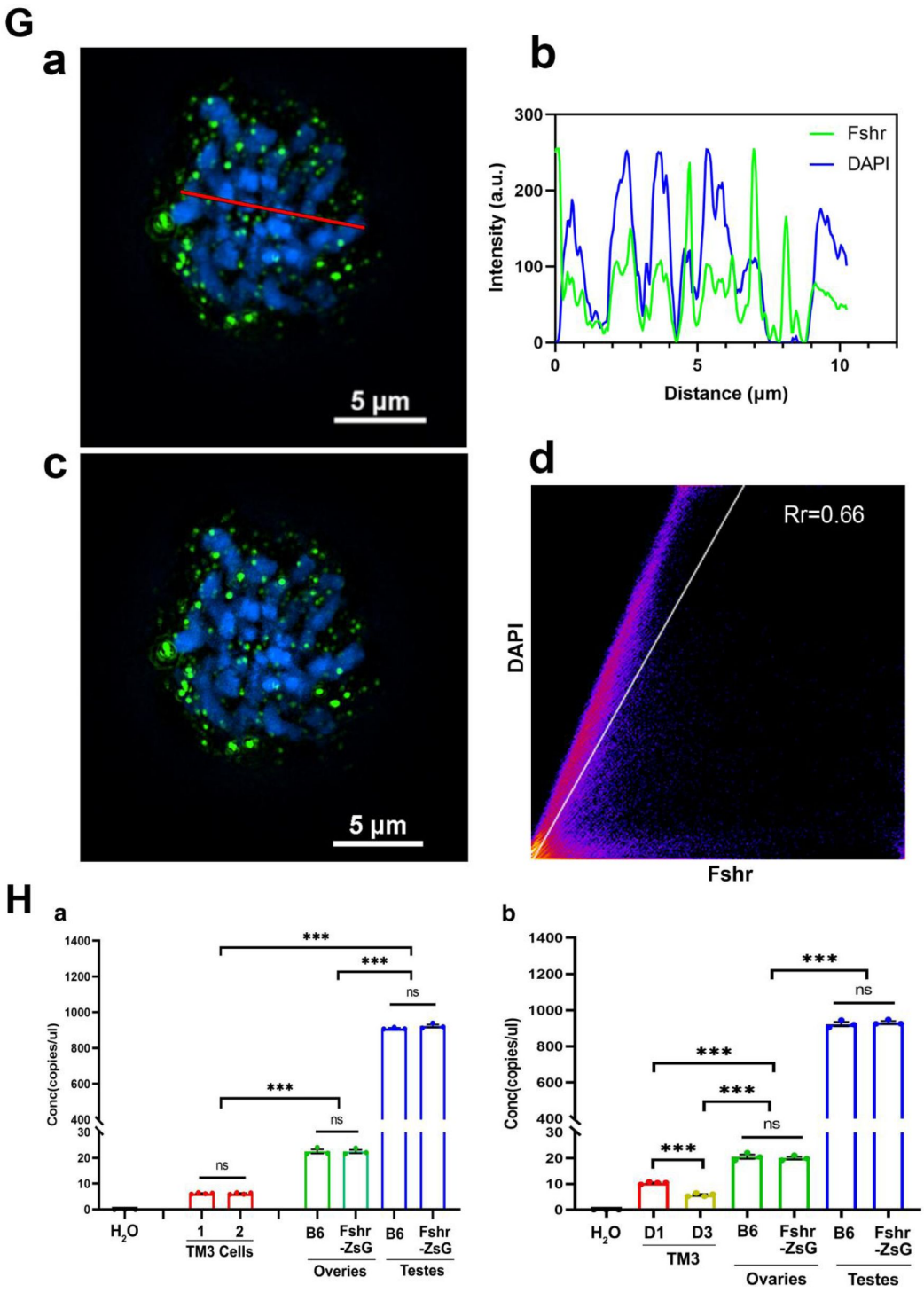

Figure 2.

Imaging of Fshr-ZsGreen expression in the reproductive system.

A. Fshr expression in the ovary. Frozen sections of the ovary were immunostained with an antibody against mouse Stra 8, followed by imaging of Fshr-ZsGreen expression and its colocalization with Stra8 staining. The entire picture of the sectioned ovary is shown in A-a. The representative images of the section were taken at 400X magnification. A-b. an area containing a corpus luteum, tertiary and ruptured follicles and a partial oviduct; A-c. an area with more

corpora lutea; A-d. oviducts. Furthermore, representative images at 1000X magnification; A-e. primordial and secondary follicles; A-f. a mature follicle; A-g. follicle cells in a corpus luteum; and A-h. ciliated epithelial cells in the oviduct. Scale bars: 100 μm for a, b, c and d, 20 μm for e to h.

B. Fshr-ZsGreen expression and its colocalization with Stra8 (a to c) and Set (d to f) in the testis. B-a, the whole image of the sectioned testis; B-b, the representative area of seminiferous tubes with interstitial cells (Leydig cells); and B-c, an seminiferous tube. White empty arrowheads indicate Leydig cells; B-d, the representative area of seminiferous tubes with interstitial cells (Leydig cells) stained for Set; B-e, an seminiferous tube stained for Set and an artery with partial areas of seminiferous tubes stained for Set. Magnifications: 40X for a, 400X for b and d, and 1000X for c, e and f . Scale bars: 500 μm for b and d, 50 μm for c and d, and 20 μm for c, e and f.

C. RNA-smFISH confirmation of Fshr expression in Fshr-ZsG mice. Mixed anti- sense probes were applied for detection of Fshr while a sense probe was taken as a negative control. The entire image of the sectioned testis is taken at 40X magnification (a and c), and two representative areas of seminiferous tubes with Leydig cells are demonstrated at 1000X magnification (b and d). White arrows indicate spermatozoa. Abbrev.: LCs-Leydig cells, and ST-seminiferous tubule. Scale bars: 50 μm.

D. RNA-smFISH confirmation of Fshr expression in B6 mice. Mixed anti-sense probes were applied for detection of Fshr while a sense probe was taken as a negative control. Three representative areas of seminiferous tubes with Leydig cells were imaged at 400X magnification (a to c for the sense probe; d to f for antisense RNA probes). White empty arrows indicate Leydig cells. Scale bars: 50 μm.

E. Fshr expression in the ovary (a) and testis (b) of B6 mice. Frozen sections of the ovary and testis were immunofluorescence stained for Fshr. Representative areas of whole the ovary or the testis image are present at 400X magnification. White arrows indicate Leydig cells.

F. Immunofluorescence staining for Fshr in TM3 cells. a. isotype control (IgG); b. positive staining for Fshr with mouse Fshr antibody, empty arrowheads indicate lower Fshr expression cells and white arrows indicate higher Fshr expression cells; c and f, higher magnification of Fshr positively stained cells (maximum intensity projected images); d and g, single layer images across the centers of the nuclei in c and f; e and h. 3D images of the nuclei showing Fshr located in the nuclei;

G. SIM images of Fshr localized in the nuclei of TM3 cells. a. a single layer of the nuclei for analysis of Fshr colocalization of DAPI, a red line indicates a single layer for analysis of colocalization; b. fluorescence analysis of colocalization of Fshr with DAPI from a. c. the whole layers of nuclei for colocalizationof Fshr with DAPI; d. Pearson coefficient analysis of the colocation by Image J-Colocalization Finder, Rr=0.66 [PCC (Rr): 0.5 to 1 indicating colocalization].

H. Comparison of Fshr expression in TM3 cells, the testes and ovaries of Fshr- ZsGreen and B6 mice assessed by ddRT-PCR. a, the first comparison of Fshr expression among TM3 cells (cultured for 1 day); the testes and the ovaries from two types of mice, two groups of TM3 cells (1 and 2) for measuring Fshr expression (n=4 per group). b. the second comparison, TM3 cells were cultured for 1 day (D1) and 3 day (D3). Three samples for each organ (n=3 mice/each organ, aged 3 months). ***p<0.001; ns-no significant difference in the comparisons.

In the testis, we found Fshr-ZsGreen expression and its colocalization with Stra8 [27] staining in the cells of seminiferous tubules (STs), including primary spermatocytes, Sertoli cells and spermatids, and particularly in interstitial Leydig cells (LCs) between STs (**Fig. 2B**). **Figure 2B-a** shows an image of the whole sectioned testis. A representative ST is displayed at two magnifications (**Fig. 2B-b** and c), demonstrating strong expression of Fshr-ZsGreen in Leydig cells, as indicated by empty white arrows. In addition, we also applied an antibody against Set to identify testis cells, whose expression was reported in multiple cell types of the mouse testis at different developmental stages [28]. In **Figure 2C**, a representative image of ST with Leydig cells is shown at a lower magnification (400X) and a higher magnification (1000X) (**Fig. 2C-a** and b),

showing colocalization of Fshr-ZsGreen and Set staining in testis cells. We found strong Set signal in Fshr-ZsGreen-positive spermatogonia, as indicated by empty white arrowheads (**Fig. 2C-b**). Fshr-ZsGreen was also observed in the arterioles of the testis (**Fig. 2C-c**).

Because of RNA in situ hybridization as the gold standard method for visualizing RNA expression and localization in cells, tissue sections, and whole organs [22,29], we further carried out single RNA molecule-fluorescence in situ hybridization to confirm Fshr expression in the LCs, using antisense probe for identifying Fshr expression in the sections of Fshr-ZsGreen and B6 mice, whereas its sense probe was used as a negative control (**Fig. 2C and D**). Additionally, we also examined Fshr expression by immunofluorescence in Leydig cell line TM3 [30] and found that the majority of TM3 cells stained for lower levels of Fshr, only a few cells showed relatively higher levels of Fshr expression (**Fig. 2E-a** and b). Interestingly, we also noticed Fshr expression located in the nuclei, demonstrated by confocal 3D images (**Fig. 2E-c**-h) and SIM images (**Fig. 2G**- a-di) of the nuclei.

We then performed ddRT-PCR to compare Fshr expression in TM3 cells, testis, and ovaries of Fshr-ZsG and B6 mice at 3 months old (**Fig 2H-a** and b, two representative of four experiments). The results showed that Fshr expression was similar in the testes and ovaries of both types of mice, indicating that the insertion of P2A- ZsGreen did not disrupt Fshr expression in Fshr-ZsGreen mice. However, Fshr expression was significantly higher in the testes compared to the ovaries, by almost 40- fold. Interestingly, TM3 cells exhibited much lower Fshr expression levels than the testes and ovaries. In fact, the levels were approximately 145-fold lower than in the testes and 3.6-fold lower than in the ovaries.

Last, we also searched for FSHR expression in scRNA-seq databses (DISCO (immunesinglecell.org/genepage/FSHR), BioGPS (*http://biogps.org/#goto=genereport&id=2492*) and CZ CELL×GENE Discover (*https://cellxgene.cziscience.com/e/535e9336-2d8d-43c3-944d-bcbebe20df8a.cxg/*), showing FSHR expression in human Leydig cells (Supplementary Data 3).

Overall, we observed Fshr-ZsGreen expression in the reproductive system, demonstrating that ZsGreen is a readout for Fshr expression. In addition to its sole expression in granulosa cells and Sertoli cells, as reported previously, our findings clearly reveal that Fshr is also expressed in other cell types in the reproductive system, particularly in Leydig cells.

2) Skeletal tissues

Fsh has been thought to have a direct role in bone [11], therefore we next examined the expression pattern of Fshr in femoral sections, as shown in **Figure 3A**, under confocal fluorescence microscopy. The representative areas are presented at two magnifications of 400X and 1000X. In the epiphyseal growth plate, we observed lower expression of Fshr in chondrocytes, as indicated by two dotted lines, compared to its expression in cells located in the sponge area above or under the dotted lines (**Fig. 3A-a**). At higher magnification, Fshr was expressed in the columns of chondrocytes from the resting zone to the transformation zone (**Fig. 3A-e**).

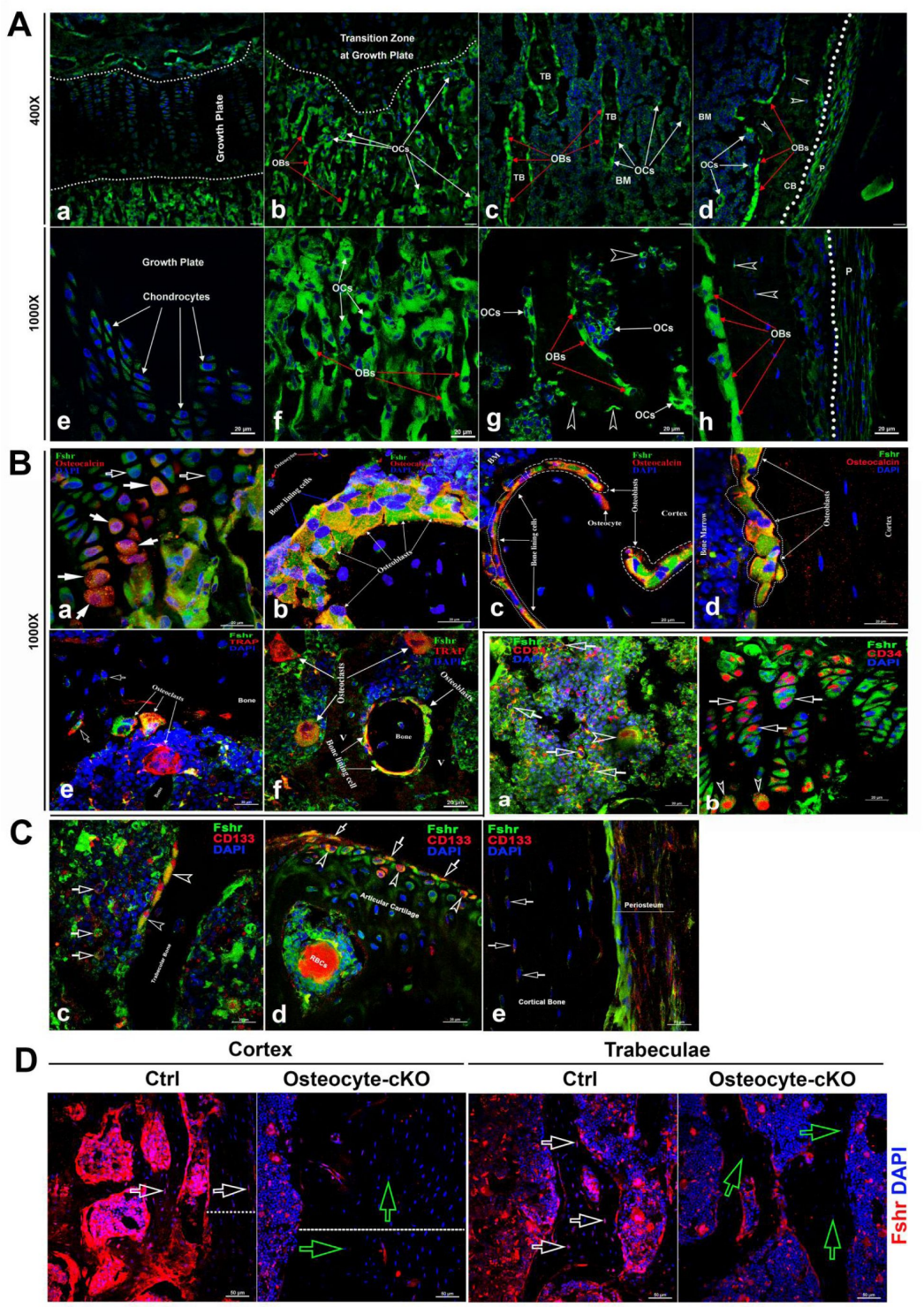

Figure 3.

Fshr-ZsGreen expression in skeletal tissues.

A. Detection of Fshr-ZsGreen expression in frozen sectioned skeletal tissues by fluorescence confocal microscopy. The upper panels show Fshr-ZsGreen-positive cells in the representative areas of skeletal tissues at low magnification (400X), while the lower panels show their corresponding cells at high magnification (1000X). These representative

areas demonstrate the Fshr-ZsGreen-positive cells in chondrocytes of the growth plate (a and e), on the surfaces of sponge bone under the growth plate (b and f), in trabecular bone in the bone marrow (c and g), and in the cortex (d and h). Abbreviations: OBs-osteoblasts; OCs-osteoclasts; BM-bone marrow; CB-cortical bone; and P-periosteum. Arrows: white empty arrowhead indicates GFP-positive osteocytes. Magnifications: 400X for a to d and 1000X for e to h; scale bars: 50 μm for a to d and 20 μm for e to h.

B. Confirmation of GFP-positive cell identities with antibodies against either osteocalcin or Trap as markers for osteoblasts or osteoclasts. Colocations of GFP expression with osteocalcin in mature chondrocytes (a), osteoblasts, bone lining cells and osteocytes on the surface of or within sponge bone (b), trabecular bone (c), and cortical bone (d). Colocations of Trap with multinucleated GFP-positive cells are shown in e and f, which represent osteoclasts on the resorptive areas and in bone marrow adjacent to bone surfaces and bone lining cells over trabecular bone. Arrows: white empty arrows indicate early chondrocytes with GFP expression but undetectable osteocalcin expression, while white arrows point to mature chondrocytes with both strong GFP and osteocalcin expression. Magnifications: 1000X for a to f. Scale bars: 20 μm for a to f.

C. Identification of stem/progenitor cells. a. Colocalization of Fshr-ZsGreen with CD34-positive staining in bone marrow, indicated by empty white arrows; an empty white arrowhead indicates multinucleated Fshr-ZsGreen cells with CD34-positive staining. b. CD34-positive stained cells in growth plates. Empty white arrows indicate spindle-shaped ZsGreen-positive chondrocytes stained positively for CD34, where empty white arrowheads point to round cells with CD34-positive staining located in the bottom of the growth plate. c. Colocalization of Fshr-ZsGreen with CD133 staining in the cells of bone marrow and on the bone surface. Empty white arrows indicate bone marrow cells positive for both Fshr-ZsGreen and CD133 staining, and empty white arrowheads indicate Fshr-ZsGreen-positive cells on the trabecular bone surface with positive staining for CD133. d. Positive staining for CD133 on Fshr-ZsGreen-positive chondrocytes on the surface of articular cartilage. e. CD133 staining in the weak Fshr-ZsGreen-positive fibroblast-like cells in the periosteum.

D. Reduced Fshr expression by Fshr cKO in osteocytes. Immunofluorescence staining with Fshr antibody was performed in decalcified frozen sections of femurs from the control and inducible osteocytes Fshr cKO mice (DMP1-CreERT^{2+}:Fshr$^{fl/fl}$ treated tamoxifen and DMP1-CreERT^{2}:Fshr$^{fl/fl}$ as the control treated with corn oil). White empty arrows-osteocytes in the control; Green empty arrows-osteocytes with reduced Fshr expression in the cKO. Dotted lines indicate the thickness of the cortex. Magnifications: 400X. Scale bars: 50μm.

In contrast, we found that Fshr was brightly expressed in osteoblasts and osteoclasts in the metaphyseal trabeculae, which were recognized based on nuclear DAPI staining- osteoblasts were stained with a single DAPI nucleus, while osteoclasts contained more than two DAPI-stained nuclei (**Fig. 3A-c** and d). Similarly, we further observed that these cells on the surfaces of trabeculae in bone marrow and cortical bone also clearly expressed Fshr-ZsGreen, as shown in **Fig. 3A-e** and f (trabeculae) and-g and h (cortex). Importantly, we noted Fshr-ZsGreen expression in osteocytes (indicated by empty white arrowheads, **Fig. 3A-d**, g and h),the most abundant cell in the skeleton. These were embedded in trabecular and cortical bone, as well as in the periosteum (P) (**Fig. 3A-h**).

To confirm the identification of osteoblasts/osteocytes and osteoclasts that expressed Fshr, we performed immunofluorescence (IF) staining using an antibody against osteocalcin, a marker of osteoblasts [31]. As shown in **Fig. 1B**, we observed colocalization of Fshr expression with osteocalcin staining in chondrocytes in the transforming zone, as indicated by white arrows (**Fig. 3B-a**), in cuboid and nucleated osteoblasts and bone lining cells on the trabecular and endosteal surfaces (**Fig. 3B-b** and c), cortical bone, and osteocytes within the mineralized matrix (**Fig. 3B-b**, c and e).

To identify osteoclasts, we performed fluorescence immunostaining with an antibody against Trap, an osteoclast marker [32]. Osteoclasts were recognized by positive staining for TRAP with more than two DAPI-stained nuclei. Multinucleated Fshr-ZsGreen-positive cells were stained

positively for Trap located on the surface of the resorptive bays or areas adjacent to the trabecular bone (**Fig. 3B-e** and f).

To examine whether skeletal stem/progenitor cells express Fshr, we performed IF staining for stem markers with antibodies against CD34 or CD133 [33–37]. Using these well- known stem markers, we identified Fshr-ZsGreen-positive cells as stem/progenitor cells located in the bone marrow, growth plate/articular cartilage, and periosteum, as shown in **Figure 2C-a**, b, c, e and d, respectively. These cells also featured an increased nuclear- cytoplasmic ratio, except for these cells on the trabecular surface and in the periosteum.

We also examined Fshr expression in osteocytes from DMP1-CreERT^{2+}:Fshr$^{fl/fl}$ mice (osteocyte-specific Fshr cKO) where the control mice (DMP1-CreERT[2]:Fshr$^{fl/fl}$) as a positive control. We noticed a significant drop of Fshr expression in osteocytes in Fshr cKO mice when tamoxifen was intraperitoneally administrated to the mice (**Fig. 3D**). We also found an increased thickness of cortex triggered by Fshr cKO (**Fig. 3D**-the left panels, the thickness indicated by dotted lines). The finding further demonstrated Fshr present in osteocytes, the largest cell population in bones, and the specificity of the Fshr antibody.

3) Adipose tissues

Because our previous works and others have provided evidence on the role of Fsh in adipose tissues, we then examined Fshr-ZsGreen expression in adipose tissues. As expected, we found Fshr-ZsGreen expression in adipocytes of the frozen sectioned inguinal WAT, as shown in the left panel of **Figure 4A** at a low magnification (40X), which was further confirmed under a higher magnification (400X) in the three representative areas, demonstrating that Fshr- ZsGreen was expressed in the cellular membranes of individual adipocytes (**Fig. 4A-a**, b and c).

Figure 4.

Fshr-ZsGreen expression in adipose tissues.

A. Confocal imaging of Fshr-ZsGreen expression in frozen sections of inguinal WAT. The whole image of a piece of the inguinal WAT was imaged under confocal microscopy with a low magnification (40X), and three representative areas were also presented with a higher magnification (400X) showing low and high cellular densities (low-b and high-a and c). These images demonstrate Fshr-ZsGreen expression in the cellular membranes of adipocytes.

B. IF staining of Fshr-ZsGreen-positive adipocytes with an antibody against mouse Ucp1. To identify the beige cells in WAT, we performed IF staining with an antibody against mouse Ucp1. Positive staining for Ucp1 was colocalized within Fshr-ZsGreen- positive cells in the areas with a higher cell density (a and b) imaged at low magnification, as shown in the left panels, while higher magnification images are shown in the right panels (a and d). In addition, strong Fshr-ZsGreen expression was observed in the arterioles of WAT (c and d). Arrows: white empty arrows indicate beige cells; white arrows point to white adipocytes, and empty arrowheads indicate GFP-positive arterioles. Magnifications: 400X for a and c; 1000X for b and d. Scale bars: 50 μm for a and c and 20 μm for b and d.

C. Fluorescence images of Fshr-ZsGreen expression in frozen sectioned BAT. A whole image of BAT was imaged under confocal fluorescence microscopy at low magnification (a, 40X). Three representative areas are also presented at a higher magnification (b, c and d, 400X), which clearly show the Fshr-ZsGreen expressed in the cells of BAT and skeletal muscles in the right parts of the images (b and c). Abbreviation: M-muscle. Arrows: white arrows indicate strong Fshr-ZsGreen expression in BAT cells. Magnifications: 40X for a and 40°C for b, c and d. Scale bars: 100 μm for a and 50 μm for b, c and d.

D. Identification of brown adipocytes in BAT by IF staining. Brown fat cells were identified using an antibody against mouse Ucp1. Ucp1 staining is shown at lower magnification (40X) in the left panel covering a whole piece of BAT. Three representative areas are imaged at higher magnifications (a, b and c, 400X and 1000X), showing Fshr- ZsGreen colocalization with Ucp1-positive staining. Magnifications and scale bars are indicated in the figure.

E. Examination of peripheral neural fibers within BAT. To determine whether Fshr- ZsGreen is expressed in the peripheral nerves in BAT, we performed IF staining with an antibody against tyrosine hydroxylase (TH), a marker for peripheral sympathetic neurons. A whole piece of BAT was imaged at a lower magnification (40X) after being stained for TH, as shown in the left panel. Representative areas are presented in the right panels with higher magnifications (400X -a, b and c and 1000X-d, e and f, respectively). Arrows: red outlined arrowheads indicate Fshr-ZsGreen- and TH-positive large peripheral nerves; green outlined arrowheads point to Th-stained nerve fibrils accompanying Fshr-ZsGreen- positive nerve fibrils around a Fshr-ZsGreen-positive arteriole; red arrows indicate Fshr- ZsGreen- and TH-positive nerve fibrils; and white arrows indicate brown adipocytes with both Fshr-ZsGreen and TH expression. Magnifications: 40X for the whole image of BAT in the left panel; 400X for a, b and c; and 1000X for a, e, and f. Scale bars: indicated in the images.

F. Further confirmation of Fshr-ZsGreen expression in the peripheral nerves. To confirm Fshr-ZsGreen expression in peripheral neurons, we also employed another antibody against Peripherin (Peri), a 57-kD type III intermediate filament that is a specific marker for peripheral neurons, to further identify peripheral neurons in BAT. The left panel shows an entire image of the BAT stained for Peri at a lower magnification (40X). The three representatives are shown in the right panel: a. the first area located in the edge of the BAT with more white adipocytes; b. the second area with more brown adipocytes and a large peripheral nerve; c. the last area enriched with brown adipocytes. Their corresponding higher magnifications (1000X) are shown in a, e and f, respectively. Abbrev.: LNF-large never fibril. Arrows: Empty white arrows-small peripheral fibrils; white arrow-Fshr-ZsGreen-positive fibrils and empty white arrows-both Fshr-ZsGreen- and Peri-positive brown adipocytes. Magnifications: 40X for the t panel; 400X for a, b, and c and 1000X for d, e and f. Scale bars: 1000 μm for the whole images in the left panel; 50 μm for a, b and c, and 20 μm for d, e and f.

G. Detection of Fshr expression in adipose tissues of B6 mice. Immunofluorescence staining for Fshr expression was carried out in frozen sections of white adipose tissue (the left panels) and brown fat (the right panels) from B6 mice at age of 3 months. Magnifications: 40X and 400X. Scale bars: 500 μm and 50 μm.

To confirm adipocyte identification, we performed IF with an antibody against mouse Ucp1 [12] to recognize adipocytes, showing that the majority of Fshr-ZsGreen-positive cells were stained positively for Ucp1, and found two types of $Fshr^{+}$ adipocyte populations: one with colocalization of the two markers only in the membrane (indicated by empty white arrowheads) and another with two markers in both the membrane and cytoplasm (indicated by white arrows) (**Fig. 4B-a** and b). In addition, we observed that Fshr-ZsGreen was expressed in arterioles in adipose tissue, denoted by white empty arrowheads in **Figure 4B-c** and a dotted circle in **Figure 4B-d**.

We further examined Fshr-ZsGreen expression in BAT. Fshr-ZsGreen was observed across the whole section of examined BAT at a lower magnification (**Fig. 3A-a**). At a higher magnification (400X), three representative areas are presented, as shown in **Figure 3A-b**, c and d, in which Fshr-ZsGreen was expressed not only in the cellular membranes but also in areas of cytoplasm close to the membranes, as indicated by white arrows (**Fig. 4C-b**, c, and d).

Furthermore, we also performed IF with three antibodies against Ucp1, Th and Peri to identify brown cells and peripheral fibers in the Fshr-positive section. We found that several areas in the section were strongly stained for Ucp1 at low magnification (40X), as shown in **Figure 4D-a**. Under higher magnifications of 400X and 1000X, we colocalized Fshr-ZsGreen with Ucp1 in the three representative areas, in which some locations had higher Fshr-ZsGreen expression and others had higher Ucp1 expression (**Fig. 4D-a**, b and d).

To examine whether peripheral neural fibers express Fshr, we used antibodies against Th and Peri that can recognize peripheral neural fibers. We found that neural fibers stained positively and surrounded Fshr-ZsGreen-positive arterioles in BAT (**Fig. 4E-a** and b). In addition, Fshr-ZsGreen was expressed in the nodes of Ranvier of TH-stained small neural fibers (indicated by empty red arrows, **Fig. 4E-e**). We further confirmed Fshr- ZsGreen expression in peripheral neural fibers by IF with an antibody against peripherin (Peri), which is a type III intermediate filament protein found predominantly in peripheral nerves, specifically in sensory and autonomic neurons (**Fig. 4F**). We noted colocalization of Fshr-ZsGreen and Peri staining in large neural fibers (**Fig. 4F-b**, d and e). Interestingly, we observed that both markers for peripheral neural fibers were also expressed in the cytoplasm of BAT cells, in which Fshr-ZsGreen was strongly expressed (**Fig. 4E-b, c** and f; **Fig. 4Fe, c** and f).

To further ensure Fshr expression in adipose tissues, we also performed immunofluorescence staining with Fshr antibody in white and BAT adipose sections of B6 mice. The results showed the similar expression pattern as seen in Fshr-ZsGreen mice (**Fig. 4G**).

Taken together, the above-described findings on Fshr-ZsGreen expression in reproductive, skeletal, and adipose tissues convincingly demonstrate that Fshr-ZsGreen is a reliable readout of Fshr expression. Furthermore, we identified Fshr expression in Leydig cells and follicles at different developmental stages, cells of osteoblast lineage and peripheral nerve fibers. With confidence that Fshr-ZsGreen is a reliable readout, we used this powerful tool to further examine Fshr expression in other tissues and organs.

4) Heart and aorta

To examine Fshr expression in the cardiovascular system, we used the heart and aorta as key organs/tissues to detect Fshr-ZsGreen expression. As expected, we observed strong Fshr-ZsGreen expression in the myocardium (**Fig. 5A-a**) and large muscular arteries (a representative is

shown in **Fig. 5A-b**). Then, we further confirmed Fshr-ZsGreen expression by IFs with two antibodies against α-SMA and EMCN [21] that recognize alpha smooth muscle actin of smooth muscle and endomucin of endothelial cells at higher magnifications. With IF staining for α-SMA, we imaged several areas of both heart and blood vessels, as shown in the left image of the upper panel (40X). In the heart, we observed that Fshr-ZsGreen was highly expressed in cardiomyocytes in longitudinal and transverse orientations of the myocardium, which were positively stained for α-SMA (**Fig. 6B-a**, b and c). At a magnification of 1000X, it was also expressed in the endothelial layer of arterioles between muscle fibers (**Fig. 5B-i**).

Figure 5.

Imaging of Fshr-ZsGreen expression in the heart and aorta.

Fshr-ZsGreen expression was imaged in frozen sections of the heart (A): cardiomyocytes (a) and smooth muscles (b). Then, IF staining with antibodies against α- SMA (B) and EMCN (C) was carried out to identify cardiomyocytes and smooth muscles. The whole image of the heart with Fshr-ZsGreen expression and staining for α-SMA is shown in the left upper panel of B. Its representative areas are presented at two magnifications of 400X (B-a to h) and 1000X (B-i to n), respectively, in the following: (1) 400X magnification: a-cross-oriented cardiomyocytes; b-longitudinally oriented cardiomyocytes; c-cross-oriented smooth muscle of the ascending aorta with brown adipose tissue; d-smooth muscle of the left pulmonary artery with brown adipose tissue; e-brown adipose tissue attached to a large artery; e-layer of endothall cells of the superior vena cava (SVC); g. connective tissues between arteries containing brown adipose, different sized nerves and arteries; h. another part of the SVC with layers of smooth muscles and connective tissue. (2) 1000X magnification: i, cardiomyocytes with an arteriole; j. brown adipose tissue attached to the circulation system above the heart; k. the layers of endothelial cells and smooth muscles of a bronchial artery; m. transverse section of nerve fibers; n. the layers of ECs and SM of the SVC. In addition, imaging of the IF staining for EMCN is shown in C. The whole image of Fshr-ZsGreen and EMCN staining in the heart at a magnification of 40X in the left upper panel, from which a representative of pulmonary artery at a magnification of 400 is shown in a at a magnification of 400X (a); a representative of aorta is presented in b. Representative images at higher magnification of 1000X: c-cardiomyocytes in transverse orientation with a venule and d-a layer of endothelial cells of pulmonary artery. Abbrev.: CM- cardiomyocytes; SM-smooth muscle; ECs-endothelial cells; N-never; B-brown adipose. Magnifications and scale bars are indicated as in the figure.

Two orientations of the ascending aorta were examined for Fshr-ZsGreen after staining for α-SMA or EMCN: the longitudinal section (D-a to c) and the cross section (D-d to f)). D-a shows the entire image of the ascending aorta stained for α-SMA at a magnification of 100X, while representative images at a higher magnification of 1000X are presented in D-b for α-SMA staining and D-c for EMCN staining. The entire image of the transversely sectioned aorta (D-d) and representative images at a higher magnification of 1000X for α-SMA (D-e) and EMCN (D-f). Abbrev.: TI-tunica intima, TM- tunica media, AV- aortic valve, SM- smooth muscles, Sub. CT-subendothelial connective tissue. Arrows: empty white arrows indicate arterioles positively stained for α-SMA in b; empty arrowheads point to endothelial cells positively stained for either α-SMA or EMCN. Scale bars: 100 μm for a and d and 20 μm for b, c, e, and f.

Figure 6.

Fshr-ZsGreen expression in the lung and kidney.

Detection of Fshr-ZsGreen expression and IF staining with PD-L1 was performed in lung sections at different magnifications. The whole image of the frozen sectioned lung is shown in the left panel at 40X magnification (A-left panel). Representative areas are shown in the right panels at magnifications of 400X (**Figure 6A-a** to d) and 1000X (A-e to h). They are the ciliated columnar cells of primary bronchi (a and c), the bronchioles with alveoli (b and f), respiratory bronchiole with bronchial gland (c and g) and alveoli (d and h). Arrows: empty white arrowheads-type I pneumocytes, white arrowheads-type II pneumocytes and white arrows-macrophages. Abbrev.: C-ciliated epithelium; PA- pulmonary arteriole; L-lumen; RB-respiratory bronchiole; BG-bronchial gland; A-alveoli; AD-alveolar duct. Magnifications: 40X for the left mage of the whole section, 400X for a to d, and 1000X for e to h. Scale bars: 1000 μm for the left panel, 50 μm for a to d and 20 μm for e to h.

Fshr-ZsGreen expression and staining with Col1a1 were examined in the sectioned kidney under confocal fluorescence microscopy at three magnifications (B). The images in the top panel are images of the whole section at 40X magnification (a-d). The images in the middle panel show the colocalization of Fshr expression with positive staining for Col1a1 in the glomerulus and renal tubes (proximal and distal convoluted tubes) at 400X magnification (e and f), while the bottom panel shows images of the glomerulus (g) and arteriole (h) at 1000X magnification. Magnification: 1000X. Scale bars: 100 μm for a-d, 50 μm for e and f and 20 μm for g and h. Abbrev. A-arteriole; PCT-proximal convoluted tubule; DCT-distal convoluted tubule; g-glomerulus.

In addition to the cardiomyocytes, we also observed Fshr-ZsGreen in α-SMA-stained smooth muscles and endothelial cells of large blood vessels above the heart (**Fig. 7B-d**). Interestingly, we found Fshr-ZsGreen in adipose tissue around the blood vessels, and the adipocytes morphologically appeared to be brown adipose cells, as the majority of these brown-like cells were full of ZsGreen-positive cytoplasm, instead of single large fat droplets with Fshr-ZsGreen expression in cellular membranes (**Fig. 5B-c**, d, e and j). The adipose tissue was stained positively for α-SMA, suggesting that the ZsGreen^{+} structures costained for α-SMA are blood vessels within the beige tissues, which are indicated by white empty arrowheads (**Fig. 5B-e** and j).

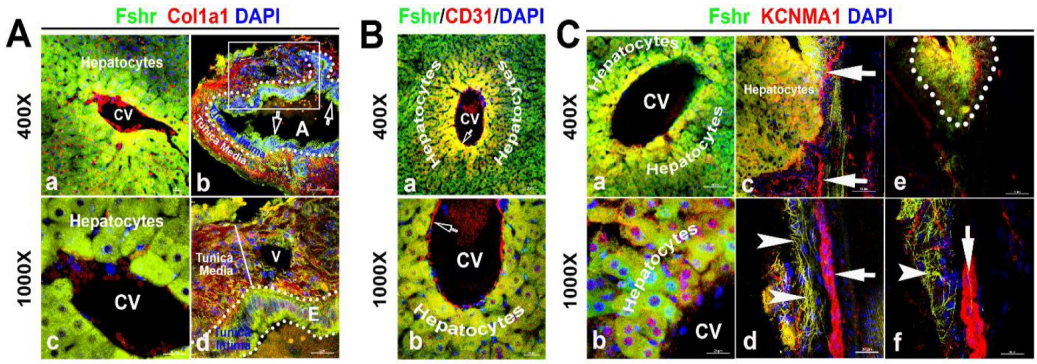

Figure 7.

Identification of Fshr-ZsGreen expression in the liver.

Frozen sectioned liver tissue was stained for Col1a1 (A), CD31 (B) or KCNMA1 (C), followed by florescent imaging for Fshr-ZsGreen and each of these stained molecules simultaneously. In the section stained for Col1a1 (A), two representative areas are shown at magnifications of 400X and 1000X as indicated: (1) hepatic cells with a central vein

(CV) (a and c) and (2) hepatic artery (b and d). In the section stained for CD31 (B), a representative area of hepatic cells with a CV is shown at lower (a) and higher (b) magnifications. In the section stained for KCNMA1, three representative areas are presented at two magnifications as follows: (1) hepatic cells with a CV (a and b); (2) hepatic cells with peripheral nerve fibers (c and d); and (3) small nerve fibers located around a vein (e and f).

Furthermore, we observed bright Fshr-ZsGreen expression with slightly weak staining for α-SMA in the layer of endothelial cells of the large vein in **Figure 5B-f** and h. Under the endothelial cells, a cluster of smooth muscles showed colocalization of Fshr-ZsGreen with positive staining for α-SMA (**Fig. 5B-f** and h). In contrast to the vein, we observed a thin layer of endothelial cells (tunica intima) and stronger Fshr-ZsGreen expression with positive staining for α-SMA in the large artery (tunica media); Fshr-ZsGreen was also present in the cells in the tunica adventitia (**Fig. 5B-k**). In frozen sections of hearts, we observed strong Fshr-ZsGreen expression in neural fiber clusters that were in adipose tissue, as shown in **Figure 5B-g** and m.

Using an antibody against EMCN, a marker for endothelial cells, we further confirmed Fshr-ZsGreen expression in the layer of endothelium (tunica intima), which showed visible positive staining for EMCN when imaged at 400X and 1000X (**Fig. 5C-a**, b and d). In addition, Fshr-ZsGreen^{+} cardiomyocytes and smooth muscles under the endothelial layer were positive for EMCN staining (**Fig. 5C-a**, b and c).

In addition to large blood vessels on the heart, we also took a close look at the ascending aorta. We obtained two types of sections with longitudinal and transverse orientations for IFs with the two antibodies as above. In both sections, we found that Fshr-ZsGreen^{+} smooth muscle fibers were strongly stained for α-SMA in the first layer of SM close to the endothelium, where the second layer of smooth muscle was relatively weak for staining with α-SMA (**Figs. 5D-a** and 6B-e). Fshr-ZsGreen was also present at the endothelium, which was costained positively for α-SMA (**Fig. 6A-a** and 6B-e). Using an anti-EMCN antibody, we noticed that positive staining was in the upper part of Fshr- ZsGreen^{+} endothelial cells facing the lumen of the examined blood vessels (**Fig. 5A-c** and 5B-f). In addition to Fshr-ZsGreen expression in the endothelium of the tunica intima, it was also observed in the areas of subendothelial connective tissue and tunica media (smooth muscle), but these areas were not stained for EMCN (**Fig. 5A-c** and 5B-f).

5) Lung and kidney

To identify whether Fshr is expressed in epithelial cells, we first detected Fshr- ZsGreen in the lung. Unexpectedly, we observed high Fshr-ZsGreen expression in the lung (**Fig. 6A**). Fshr-ZsGreen was brightly expressed in the columnar epithelium of the respiratory conducting zone/tract, including the trachea, bronchus, bronchi and bronchiole, at low magnification (**Fig. 6A**-left panel). At higher magnifications, it was clearly shown that Fshr-ZsGreen was expressed not only in the columnar epithelium but also in the bronchial gland and alveoli (**Fig. 6A-a**, b, d, e, f and g). In the alveoli, Fshr-ZsGreen was observed in the respiratory portion of both type I and II cells, as indicated by empty arrowheads and white arrows, respectively (**Fig. 6A-d** and h). We confirmed the identification of respiratory cells by IF with an anti-PD-L1 antibody, which showed the colocalization of Fshr-GFP with PD-L1 [38] staining (**Fig. 6A**).

Then, we aimed to examine Fshr expression in epithelial cells of the kidney. In the frozen section of the kidney, it was astonishing to observe high expression of Fshr- ZsGreen in the proximal and distal convoluted tubules (**Fig. 6B-e** and f), whereas relatively weak expression was observed in the glomerular capillaries at different magnifications (**Fig. 6B-e** and f at 400X and g at 1000X). Again, we observed Fshr-ZsGreen expression in the endothelial layer of the arteriole in the kidney tissue (**Fig. 6B-h**). We also observed colocalization of Fshr-ZsGreen with positive staining for Col1a1 [34] in the kidney (**Fig. 6B**).

6). Other key tissues and organs (liver, pancreas, thyroid, skin and skeletal muscle, spleen, bone marrow, and brain)

With the power of Fshr-ZsGreen, we characterized Fshr-ZsGreen expression in the liver. We observed Fshr-ZsGreen expression in the hepatocytes and arteries inside the hepatocytes, which were positively stained for Col1a1 or CD31 [39,40], respectively (**Fig. 7-A** and B). Although it is weakly expressed inside large nerve fibers, Fshr-ZsGreen is strongly expressed in small neural fibers and shows a costaining pattern with KCBMA1 [41], a marker used for the detection of peripheral nerve fibers (**Fig. 7-C**, indicated by white arrowhead, whereas large nerve fibers are indicated by white arrows).

We then examined Fshr-ZsGreen expression in the pancreas and found that it was expressed not only in acinar cells but also in islets of Langerhans at low and high magnifications (**Fig. 8-A**-a and b). We then confirmed the identification of α and β-cells by IFs with antibodies against NG3, insulin or glucagon. The imaging results clearly demonstrated that Fshr-ZsGreen was expressed in both α and β-cells as well as acinar cells at 400X and 1000X magnifications, respectively (**Fig. 8-A**, -B and -C).

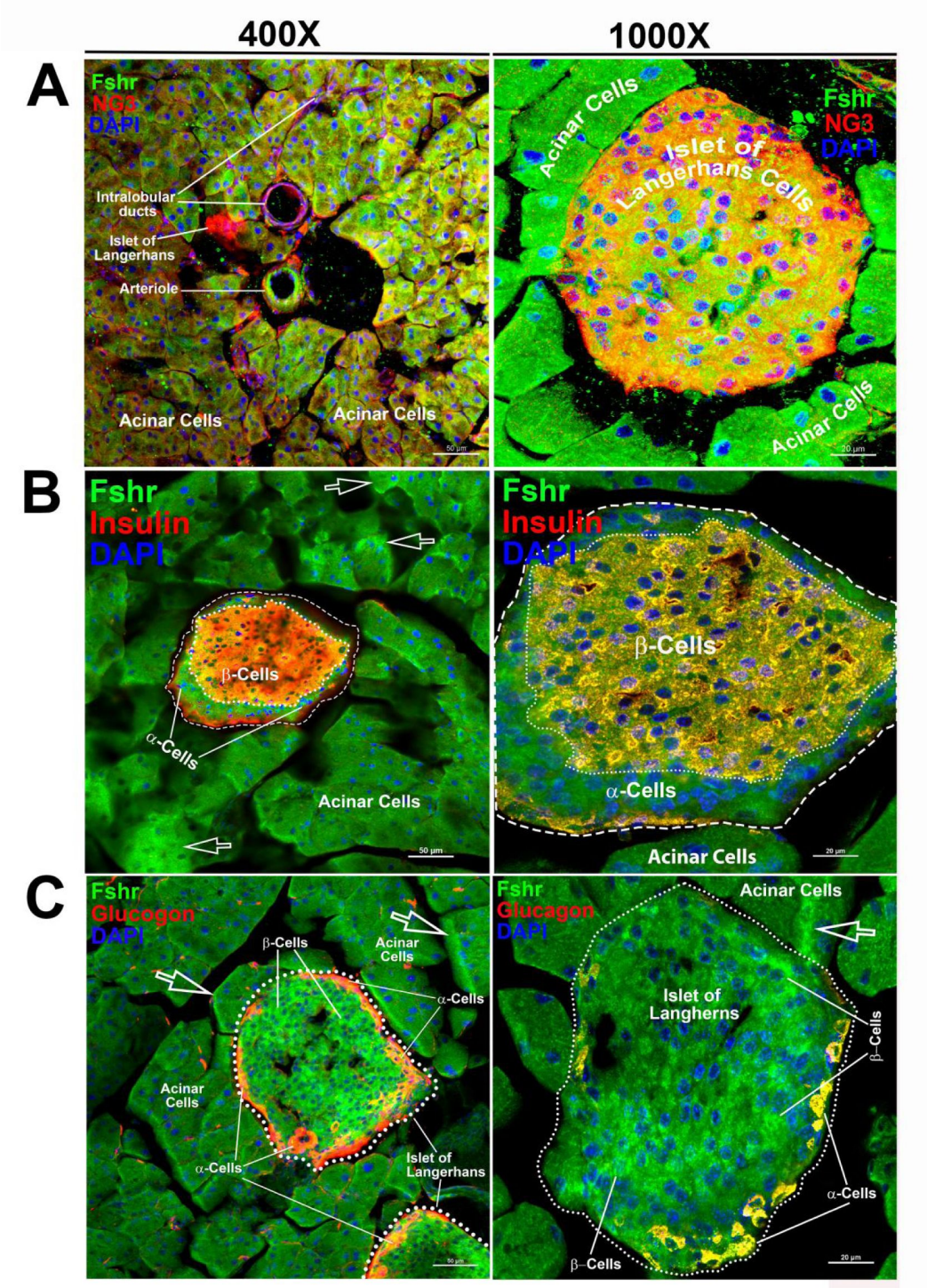

Figure 8.

Visualization of Fshr-ZsGreen expression in the pancreas.

Visualized Fshr-ZsGreen expression was obtained in frozen sections of the pancreas under fluorescence microscopy after immunostaining with antibodies against NG3, insulin or glucagon at two magnifications (400X and 1000X). Images of Fshr- ZsGreen expression with NG3, insulin and glucagon staining are shown in A, B and C, respectively.

Regarding Fshr-ZsGreen expression in the thyroid, we found Fshr-ZsGreen in both follicular cells and parafollicular cells (C-cells) at low and high magnifications (400X and 1000X) (**Fig. 9-A**-a, b, c, d and e). We further used an anti-Tsh receptor antibody to confirm Fshr-ZsGreen-positive cells, which showed that follicular cells were stained positively for Tshr in the nuclei, as indicated by dotted circles and white arrowheads, and C-cells were indicated by white arrows (**Fig. 9-b** to e).

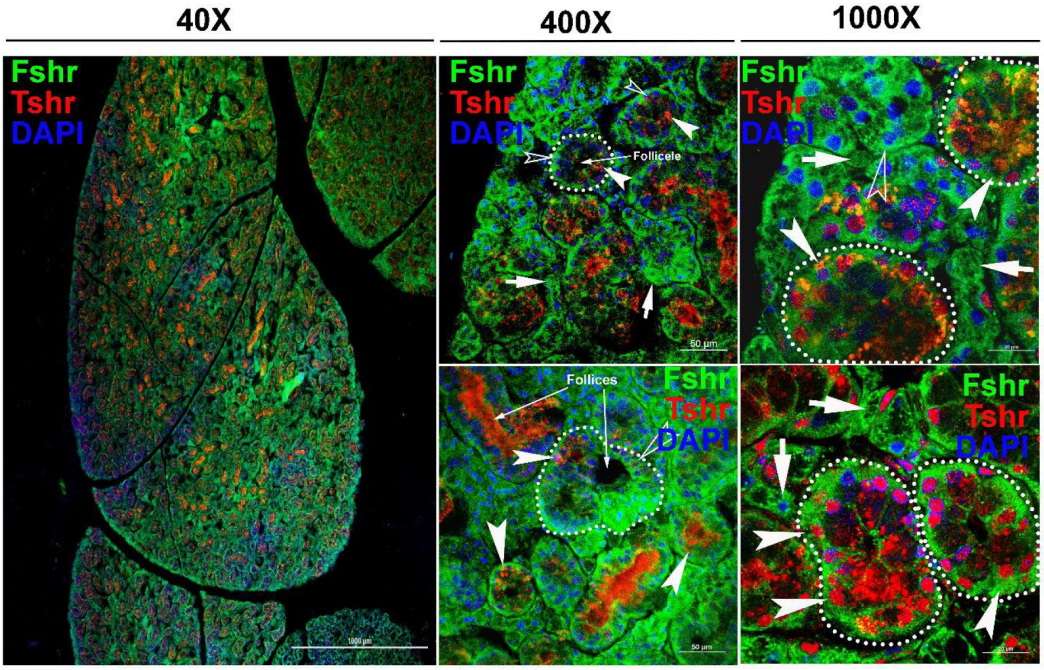

Figure 9.

Fshr-ZsGreen expression in the thyroid.

Fshr-ZsGreen expression was detected by its colocalization with immunostaining of TSH in frozen thyroid sections. The left panel is an entire image of the section, and two representative areas are in the right panels at higher magnifications, demonstrating Fshr-ZsGreen expression in follicular cells and parafollicular cells (C cells) at the edge (a and b) and the center of the thyroid (c and d). Arrows: white arrowheads indicate follicular cells, and white arrows indicate parafollicular cells. Magnification: 40X for the whole image.

Next, to examine Fshr-ZsGreen expression in the skin, we used two types of skin sections: thick skin from the tail and thin skin from the abdomen (**Fig. 10-A**-a and b). Although a dermis layer was not included in the image taken for a thick sample, we observed that Fshr-ZsGreen was expressed in hair follicle (HF) and sweat gland cells and fibroblasts in the dermis and hypodermis (**Fig. 10-A**-a). Similarly, Fshr-ZsGreen was present in HFs and fibroblasts in the dermis and keratinocytes in the epidermis of the thin skin (**Fig. 10-A**-b). As we detected Fshr-ZsGreen expression in hair follicles, we wondered whether stem cells in HFs express Fshr-ZsGreen. To address this question, we carried out IF with an antibody against CD34, a stem cell marker. Not surprisingly, we found that

Figure 10.

Detection of Fshr-ZsGreen expression in the skin.

Fluorescence images of Fshr-ZsGreen were taken in two types of skin (A): thick skin (A-a) and thin skin (A-b). Then, IF staining was performed using an antibody against CD34 to identify stem cells with Fshr-ZsGreen expression in the hair follicles (B) at lower (B-a) and higher (B-b) magnifications (400X and 1000X, respectively). Abbrev.: HF-hair follicle; SG-sweat gland; FT-fat tissue; DP-dermal papillae. Magnifications: 400X for A and B-a, 1000X for B-b. Scale bars: 50 μm for A and B-a and 20 μm for B-b.

CD34 staining was colocalized with cells with Fshr-ZsGreen in Bulge as quiescent stem cells and in the dermal papilla (DP) and epidermis as active stem/progenitor cells, as shown in Figure S4-B-a and b. Therefore, these results indicate Fshr-ZsGreen expression in stem/progenitor cells in the skin (**Fig. 10B-a** and d).

We then detected Fshr expression in skeletal muscle (gastrocnemius), followed by IF staining using three antibodies against αSMA, PAX7 and TH for the identification of satellite cells and peripheral nerve fibrils. We observed Fshr-ZsGreen across the muscle sections at a lower magnification of 40X (**Fig. 11a**). At higher magnifications, we found that Fshr-ZsGreen was present in the muscle fibers, in which one type had higher Fshr- ZsGreen expression (indicated by white arrowheads) and another type had lower Fshr- ZsGreen expression (**Fig. 11b** to h). Fshr-ZsGreen was also highly expressed in satellite cells stained positively for either αSMA (**Fig. 11-b** to e) or PAX7 (**Fig. 11-f** and g) in both longitudinal and transverse sections, as indicated by white arrows. In addition, we detected Fshr-ZsGreen expression in the peripheral neural fibers identified by positive staining for TH, which were around vascular structures in the muscle tissue, as indicated by red arrowheads (**Fig. 11-h** and i).

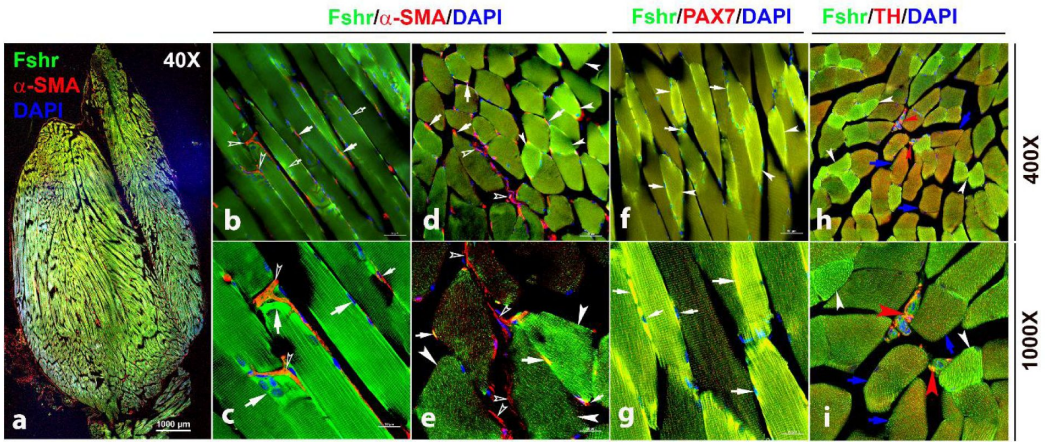

Figure 11.

Fshr-ZsGreen expression in skeletal muscle.

The whole image of frozen sectioned skeletal muscle (gastrocnemius) was taken at a lower magnification (40X) after the section was stained with anti-α-SMA antibody, as shown in the left panel (a). Then, longitudinal sections (b and c) and cross-sections (d and e) were imaged at higher magnifications (400X and 1000X), respectively. In addition, frozen sections stained with antibodies against PAX7 (f and g) and TH (h and i) were imaged at two magnifications (400X and 1000X) as indicated. Arrows: (1) In b-e, empty white arrowheads indicate both Fshr-ZsGreen- and α-SMA-positive

satellite cells; empty white arrows point to only Fshr-ZsGreen-positive satellite cells without α-SMA staining; white arrowheads indicate muscle fibrils with strong Fshr-ZsGreen expression but no α- SMA staining. (2) In f and g, white arrowheads indicate muscle fibrils with strong Fshr- ZsGreen expression, blue arrows point to muscle fibrils with both Fshr-ZsGreen and TH expression, and red arrowheads indicate peripheral nerves with both Fshr-ZsGreen and TH expression. Magnifications: 40X for a, 400X for b, d, f and h, and 1000X for c, e, g and i. Scale bars: 1000 μm for a, 50 μm for b, d, f and h, and 20 μm for c, e, g and i.

To detect Fshr expression in immune cells, we examined Fshr-ZsGreen expression in the spleen and bone marrow using antibodies against CD11b and CD3, as integrin αM (CD11b) is expressed in myeloid-lineage cells such as monocytes/macrophages, neutrophils, eosinophils, and basophils and in lymphoid cells such as NK cells and B-1 cells [42], while CD3 marks T cells [43]. We imaged frozen sections of the spleen under magnifications of 40X, 400X and 1000X and observed that Fshr-ZsGreen was highly expressed in trabeculae and cells in both red and white pulps (RP and WP). The Fshr- ZsGreen-positive cells were further identified by IFs with antibodies against CD11B or CD3, indicating that Fshr is expressed in immune cells, such as monocytes/macrophages, neutrophils, eosinophils, basophils, NK cells, B cells and T cells (Fig. 12-A and B). In addition, we further confirmed Fshr-ZsGreen expression in macrophages of bone marrow, which were identified with anti-CD4/80 antibody, as shown in two representative images of BM-one from an area close to cortical bone (Fig. 12-C-a) and another located in the center of BM (Fig. 12C-b) at 1000X magnification (empty white arrows indicate the colocalization of Fshr-ZsGreen and CD11B, CD3 or CD4/80 in the RPs, while white arrows point to their colocalization in the WPs).

Finally, we examined Fshr-ZsGreen expression and its colocalization with markers for either astrocytes, microglia, or neurons in the brain. As expected, we observed Fshr expression across the brain sections and the three representatives from the olfactory bulbs, pallidum, and hippocampus (CA3) are shown in Figure 12, demonstrating that Fshr is indeed expressed in astrocytes (**Fig. 13-a** to c), microglia (Fig. 12-d to f) and neurons (**Fig. 13-g** to j), as well as neuronal fibers (synapses or projections). Other cell types are needed to be further defined.

Figure 13.

Examination of Fshr-ZsGreen expression in the spleen and bone marrow

To identify Fshr-ZsGreen expression in immune cells of the spleen, IF staining was performed in frozen sections of the spleen. Two antibodies against either CD11B or CD3 were used to identify myeloid-lineage cells or T cells. Fshr-ZsGreen expression in myeloid-lineage cells is shown in A, in which the left panel is the whole image of the spleen at a low magnification and its three representative areas are presented at higher magnifications (400X and 1000X): (1) an area located at the edge showing strong Fshr- ZsGreen and CD11B expression (a and b); (2) an area of red pulp c and d); (3) an area of white pulp (e and f). Abbrev.: RP-red pulp, WP-white pulp, BM-bone marrow, F-fibroelastic capsule and MZ- marginal zone. Scale bars are indicated in each image.

3. Confirmation of Fshr-ZsGreen expression with a Fshr-specific antibody and ddRT- PCR

Finally, to confirm the accuracy of the above results obtained from Fshr-ZsGreen mice, we performed fluorescence immunostaining with a specific antibody against mouse Fshr and accurate droplet digital RT−PCR (ddRT-PCR) with mouse Fshr-specific primers to confirm the above data. An isotype-matched rabbit IgG was used as a negative control for IFs with anti-Fshr antibody using sections from Fshr-ZsGreen mice. Imaging was performed under the same conditions to record each corresponding tissue/organ stained with anti-Fshr antibody. The images of negative controls are shown in Supplementary Data 2, showing specific binding of the secondary antibody to anti-Fshr antibody without any nonspecific binding of the secondary antibody to the examined sections.

As shown in **Figure 14A**, in all the examined tissues, including bone, BAT, thyroid, cardiac muscle, kidney, liver, lung, aorta, ovary and testis, we observed colocalization of Fshr-ZsGreen with positive staining for Fshr, further confirming the specific expression of Fshr-ZsGreen in the examined tissues/organs.

Figure 14.

Fshr-ZsGreen expression in the representative areas of the brain.

Fshr expression in three representative areas of the brain-the olfactory bulbs (a, d, and g), pallidum (b, e and h) and hippocampus (c, f and j). Each section was immunofluorescently stained with antibodies against GFAP, Iba1 or NeuN that recognized markers for astrocytes (a-c), microglia (d-f) or neuron (g-j), respectively. Their colocalizations are indicated by white arrowheads. Abbrev.: OLB-olfactory bulb. Magnifications: 400X for a, c and f, and 1000X for b, d, e, f g and h. Scale bars are indicated in each image.

We also obtained total RNA from the following tissues: lung, kidney, thoracic vertebra, calvaria, femur, jejunum, liver, teeth, tibia, skeletal muscle, tails, cartilage, skin, spleen, stomach, heart, bladder, tongue, BAT, WAT, thyroid, brain, pancreas and duodenum. After reversing mRNA from total RNA, we performed ddRT-PCR with mouse-specific primers to check Fshr expression at the transcriptional level as described in the Methods section. The results demonstrated Fshr expression in these tissues, and the expression profile was categorized into three groups: 1) high expression in the lung and kidney tissues; 2) moderate expression in the thoracic (T) vertebrae, calvaria, femur, jejunum, liver, teeth, tibia, and muscle; and 3) low expression in the tail, cartilage, skin, spleen, stomach, heart, bladder, tongue, BAT, WAT, brain, pancreas, and duodenum (**Fig. 14B**).

Finally, we also searched Fshr expression at single cell level in 5 single cell databases including DISCO (a database of Deeply Integrated Single-Cell Omics data, (*https://www.immunesinglecell.org/*), BioGPS (A free extensible and customizable gene annotation portal, a complete resource for gene expression and protein function, *http://biogps.org/exrna/#goto=welcome*), Single Cell Portal (SCP, an interactive home for single-cell genomics data, *https://singlecell.broadinstitute.org/*), Genotype-Tissue Expression (GTEx portal, *https://gtexportal.org*), CZ CELLxGENE Discover (*https://cellxgene.cziscience.com/*).

The selected results from these databases are presented in Supplementary Data 3, which further support our findings of the widerspread express pattern of Fshr described as above. In particular, Fshr expression was detected in Leydig cells by scRNA-seq as shown in DISCO (immunesinglecell.org/genepage/FSHR), BioGPS (*http://biogps.org/#goto=genereport&id=2492*) and CZ CELLxGENE Discover (human- *https://cellxgene.cziscience.com/e/535e9336-2d8d-43c3-944d-bcbebe20df8a.cxg/* and mouse- *https://cellxgene.cziscience.com/e/a13bda79-9134-46c9-9ed1-a2858be9aafe.cxg/*).

Taken together, these data further confirmed Fshr-ZsGreen expression patterns from the Fshr-ZsGreen reporter line, convincingly demonstrating that Fshr is not limited to previously reported cells, tissues, or organs, such as the reproductive system, osteoclasts, adipose, endothelium in tumors, and neurons in the brain, but rather has a wide expression in the cells, tissues, and organs in the body, particularly in the lung, kidney, and heart, as well as Leydig cells in the testis, which has not previously been recognized.

Discussion

Although numerous efforts have been made to characterize Fshr expression in tissues/cells, defining the locations of Fshr expression remains an imperative challenge in Fsh-Fshr biology, primarily because of concerns about the specificity of available antibodies against Fshr

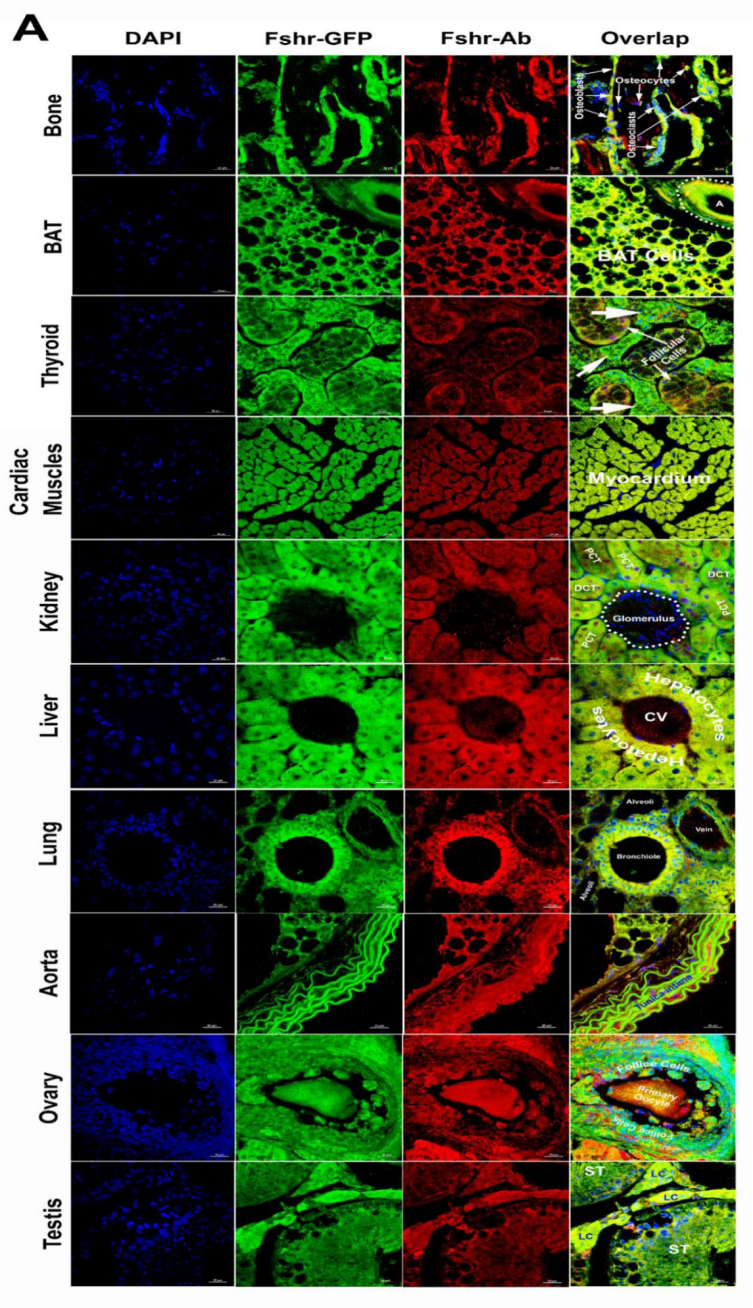

Figure 15.

Confirmation of Fshr-ZsGreen expression by IF staining with a specific antibody against mouse Fshr and ddRT-PCR.

The Fshr-ZsGreen expression described above was further confirmed by IF staining using an antibody against mouse Fshr and ddRT−PCR. The frozen tissue sections used for this confirmation include bone, BAT, thyroid, cardiac muscles, kidney, liver, lung, aorta, ovary and testis (A), demonstrating Fshr-ZsGreen colocalization with Fshr-positive staining in these tissues/organs. Fshr expression at the mRNA level in different tissues/organs was examined by ddRT−PCR (B) (the representative of two experiments). The results indicate that Fshr is expressed in all examined tissues/organs. Based on their expression levels, they can be categorized into three groups: (1) high (H), including lung and kidney, ranging from 1005 to 1843 copies/μL; (2) middle (M), including thoracic (T) vertebra, skull, femur, jejunum, liver, tooth, tibia and muscle, ranging from 173 to 475 copies/μL; and (3) low (L), including duodenum, pancreas, brain, WAT, thyroid, BAT, tongue, bladder, heart, stomach, spleen, skin, cartilage and tail, ranging from 5.4 to 81 copies/μL.

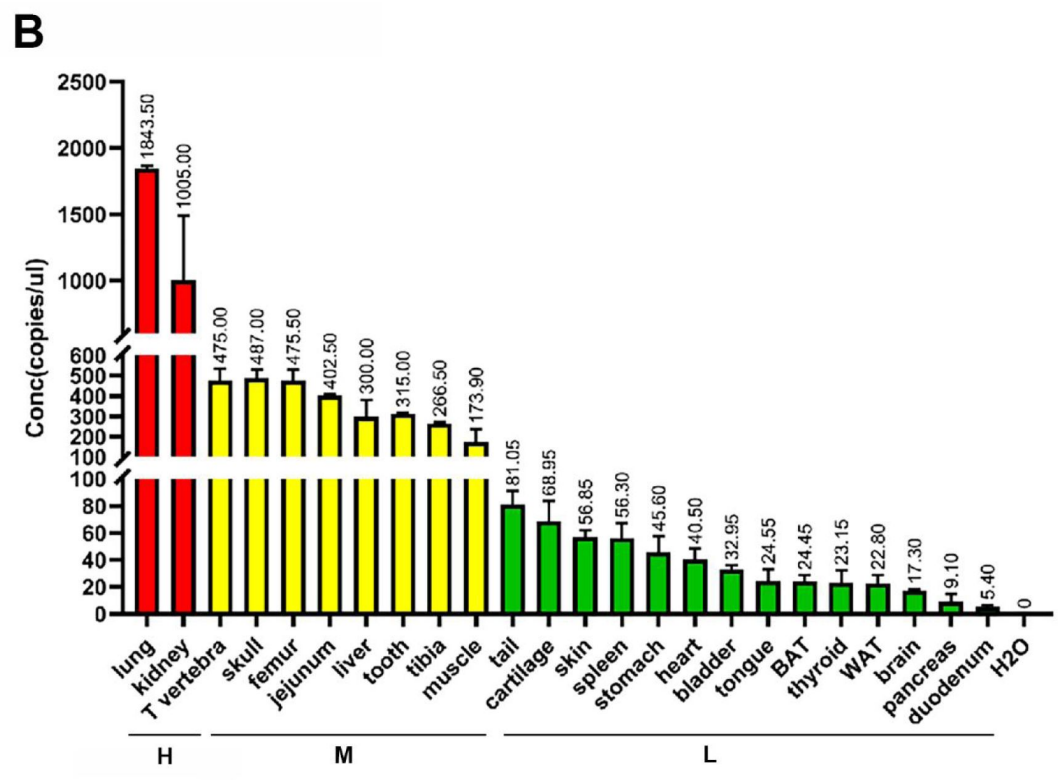

Figure 15. (continued)

[2],[15],[16]. In this case, we developed CRISPR/Cas9-mediated Fshr- ZsGreen knockin reporter mice to address this issue.

To maintain the integrity of the splicing acceptor, donor, and gene promoter regions, we designed and inserted the ZsGreen (ZsG) reporter into the the C-terminus of Fshr by sequence-specific gRNA guided CRISPR/Cas9-mediated precise genome modification with a long ssDNA template to create the Fshr-P2A-ZsG reporter mice [44]. Because of its high turnover of Fshr mRNA and a difficulty in detection of Fshr expression by rt-PCR and Northern blotting, in this reporter line, we utilized ZsG as a GFP reporter, as ZsGreen, also called ZsGreen1, is an exceptionally bright green fluorescent protein derived from a Zoanthus sp. reef coral [45] that has been modified for high solubility, bright emission, and rapid chromophore maturation. ZsGreen is the brightest commercially available green fluorescent protein—up to 4X brighter than EGFP with the half life of 26 hours and is ideally suited for whole-cell labelling and promoter-reporter studies to indicate the promoter activity of a gene of interest, which has been used in numerous GFP reporter mice [46]–[55]. In addition, we also employed a short and conserved picornavirus-derived 'self-cleaving' 2A peptide to allow bicistronic expression of Fshr and ZsG, as the 19-amino acid P2A has the highest cleavage efficiency [56],[57]. The cleavage is triggered by ribosomal skipping of the peptide bond between the proline (P) and glycine (G) in C-terminal of P2A peptide, resulting in the peptide located upstream of the 2A peptide to have extra amino acids on its C-terminal end, while the peptide located downstream the 2A peptide will have an extra proline on its N-terminal end. Therefore, P2A can nearly equalize the expression of genes upstream and downstream. As a result, Fshr is normally expressed without interruptions and ZsG expression indicates Fshr promoter activity in the defined cells, demonstrated by the comparison of Fshr expression in the testes and ovaries between Fshr-ZsGreen and B6 mice (**Fig. 2G**).

The P2A-ZsGreen construct was precisely inserted into the site between the last exon (exon 10) and the stop codon of the Fshr locus, which was confirmed by integration detection PCR, sequencing of PCR fragments and Southern blotting with Fshr locus- specific enzyme restriction digestions. Successful insertion allows the endogenous promoter of Fshr to drive ZsGreen reporter expression. Because of the site-specific insertion of the P2A ZsG vector to produce Fshr-ZsG reporter, we only used one founder line for characterizing Fshr-ZsG expression, rather than multiple founders when random insertions of a transgene were used previously for generating transgenic mice.

This approach greatly enhanced our understanding of this critical cellular pathway in several ways. Firstly, employing the native regulatory element responsible for governing the expression of the target gene ensures that the expression pattern of the GFP reporter closely mirrors that of the gene of interest, Fshr, within its natural context. Consequently, this approach provides a more faithful representation of gene expression. Secondly, endogenous promoters often exhibit specific spatial and temporal expression patterns, driving gene expression in specific cell types or developmental stages. This capability facilitates the capture of the dynamic nature of gene regulation and enables the study of gene expression under diverse physiological conditions. Thirdly, utilizing endogenous promoters minimizes potential perturbations to the native gene regulation machinery. It avoids the need to introduce exogenous elements or artificial constructs, reducing the likelihood of altering the gene's expression behavior or interfering with its regulatory interactions. Unlike biochemical assays or immunostaining, using a tagged protein under endogenous regulation avoids fixation artifacts and allows detection of the target's activity in live cells. Therefore, these distinct advantages of enhanced physiological relevance, precise spatiotemporal control, preservation of regulatory elements, and minimal perturbation provide us with a powerful tool to understand Fshr expression in more accurate and context-specific ways compared to other methods, such as using antibodies, Northern blotting, RT–PCR and in situ hybridization.

In this study, we systemically investigated Fshr expression at the single-cell level in this reporter line with confocal fluorescence microscopy and further confirmed the location of Fshr-ZsGreen expression by IF staining, in situ hybridization and ddRT−PCR. The results from this work demonstrate that as a receptor for Fsh, Fshr is widely expressed in virtually every cell at variable levels in the examined tissues/organs of mice. As expected in the examined testis, we noticed Fshr expression in Sertoli cells in the testis and granular cells in the ovary. Surprisingly, we observed that Fshr was also more strongly expressed in Leydig cells than in Sertoli cells. This expression was also detected in spermatocytes, spermatids, spermatozoa and spermatogonia. Although this finding is different from present thoughts that Fshr is only present in Sertoli cells but not in other cell types of the testis, our finding is in line with previous works in fishes (including African catfish, zebrafish, teleosts, and Japanese eels) [58–63], rats [64], dogs [65] and humans [66] performed by IHC and in situ hybridization. In humans, Fshr was also highly expressed in Leydig cells, although it was taken as non-specificity of the anti-Fshr antibodies. However, as shown in this study, this is not the case, because Fshr is widely expressed, as demonstrated in our work.

Furthermore, our findings are supported by a report of the failure of normal Leydig cell development resulting from the deficiency of Fshr but not Fsh-beta [67] and single cell RNA-seq studies in Hu sheep (originated from Mongolian sheep) [68] and in human as shown in Supplementary Data 3 [DISCO (immunesinglecell.org/genepage/FSHR), BioGPS (*http://biogps.org/#goto=genereport&id=2492*) and CZ CELLxGENE Discover (*https://cellxgene.cziscience.com/e/535e9336-2d8d-43c3-944d-bcbebe20df8a.cxg/*)].

Fshr expression in Leydig cells strongly indicates that Fsh-Fshr plays a role in the production of steroids in males. Unexpectedly, Leydig cell line TM3 expresses much lower Fshr, compared to the Leydig cells *in vivo* (**Fig. 2B-G**). It may explain that these cells do not respond well to FSH treatments [30] and indicates that this cell line may be not a typical Leydig cell population and new Leydig cell lines should be established in the future.

In the ovary, Fshr is highly expressed in follicles at different stages, from primordial cells, primary follicles, and secondary follicles to mature/Graafian follicles and the corpus luteum. In addition to granulosa cells, Fshr expression was observed in oocytes of follicles. Taken together, these data indicate that Fshr plays an intragonadal role in the ovary and testis beyond the granulosa and Sertoli cells.

In the skeletal system, we observed Fshr expression in vivo not only in osteoclasts, as reported previously [11,69,70], but also, interestingly, in osteoblast lineage cells, such as osteoblasts, bone lining cells, osteocytes and progenitor cells of the periosteum, as well as in chondrocytes. In previous reports, Fshr expression in osteoclasts was detected only by RT−PCR, Western blot and immunostaining in cultures of primary murine precursors [11,69,70]. Using the Fshr-ZsGreen reporter line, we visualized Fshr expression in multinucleated osteoclasts in frozen sections, clearly demonstrating Fshr expression in osteoclasts. Intriguingly, this powerful tool enabled us to examine Fshr expression in other cell types in bone. Surprisingly, we observed Fshr expression in cells of the osteoblast lineage, from osteoprogenitor cells and osteoblasts to osteocytes and bone lining cells. This finding indicates that Fsh may regulate not only osteoclast-mediated bone resorption but also osteoblasts for bone formation. To functionally prove the presence of Fshr in osteoblasts/osteocytes, we also deleted Fshr in osteocytes in an inducible model. The Fshr cKO induced in osteocytes significantly reduce Fshr expression and triggered an increase in the cortical thickness (**Fig. 3D**) and a much more profound increase in bone mass and a decrease in fat mass than blockade by Fsh antibodies (unpublished data), illuminating Fshr expression in the osteoblast lineage.

In addition to its expression in the reproductive system and skeletal system, we also strikingly identified other cell types that highly express Fshr: endothelial cells in blood vessels and epithelial cells in the lung and kidney. In every examined tissue/organ, we found that endothelial cells

stained positively for CD34 lining on the arterioles had a higher expression of Fshr-ZsGreen than other cell types. This bright Fshr-ZsGreen is more obviously seen in large arteries, such as the ascending aorta and others located in the heart. Similarly, Fshr was detected in vessels in solid malignant tumors by immunohistochemistry or RT−PCR [71]. However, it was not seen in normal tissues or organs by these methods, possibly due to its rapid turnover, fast degradation, or selected antibodies. Strikingly, we detected the highest Fshr-ZsGreen expression in bronchial and bronchiole ciliated epithelial cells by both fluorescence microscopy and ddRT−PCR. It was also more highly expressed in other cell types in the lung, such as type I pneumocytes (alveolar lining cells), type II pneumocytes (great alveolar or septal cells), and gland cells. However, the role of this unexpectedly high Fshr expression in the lung remains unknown. Similarly, we also found the second highest expression of Fshr- ZsGreen in renal epithelial cells in proximal and distal convoluted tubules but weak expression in renal corpuscles. In addition, our finding of Fshr expression in adipose tissues is consistent with the observations from previous works [12,72]. Recently, Fshr expression was reported to be present in β-cells of the pancreas to regulate glucose-stimulated insulin secretion, further supporting our findings of the Fshr expression pattern [73].

In summary, we established and validated an Fshr-ZsGreen protein reporter in vivo that faithfully recapitulates endogenous Fshr expression at single-cell resolution. Our compelling findings reveal that in addition to gonadal tissues, Fshr is also highly expressed in extragonadal systems, such as the lung, kidney, heart, and pancreas. This will provide insight to better understand the biology of the Fsh-Fshr axis and its roles in the physiology and pathology of these tissues/organs. In addition to the above described, we detected Fshr expression in cells of the teeth and brain; those findings are not presented here because of space limitations and will be published elsewhere, except that three representative areas of the brain are shown in **Figure 14**.

Although the Fshr-ZsGreen reporter line is a powerful tool for detecting the location of Fshr expression, it is limited in the definition of individual isoforms of Fshr transcripts and the detection of their turnover, which should be addressed by specific antibodies and determined by the rates of transcription and RNA degradation, including Xrn1 for 5’-to-3’ degradation, exosomes for 3’-to-5’ degradation and nonsense-mediated decay [74,53].

Acknowledgements

This study was supported by a fund from Shanxi Medical University to PL.

Competing interests

The authors declare that we have no competing interests related to this research.

Author contributions

Hong-Qian Chen, Conceptualization, Data curation, Investigation, Methodology, Formal analysis, Project administration; Hui-Qing Fang, Data curation, Investigation, Methodology, Formal analysis; Jin-Tao Liu, Data curation, Investigation, Methodology; Shi-Yu Chang, Data curation, Investigation, Methodology; Li-Ben Cheng, Data curation, Investigation, Methodology; Ming-Xin Sun, Data curation, Investigation, Methodology; Jian-Rui Feng, Data curation and Analysis; Ze-Min Liu, Resource and Analysis; Xiao-Li Li, Data curation and Analysis; Yong-Hong Zhang, Resource,

Writing-Original draft; Clifford Rosen, Writing – original review and editing; Peng Liu, Conceptualization, Formal analysis, Funding acquisition, Investigation, Project administration, Resources, Supervision, Writing – original draft, Writing – review and editing.

Supplementary Materials 1

1. The first set of Integration detection PCR primer design and sequences:

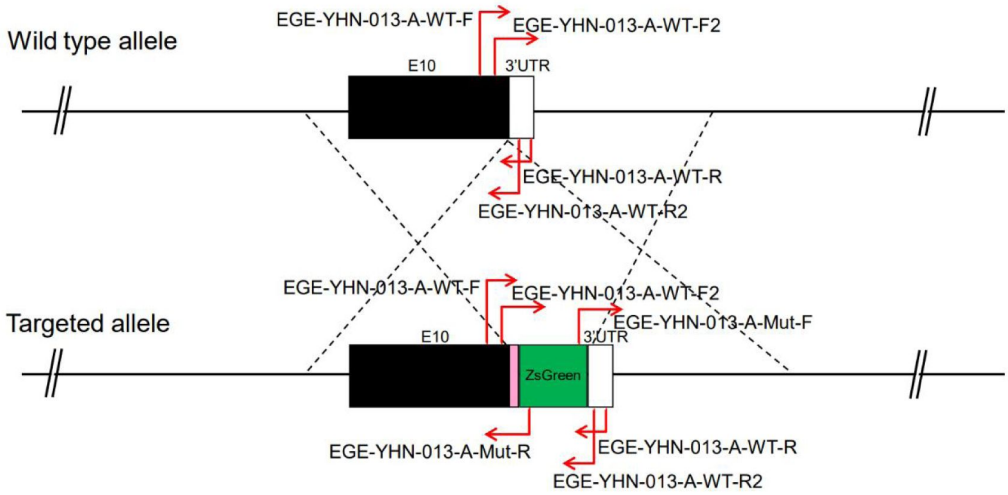

Primer	Sequence (5'-3')	Tm(℃)	Product size (bp)
EGE-YHN-013-A-WT-F2	ACTTCCACTCCAGAAAGAATCCCT	58	WT:166 Mut:937
EGE-YHN-013-A-WT-R2	CTCTTCCATAGCCCTCTCTCCAG	58	
EGE-YHN-013-A-Mut-F	CGACACCGTGTACAAGGCCAAGTC	64	Mut:316
EGE-YHN-013-A-WT-R	TAATGGTCCCTGACCTATCTGCCAT	61	
EGE-YHN-013-A-WT-F	ATCACTGTGTCCAAGGCCAAGATCC	63	Mut:542
EGE-YHN-013-A-Mut-R	TACATGAAGGCGGCGGACAAGATG	63	

Enzyme: 2x Taq Plus Master Mix II (Dye Plus)

Program: 2x Taq Plus Master Mix II (Dye Plus) progress

95 ℃	3 min	
95 ℃	15 sec	32 cycles
62 ℃	20 sec	
72 ℃	1 kb / min	
72 ℃	10 min	
4 ℃	hold	

2. The 2nd set of junction PCR primer design and sequences for genotyping F0 and F1:

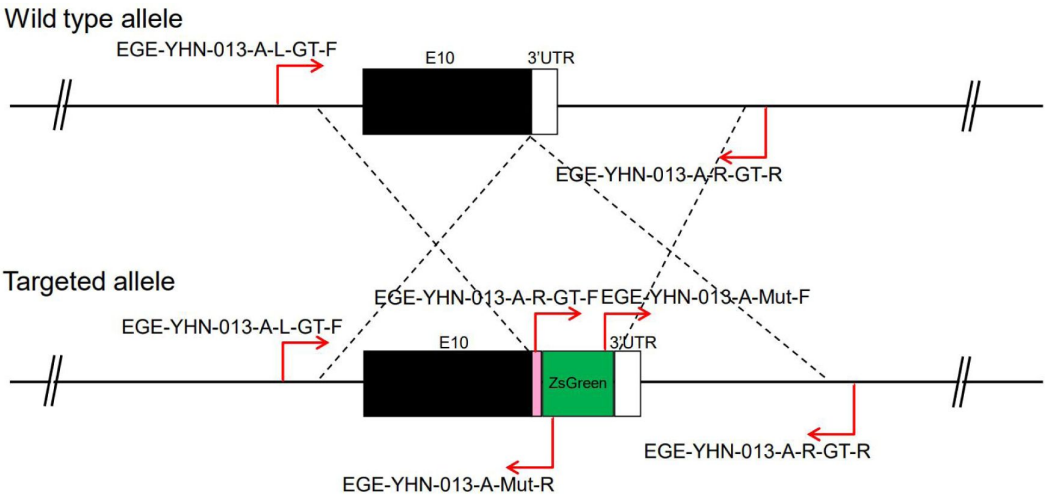

Primer	Sequence (5'-3')	Tm(℃)	Product size (bp)
EGE-YHN-013-A-L-GT-F	ACTCAGGTTGTGGCCAGATGGTTTC	63	Mut:2188
EGE-YHN-013-A-Mut-R	TACATGAAGGCGGCGGACAAGATG	63	
EGE-YHN-013-A-Mut-F	CGACACCGTGTACAAGGCCAAGTC	64	Mut:2074
EGE-YHN-013-A-R-GT-R	TGGCCTCACAAAGACAGCACAGATT	62	
EGE-YHN-013-A-R-GT-F	TGGAGGAGAACCCTGGACCTATGG	62	Mut:2636
EGE-YHN-013-A-R-GT-R	TGGCCTCACAAAGACAGCACAGATT	62	

Enzyme: KOD-FX

Program: Touchdown PCR

94 ℃	2 min	
98 ℃	10 sec	15 cycles
67 ℃	30 sec（- 0.7℃/cycle）	
68 ℃	1 kb / min	
98 ℃	10 sec	25 cycles
57 ℃	30 sec	
68 ℃	1 kb / min	
68 ℃	10 min	
4 ℃	hold	

3. PCR primer design and sequences for genotyping heterozygotes and homozygotes:

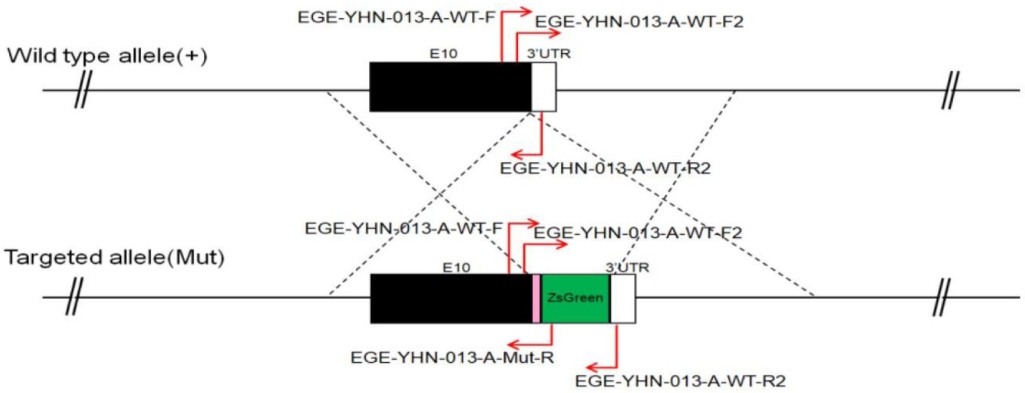

Primer	Sequence (5'-3')	Tm (℃)	Product size (bp)
EGE-YHN-013-A-WT-F2	ACTTCCACTCCAGAAAGAATCCCT	58	WT:166 Mut:937
EGE-YHN-013-A-WT-R2	CTCTTCCATAGCCCTCTCTCCAG	58	
EGE-YHN-013-A-WT-F	ATCACTGTGTCCAAGGCCAAGATCC	63	Mut:542
EGE-YHN-013-A-Mut-R	TACATGAAGGCGGCGGACAAGATG	63	

Supplementary materials 2

1. The primary antibodies used for IFs

#	Samples	The primary Abs. [rabbit anti-mouse (IgG)]	Sources	Cat. No.	Dilutions
1	WAT	Anti-Ucp1 pAb	Servicebio	GB112174	1:400
2	BAT	Anti-Ucp1 pAb	Servicebio	GB112174	1:400
		Anti-Peripherin pAb	Servicebio	GB111635	1:1100
		Anti-Tyrosine hydroxylase pAb	Servicebio	GB11181	1:800
3	Heart	Anti-Endomucin pAb	Servicebio	GB112648	1:600
		Anti--α-SMA Ab	Servicebio	GB111364	1:200
4	Liver	Anti-CD31 pAb	Servicebio	GB11063-2	1:100
		Anti-Collagen I pAb	Servicebio	GB11022-3	1:800
		Anti-KCNMA1/BK channel Ab	Bioss	bs-4775R	1:200
5	Spleen	Anti -CD3 pAb	Servicebio	GB11014	1:400
		Anti -CD11b pAb	Servicebio	GB11058	1:500
6	Lung	Anti-PD-L1/CD274 pAb	ABclonal	A1645	1:100
7	Kidney	Anti-Laminin antibody	Bioss	bs-0821R	1:300
		Anti-Col1a1 pAb	Servicebio	GB11022-3	1:800
8	Muscle	Anti-Tyrosine Hydroxylase pAb	Servicebio	GB11181	1:800
		Anti-α-SMA pAb	Servicebio	GB111364	1:500
		Anti-CD31 pAb	Servicebio	GB11063-2	1:100
		Anti-PAX7 pAb	Servicebio	GB113190	1:2500
9	Aorta	Anti-Endomucin pAb	Servicebio	GB112648	1:600
		Anti--α-SMA pAb	Servicebio	GB111364	1:200
10	Testis	Anti-Stra8 pAb	Bioss	bs-1903R	1:300
11	Pancreas	Anti-Insulin pAb	Servicebio	GB11334	1:400
		Anti-Glucagon pAb	Servicebio	GB11097	1:800
		Anti-Neurogenin3 Ab	Bioss	bs-0922R	1:300
12	Brain	Anti-NeuN pAb	Servicebio	GB11138	1:500
		Anti-GFAP pAb	Servicebio	GB11096	1:800
13	Femur	Anti-Osteocalcin pAb	Servicebio	GB11233	1:100
		Anti-Trap pAb	Servicebio	GB11416	1:400
		Anti-Tyrosine hydroxylase pAb	Servicebio	GB11181	1:800
14	Skin	Anti-CD34 pAb	Servicebio	GB111693	1:500
15	Thyroid	Anti-Tshr pAb	Servicebio	GB113007	1:500
16	Colon	Anti-CD34 pAb	Servicebio	GB111693	1:500
		Anti-CD133 pAb	Servicebio	GB113807	1:1000
17	Duodenum	Anti-Taf4 pAb	Servicebio	GB111725	1:900
18	Jejunun	Anti-CD34 pAb	Servicebio	GB111693	1:500
		Anti-CD133 pAb	Servicebio	GB113807	1:1000
19	Ovary	Anti-Taf4 pAb	Servicebio	GB111725	1:950
		Anti-CD34 pAb	Servicebio	GB111693	1:500
20	Bladder	Anti-SET pAb	Servicebio	GB113290	1:5000
21	Prostate	Anti-SET pAb	Servicebio	GB113290	1:5000
22	Testis	Anti-SET pAb	Servicebio	GB113290	1:5000

2. The sequences of sense and antisense probes for FISH in testis

1) For the sense probe

5'-ATCACTGGCTGTGTCATTGCTCTAA-3'

2) For antisense probes: a mixture of the following 5 probes used for FISH

5'-TTAGAGCAATGACACAGCCAGTGAT-3'

5’-CACCTTGCTATCTTGGCAGAGGAAG-3’

5’-AGCACAAATCTCAGTTCAATGGCGT-3’

5’-CAAGTGTTTAATGCCTGTGTTGGAT-3’

5’-GCAGGGAATAGACCTTTGTCCTTGA-3’

Supplementary Data 1

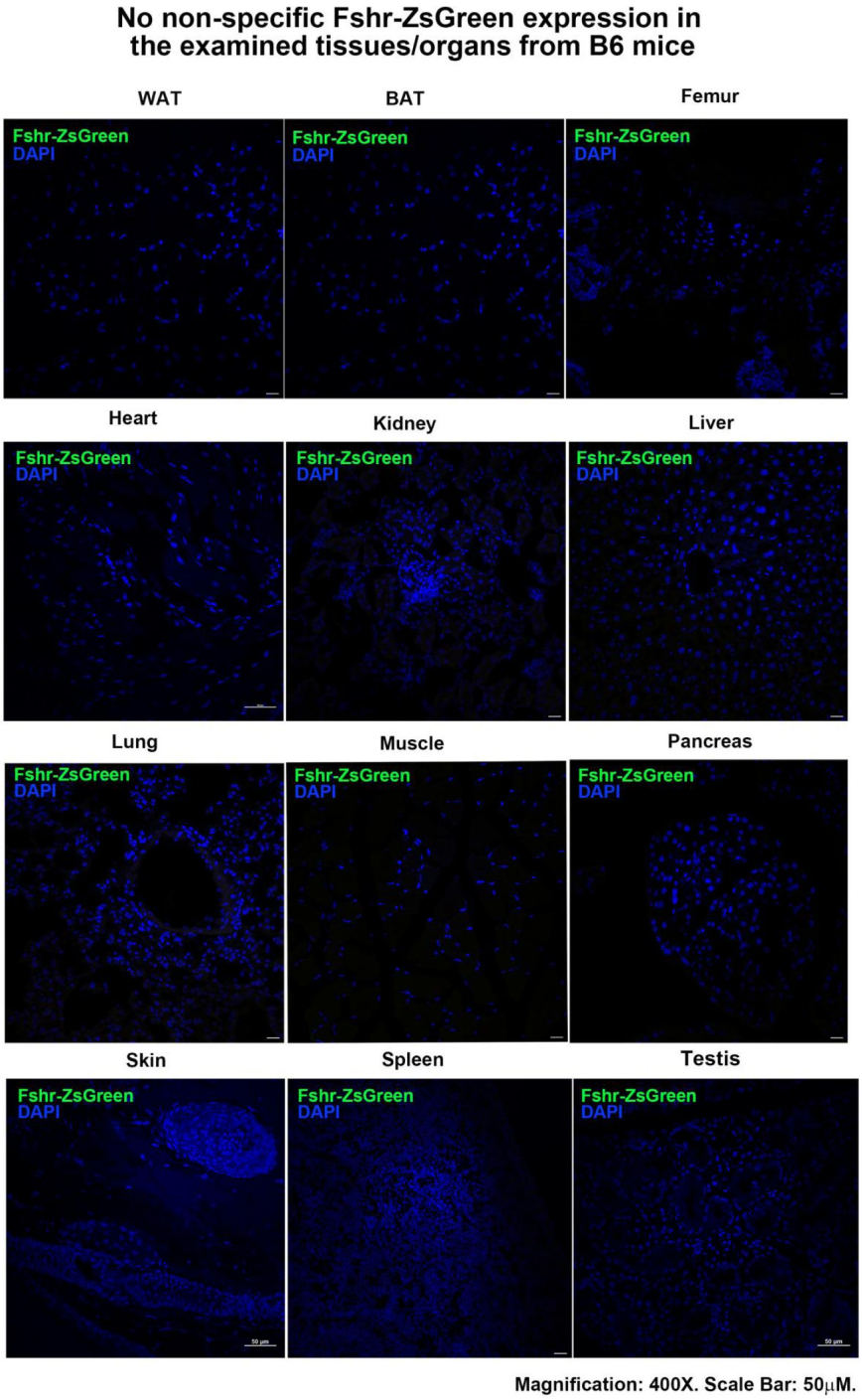

Supplementary Data 2

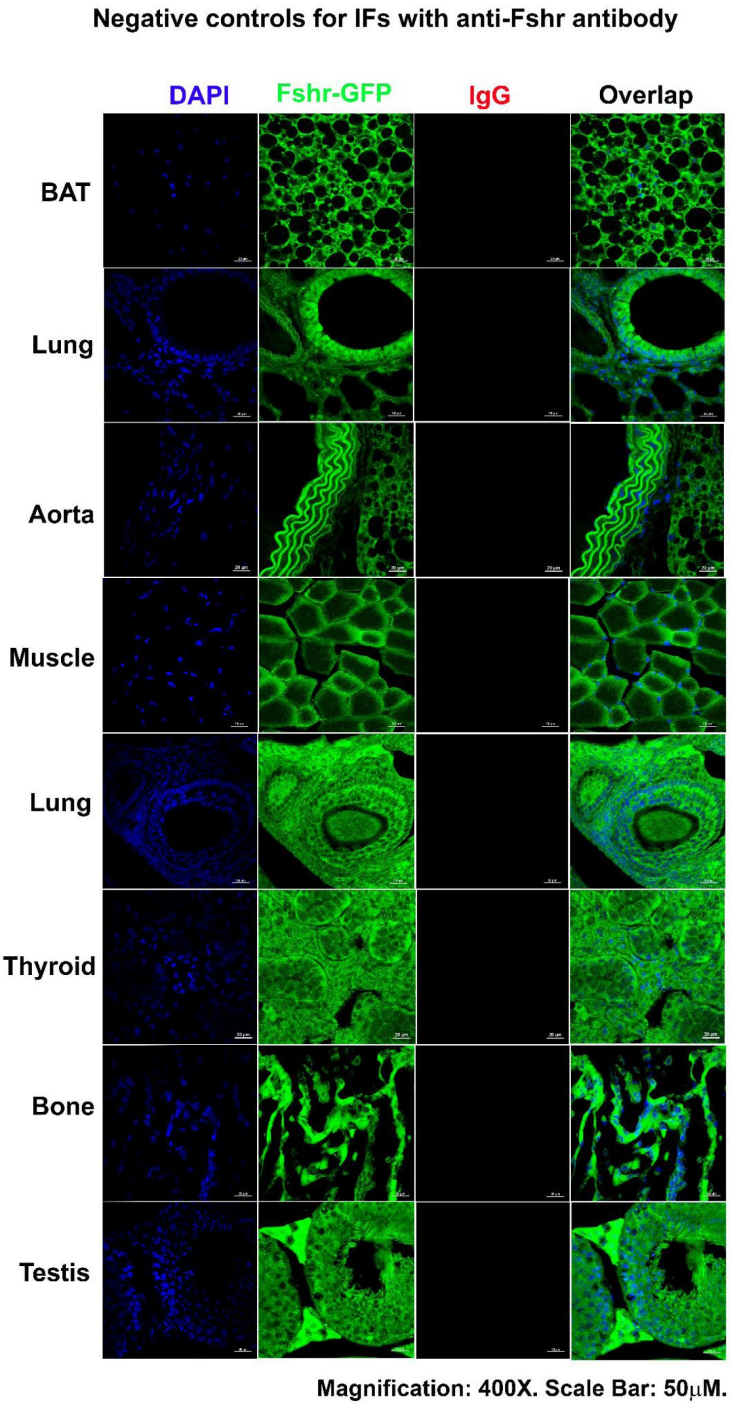

Supplementary Data 3

FSHR expression detected by scRNA-seq from 4 public single cell portals

1. DISCO (immunesinglecell.org/genepage/FSHR)

(1) Testis and ovary

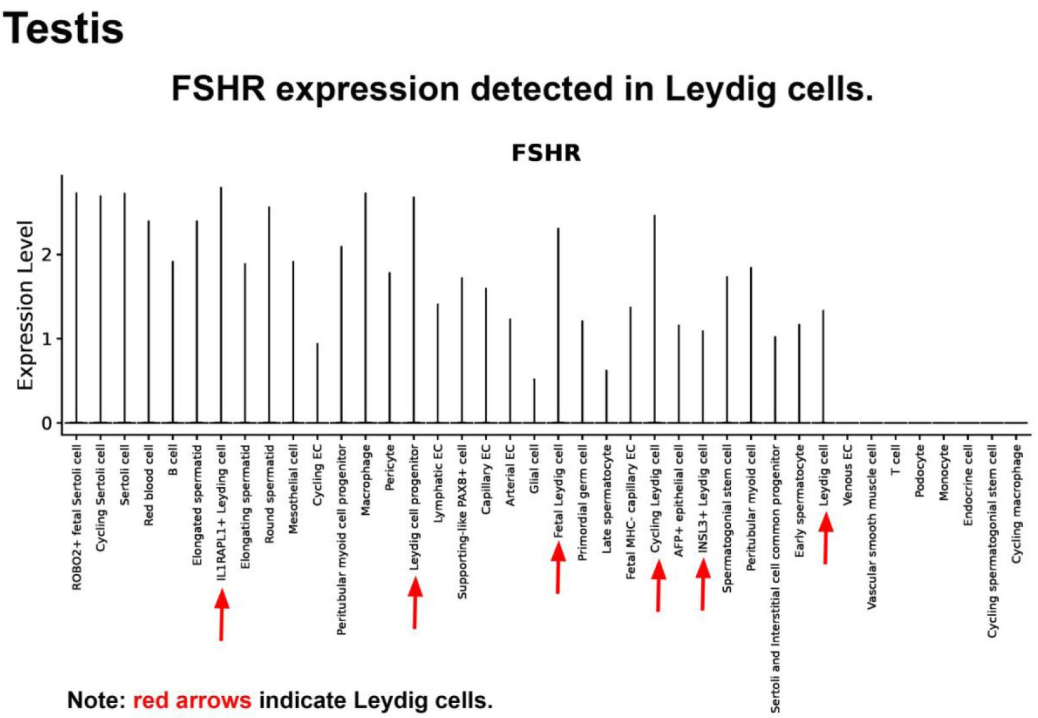

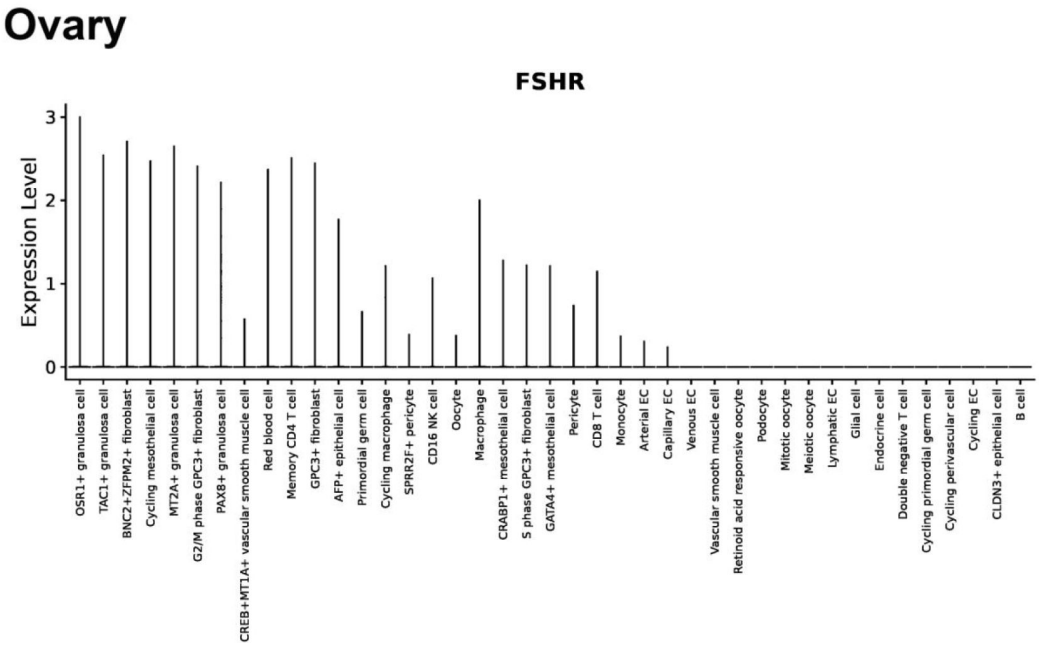

(2) Bone marrow and brain

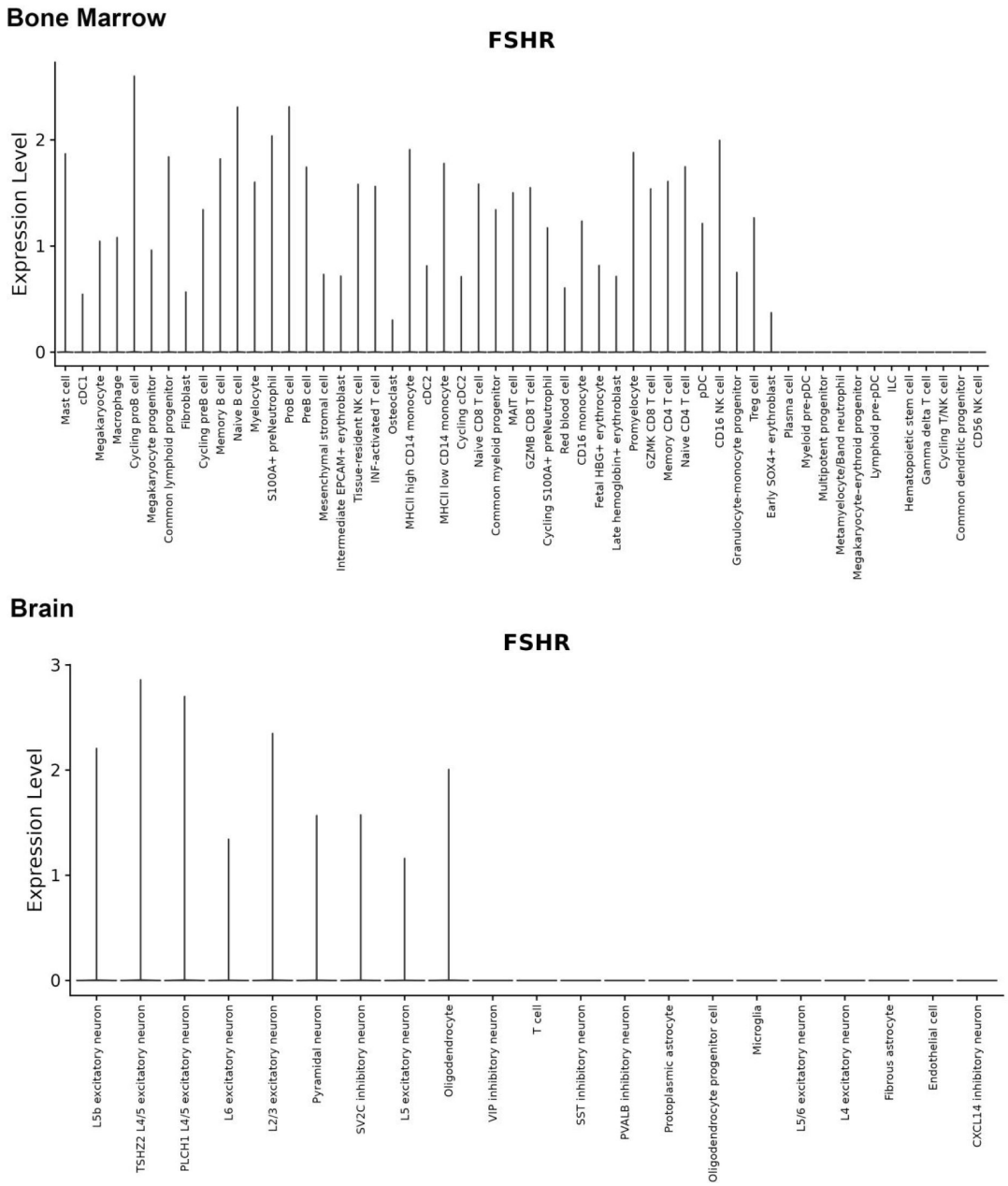

(3) Breast and Heart

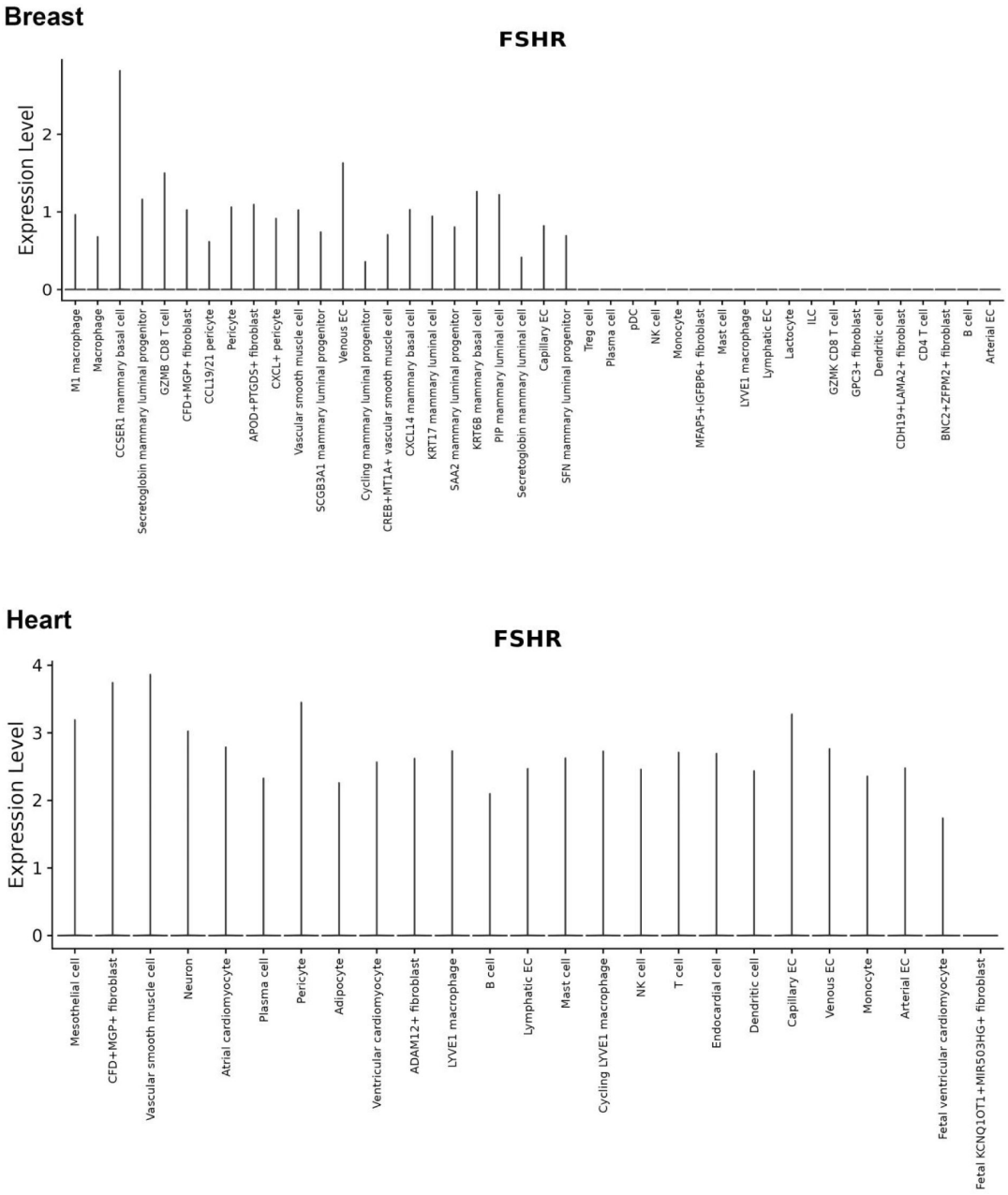

(4) Liver and Lung

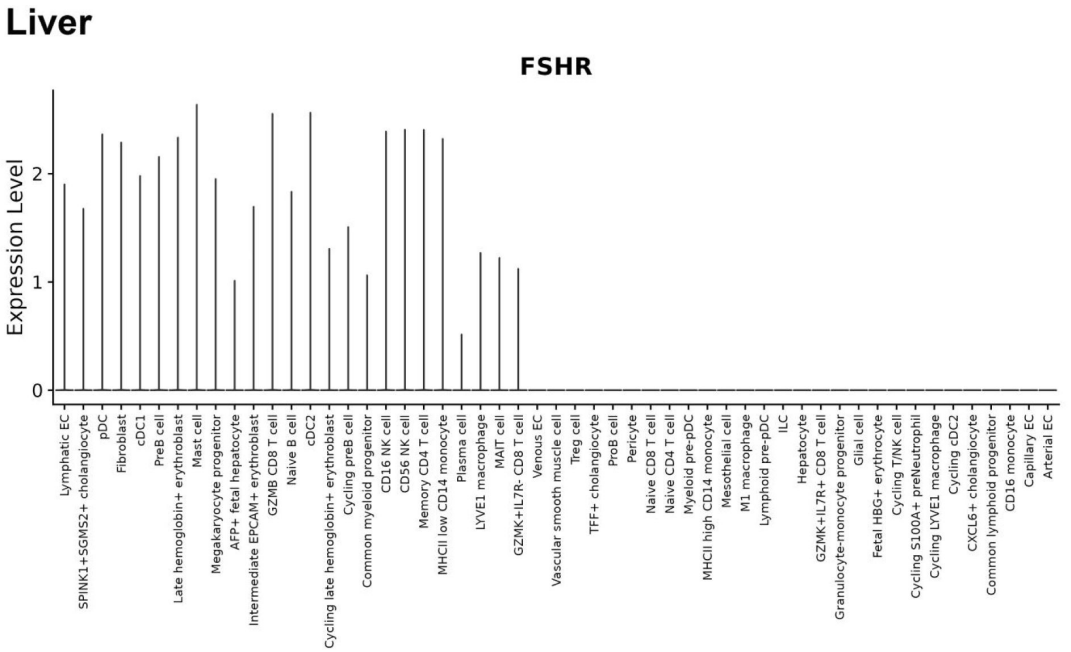

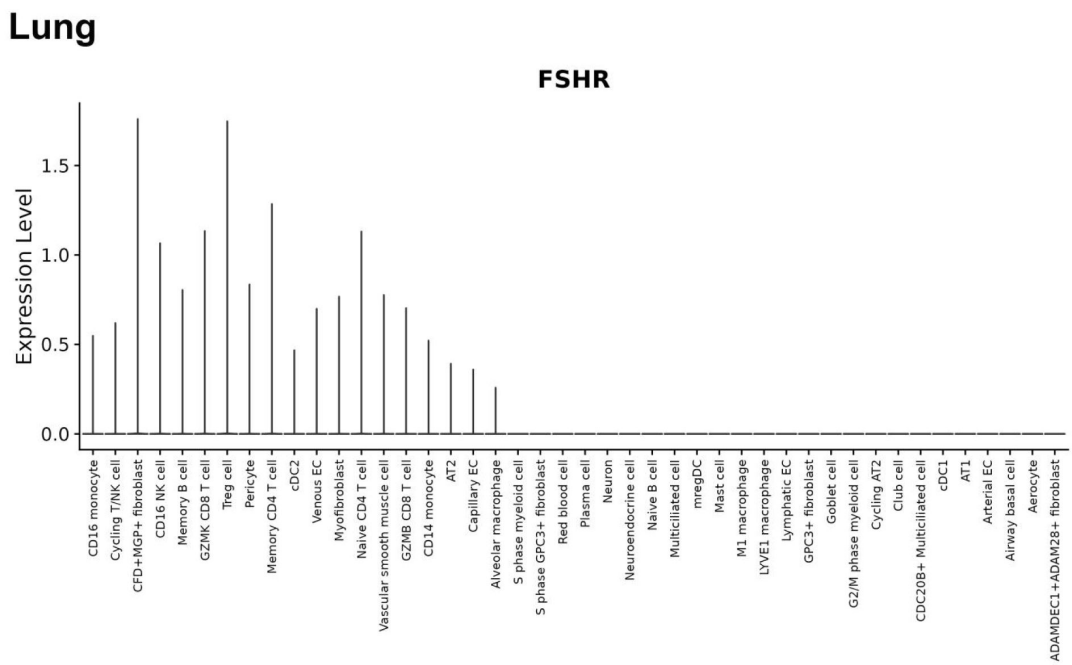

(5) Skeletal muscle and thymus

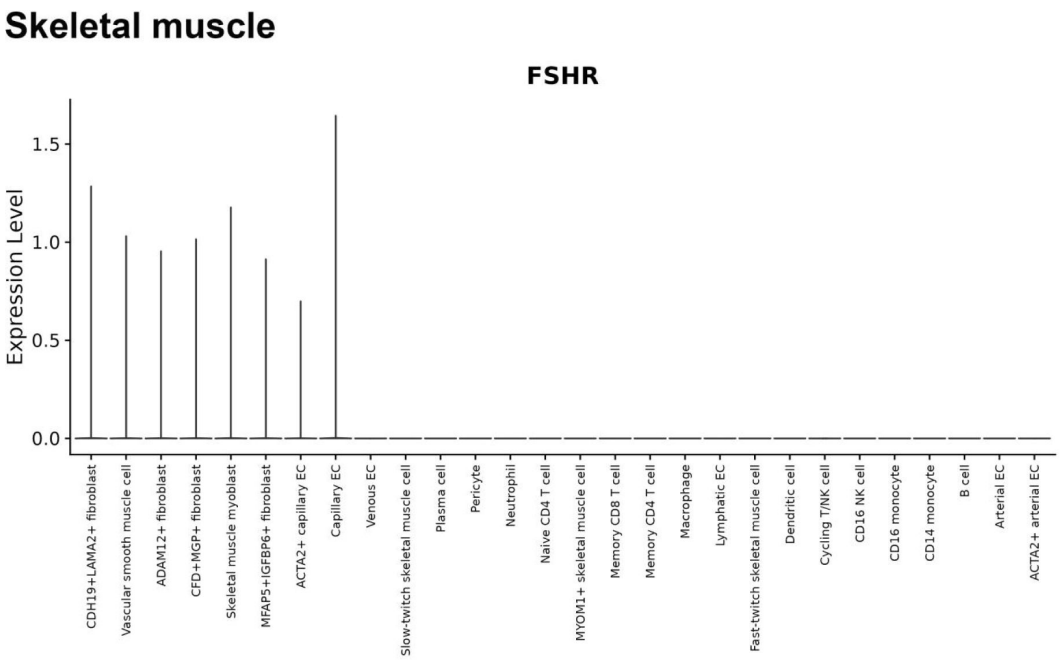

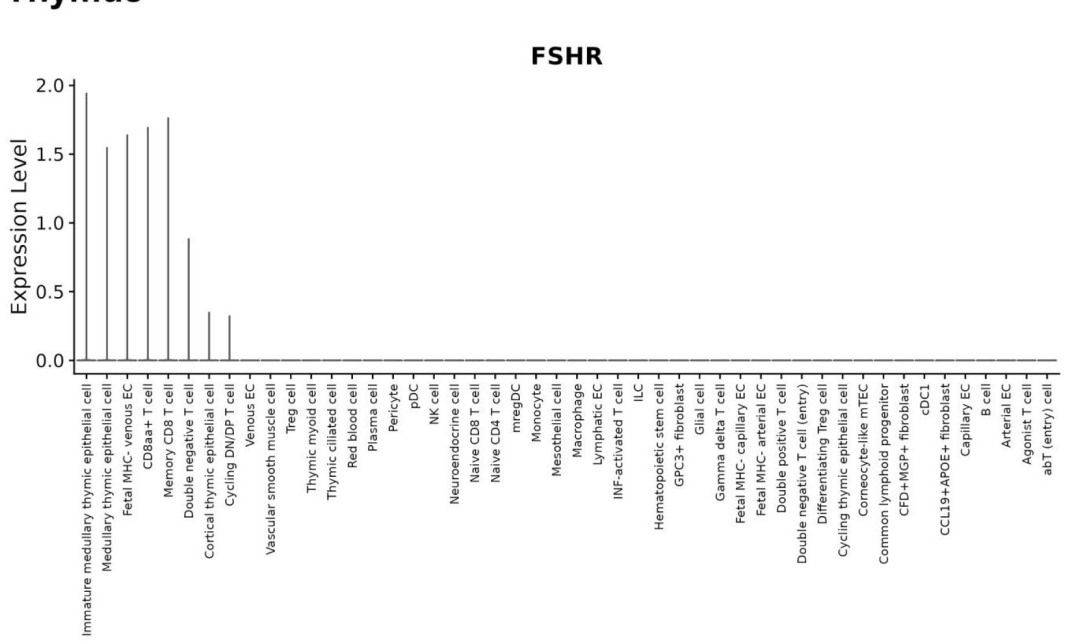

2. GTEx: *https://www.gtexportal.org/home/gene/FSHR#singleCell*

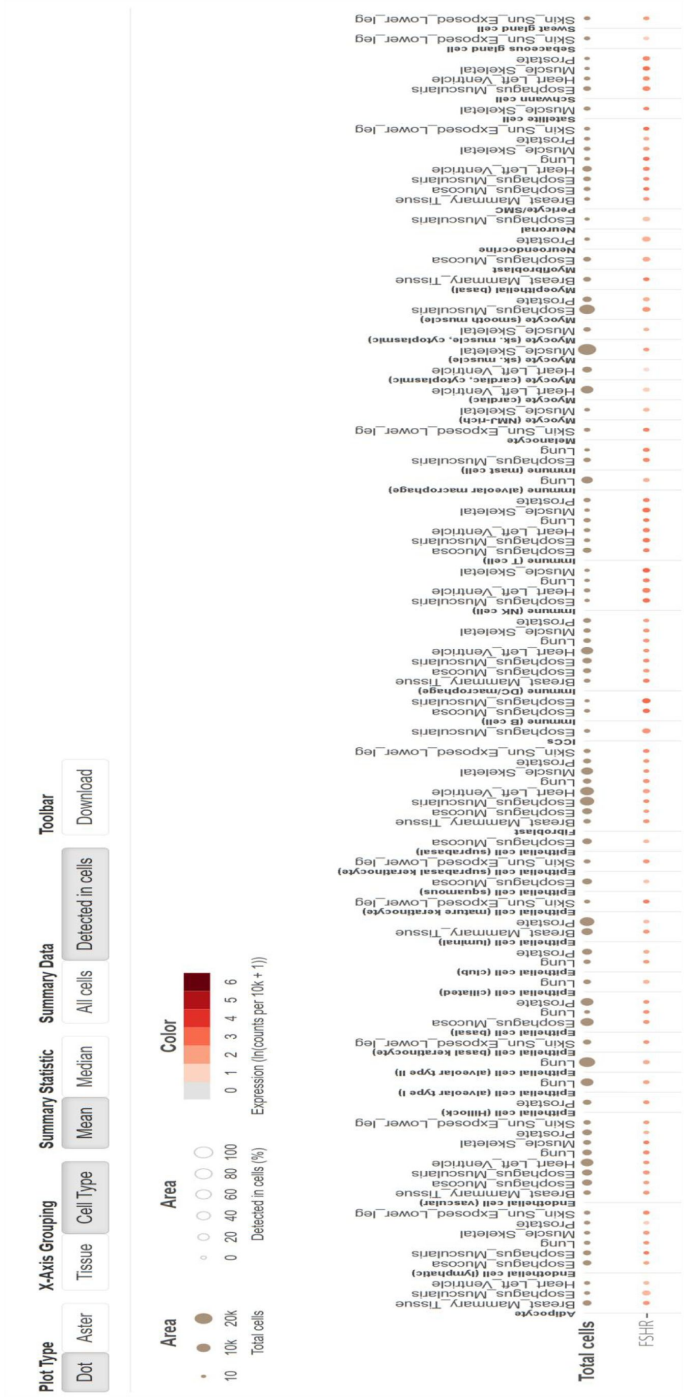

3. BioGPS: (*http://biogps.org/#goto=searchresult*)

(1) Human: ***http://biogps.org/#goto=genereport&id=2492***

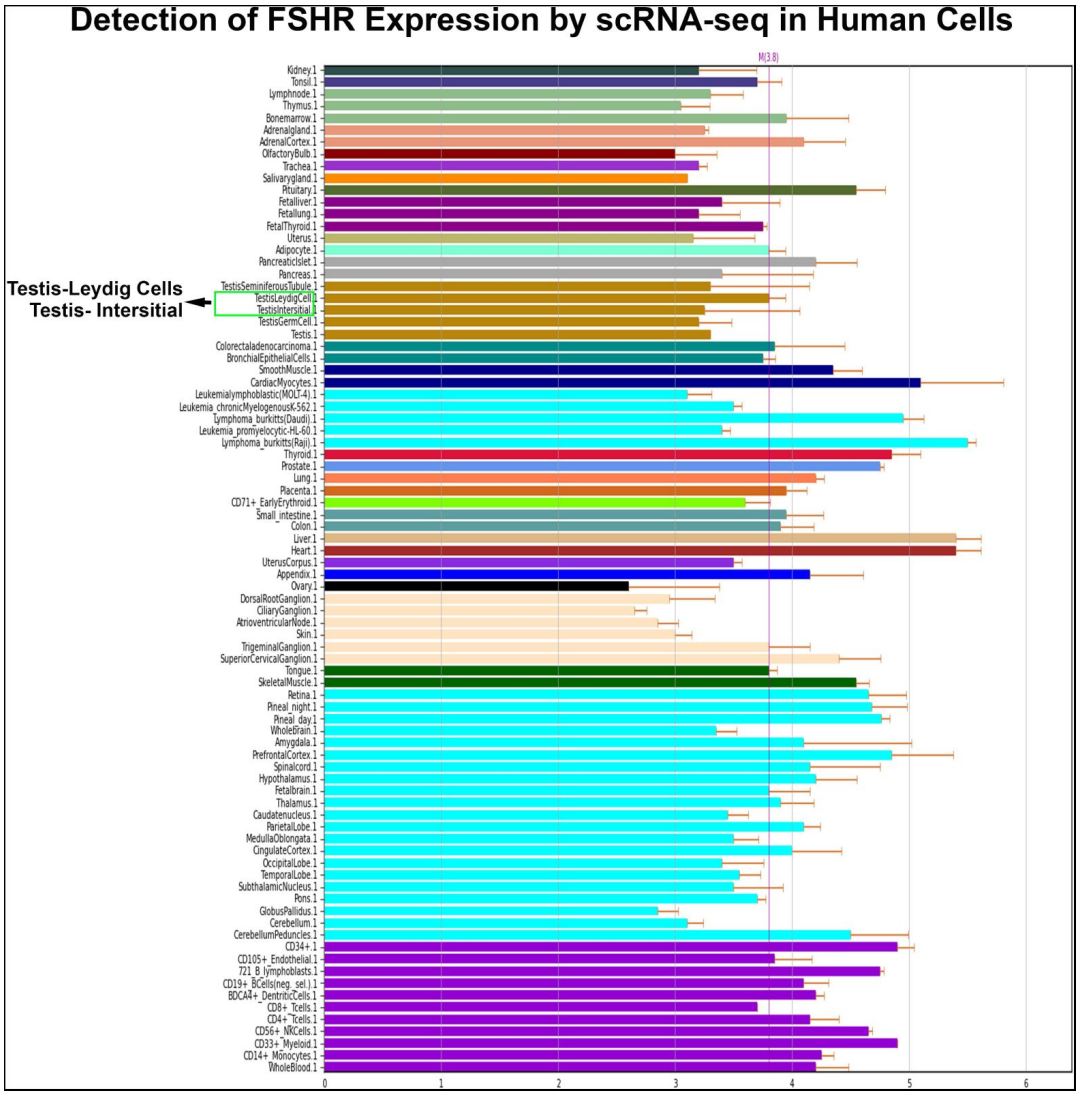

(2) Rat: ***http://ds.biogps.org/?dataset=GSE952&gene=25449***

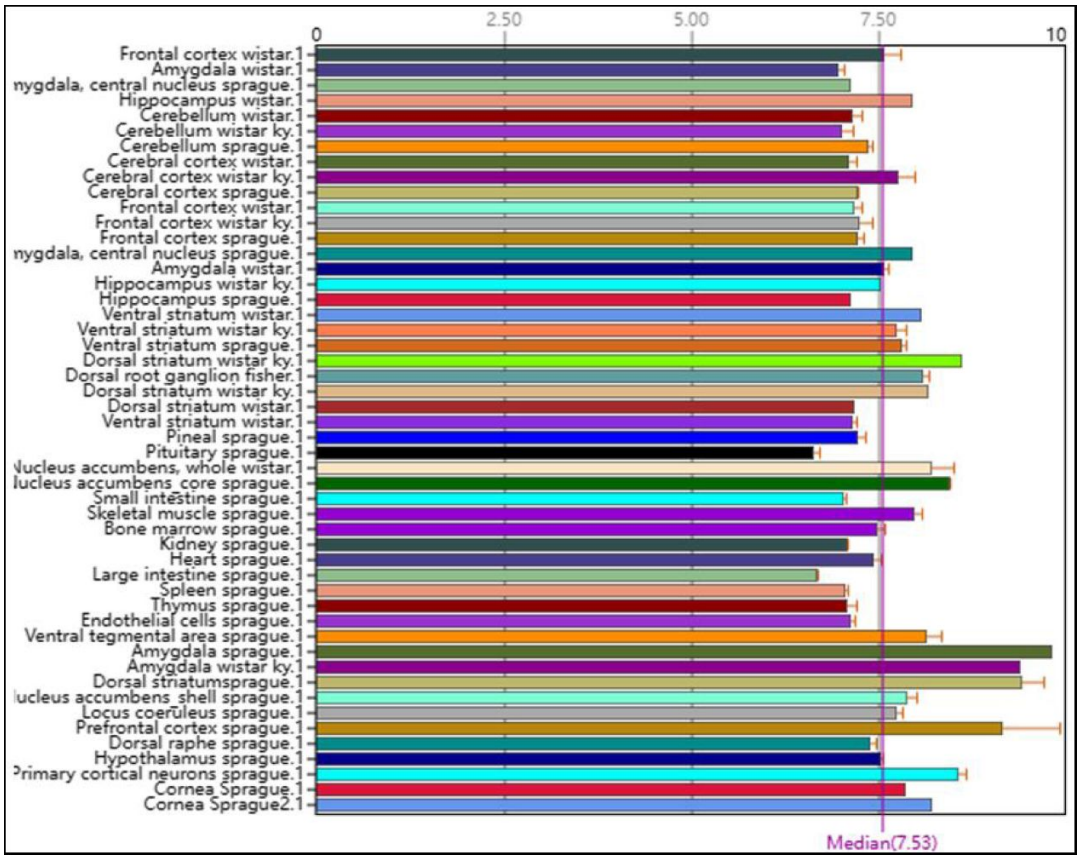

4. Single cell portal: ***https://singlecell.broadinstitute.org/single_cell***

(1) Adipose


An integrated single-cell and single-nucleus RNA-seq white adipose tissue atlas (WATLAS)
We used JOINTLY to cluster and label cells from white adipose tissue (WAT) using 6 scRNA-seq studies (Tabula Sapiens consortium, Emont et al...
294846 Cells
fshr
FSHR expression in WATLAS_clustering.txt by label_l2
Expression
ACKR1+ VEC
BTNL9+ VEC
CCR7+ DC
CD1C+ DC
CD40LG+ CD4+ T cell
CD247+ NK cell
CLEC9A+ DC
CLSTN2+ Adipocyte
CPA3+ Mast
CSF3R+ Monocyte
CTLA4+ CD4+ T cell
CXCL14+ FAP
CYP27A1+ Macrophage
DCN+ Adipocyte
DGAT2+ Adipocyte
Endothelium
FCN1+ Monocyte
GNLY+ CD8+ T cell
HES4+ Monocyte
ICAM1+ FAP
KIT+ ILC
LEC
LPL+ Macrophage
LYVE1+ Macrophage
MS4A1+ B cell
MT1E+ CD8+ T cell
PAMR1+ Mesothelial
Pericyte
PLD4+ pDC
PPARG+ FAP
PPS525+ Adipocyte
RACK1+ Macrophage
Schwann
SELL+ CD4+ T cell
SPAB1+ CD4+ T cell
SLC4A10+ CD8+ T cell
SMC
SOX5+ VEC
XCL1+ NK cell
Human Adipose SVF single cell
Performed Drop-seq on stromal vascular fraction from 10 human subcutaneous adipose tissue samples. Subjects were recruited from planned elec...
38408 Cells
fshr
FSHR expression in Allcell_UMAP by Cluster
cpm
Hs01.Pread1
Hs02.Pread2
Hs03.Pread3
Hs04.Adipocytes
Hs05.Mac/Mono1
Hs06.Mac/Mono2
Hs07.Mac/Mono3
Hs08.Dendritic1
Hs09.Dendritic2
Hs10.Tcell
Hs11.NKcell
Hs12.Mast
Hs13.Bcell1
Hs14.Bcell2
Hs15.Bcell3
Hs16.Vascular
Hs17.LEC
Hs18.Epithelial?
Hs19.Keratinocyte
Hs20.Dividing
Human Adipose SVF single cell
Performed Drop-seq on stromal vascular fraction from 10 human subcutaneous adipose tissue samples. Subjects were recruited from planned elec...
38408 Cells
fshr
FSHR expression in Allcell_UMAP by Cluster
cpm

(2) Brain

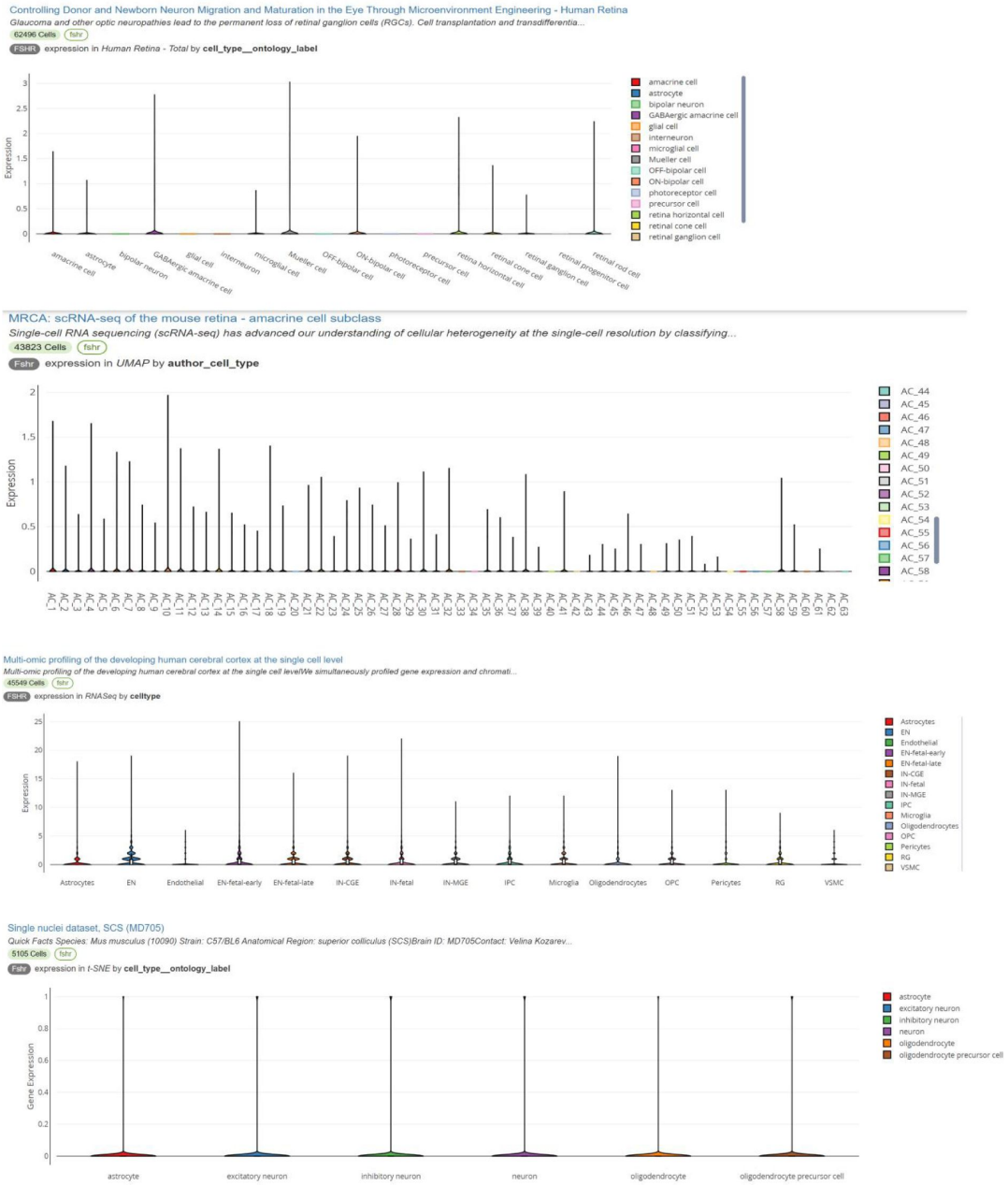
Controlling Donor and Newborn Neuron Migration and Maturation in the Eye Through Microenvironment Engineering - Human Retina
Glaucoma and other optic neuropathies lead to the permanent loss of retinal ganglion cells (RGCs). Cell transplantation and transdifferentia...
62496 Cells
fshr
FSHR expression in Human Retina - Total by cell_type__ontology_label
Expression
amacrine cell
astrocyte
bipolar neuron
GABAergic amacrine cell
glial cell
interneuron
microglial cell
Mueller cell
OFF-bipolar cell
ON-bipolar cell
photoreceptor cell
precursor cell
retina horizontal cell
retinal cone cell
retinal ganglion cell
retinal progenitor cell
retinal rod cell
MRCA: scRNA-seq of the mouse retina - amacrine cell subclass
Single-cell RNA sequencing (scRNA-seq) has advanced our understanding of cellular heterogeneity at the single-cell resolution by classifying...
43823 Cells
fshr
Fshr expression in UMAP by author_cell_type
Expression
Multi-omic profiling of the developing human cerebral cortex at the single cell level
Multi-omic profiling of the developing human cerebral cortex at the single cell levelWe simultaneously profiled gene expression and chromati...
45549 Cells
fshr
FSHR expression in RNASeq by celltype
Expression
Astrocytes
EN
Endothelial
EN-fetal-early
EN-fetal-late
IN-CGE
IN-fetal
IN-MGE
IPC
Microglia
Oligodendrocytes
OPC
Pericytes
RG
VSMC
Single nuclei dataset, SCS (MD705)
Quick Facts Species: Mus musculus (10090) Strain: C57/BL6 Anatomical Region: superior colliculus (SCS)Brain ID: MD705Contact: Velina Kozarev...
5105 Cells
fshr
Fshr expression in t-SNE by cell_type__ontology_label
Gene Expression
astrocyte
excitatory neuron
inhibitory neuron
neuron
oligodendrocyte
oligodendrocyte precursor cell

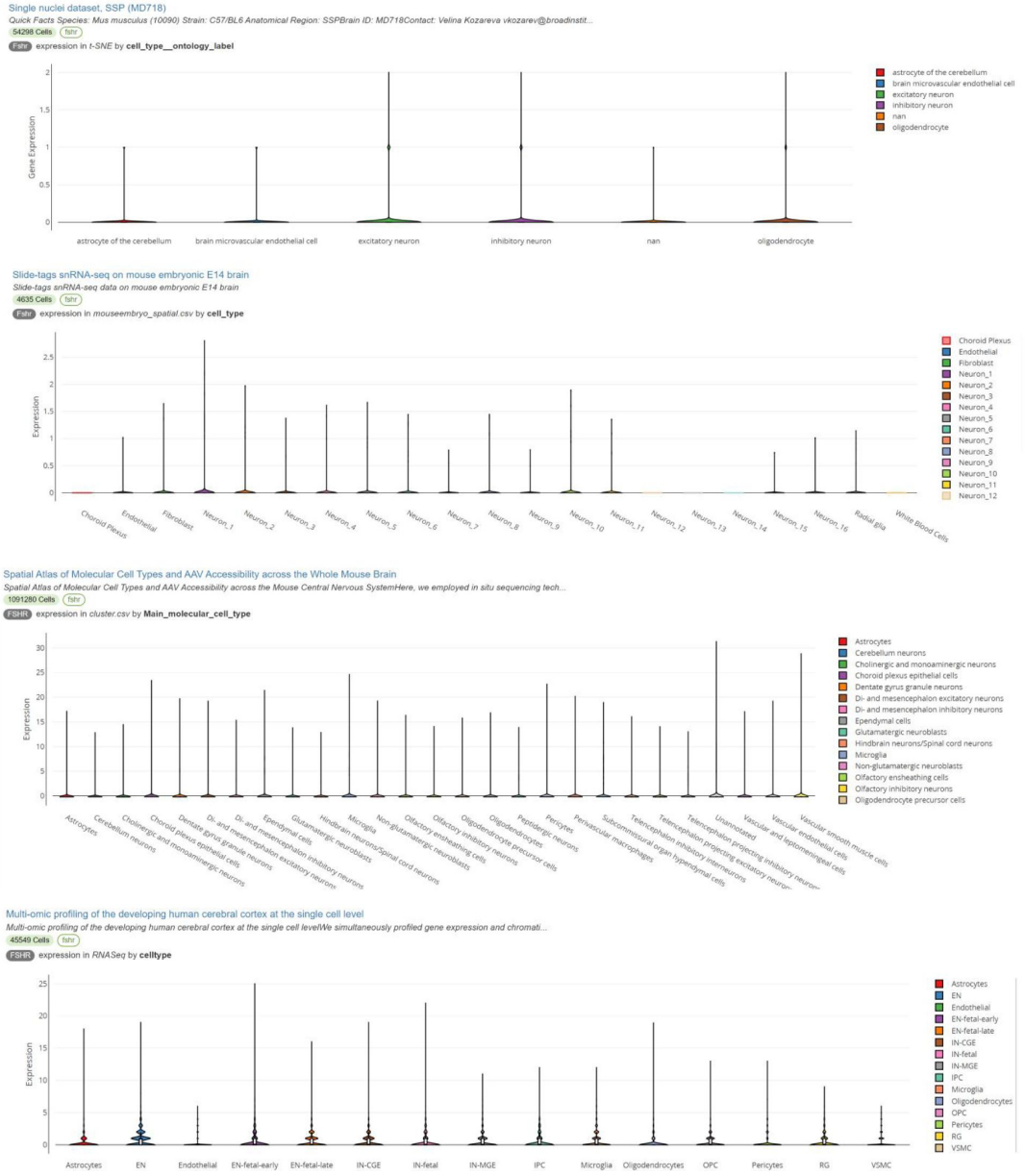
Single nuclei dataset, SSP (MD718)
Quick Facts Species: Mus musculus (10090) Strain: C57/BL6 Anatomical Region: SSPBrain ID: MD718Contact: Velina Kozareva vkozarev@broadinstit...
54298 Cells fshr
Fshr expression in t-SNE by cell_type__ontology_label
Gene Expression
astrocyte of the cerebellum
brain microvascular endothelial cell
excitatory neuron
inhibitory neuron
nan
oligodendrocyte
Slide-tags snRNA-seq on mouse embryonic E14 brain
Slide-tags snRNA-seq data on mouse embryonic E14 brain
4635 Cells fshr
Fshr expression in mouseembryo_spatial.csv by cell_type
Expression
Choroid Plexus
Endothelial
Fibroblast
Neuron_1
Neuron_2
Neuron_3
Neuron_4
Neuron_5
Neuron_6
Neuron_7
Neuron_8
Neuron_9
Neuron_10
Neuron_11
Neuron_12
Neuron_13
Neuron_14
Neuron_15
Neuron_16
Radial glia
White Blood Cells
Spatial Atlas of Molecular Cell Types and AAV Accessibility across the Whole Mouse Brain
Spatial Atlas of Molecular Cell Types and AAV Accessibility across the Mouse Central Nervous SystemHere, we employed in situ sequencing tech...
1091280 Cells fshr
FSHR expression in cluster.csv by Main_molecular_cell_type
Expression
Astrocytes
Cerebellum neurons
Cholinergic and monoaminergic neurons
Choroid plexus epithelial cells
Dentate gyrus granule neurons
Di- and mesencephalon excitatory neurons
Di- and mesencephalon inhibitory neurons
Ependymal cells
Glutamatergic neuroblasts
Hindbrain neurons/Spinal cord neurons
Microglia
Non-glutamatergic neuroblasts
Olfactory ensheathing cells
Olfactory inhibitory neurons
Oligodendrocyte precursor cells
Oligodendrocytes
Peptidergic neurons
Pericytes
Perivascular macrophages
Subcommissural organ hypendymal cells
Telencephalon inhibitory interneurons
Telencephalon projecting excitatory neuron-
Telencephalon projecting inhibitory neuron-
Unannotated
Vascular and leptomeningeal cells
Vascular endothelial cells
Vascular smooth muscle cells
Multi-omic profiling of the developing human cerebral cortex at the single cell level
Multi-omic profiling of the developing human cerebral cortex at the single cell levelWe simultaneously profiled gene expression and chromati...
45549 Cells fshr
FSHR expression in RNASeq by celltype
Expression
Astrocytes
EN
Endothelial
EN-fetal-early
EN-fetal-late
IN-CGE
IN-fetal
IN-MGE
IPC
Microglia
Oligodendrocytes
OPC
Pericytes
RG
VSMC

(3) Kidney

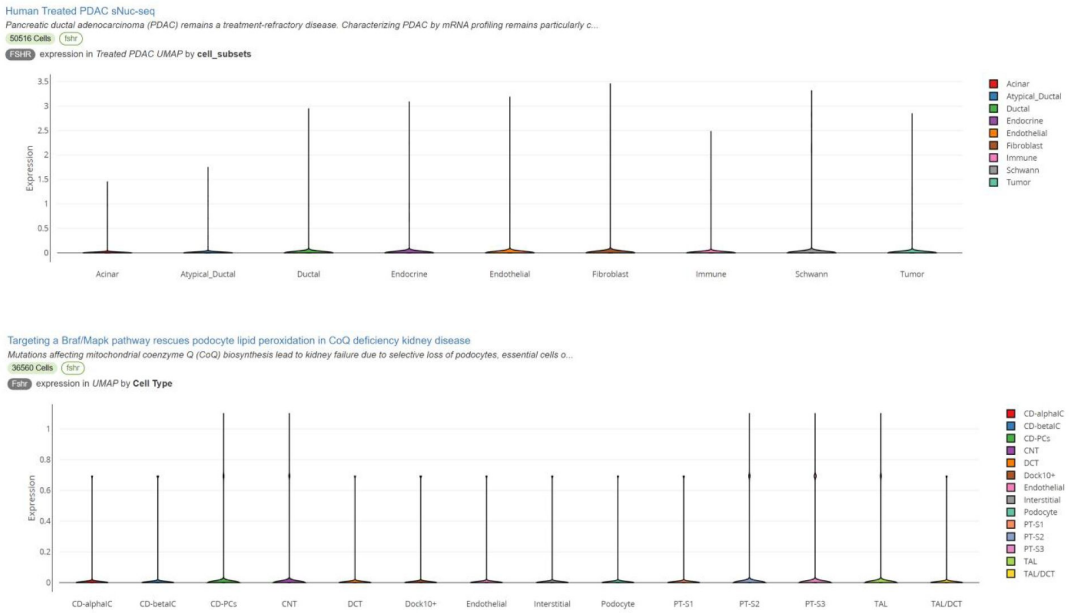

(4) Liver

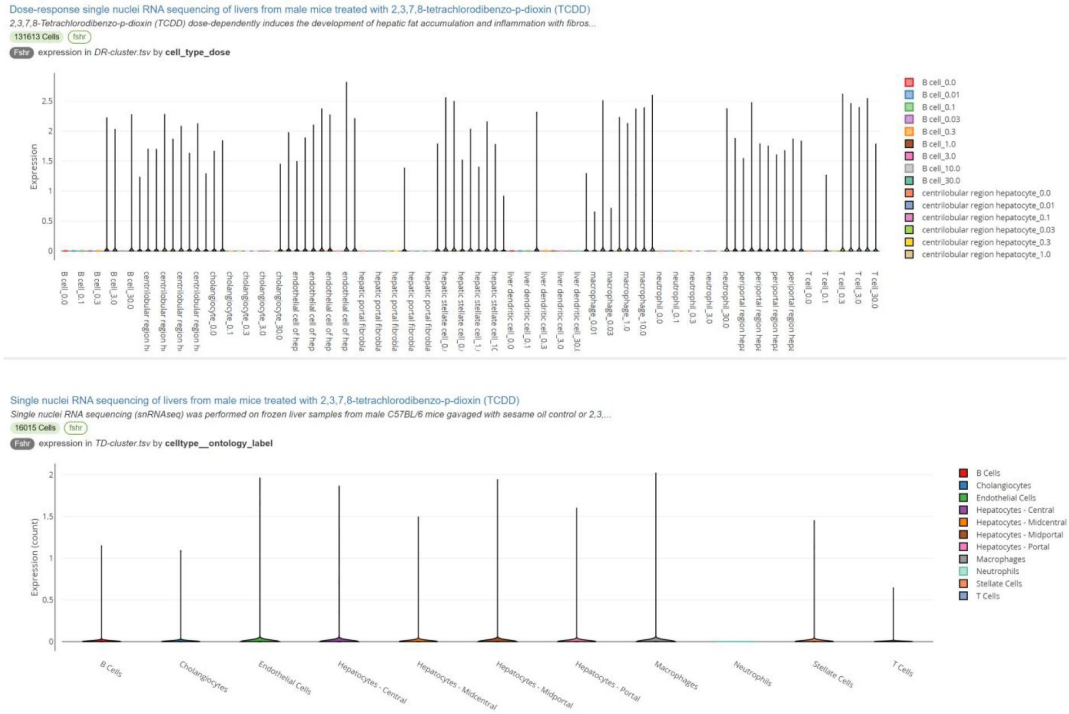

(5) Lung

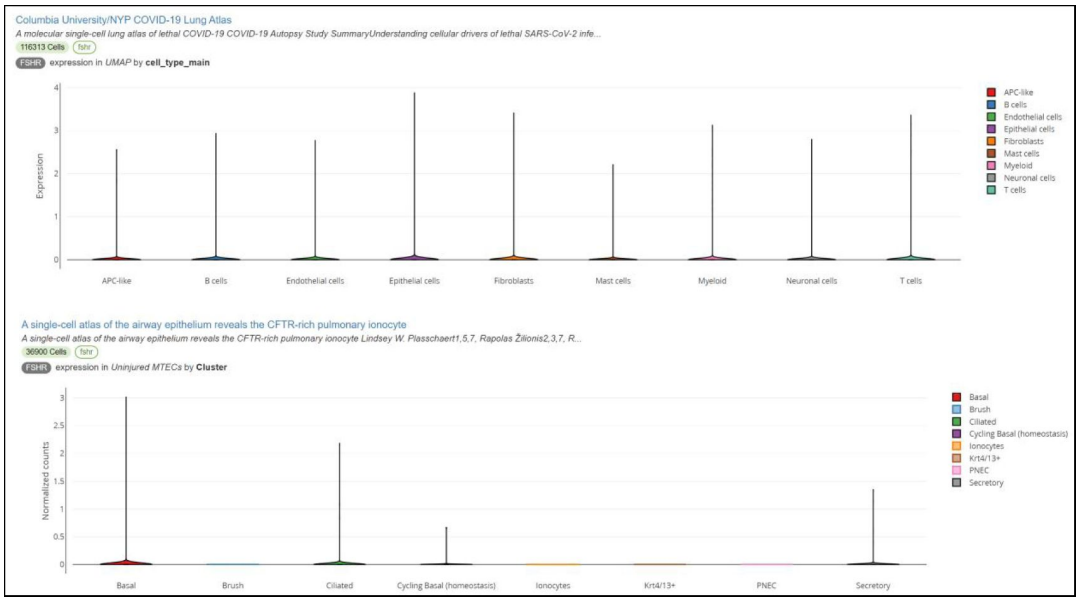

(6) Ovary and Pancreas

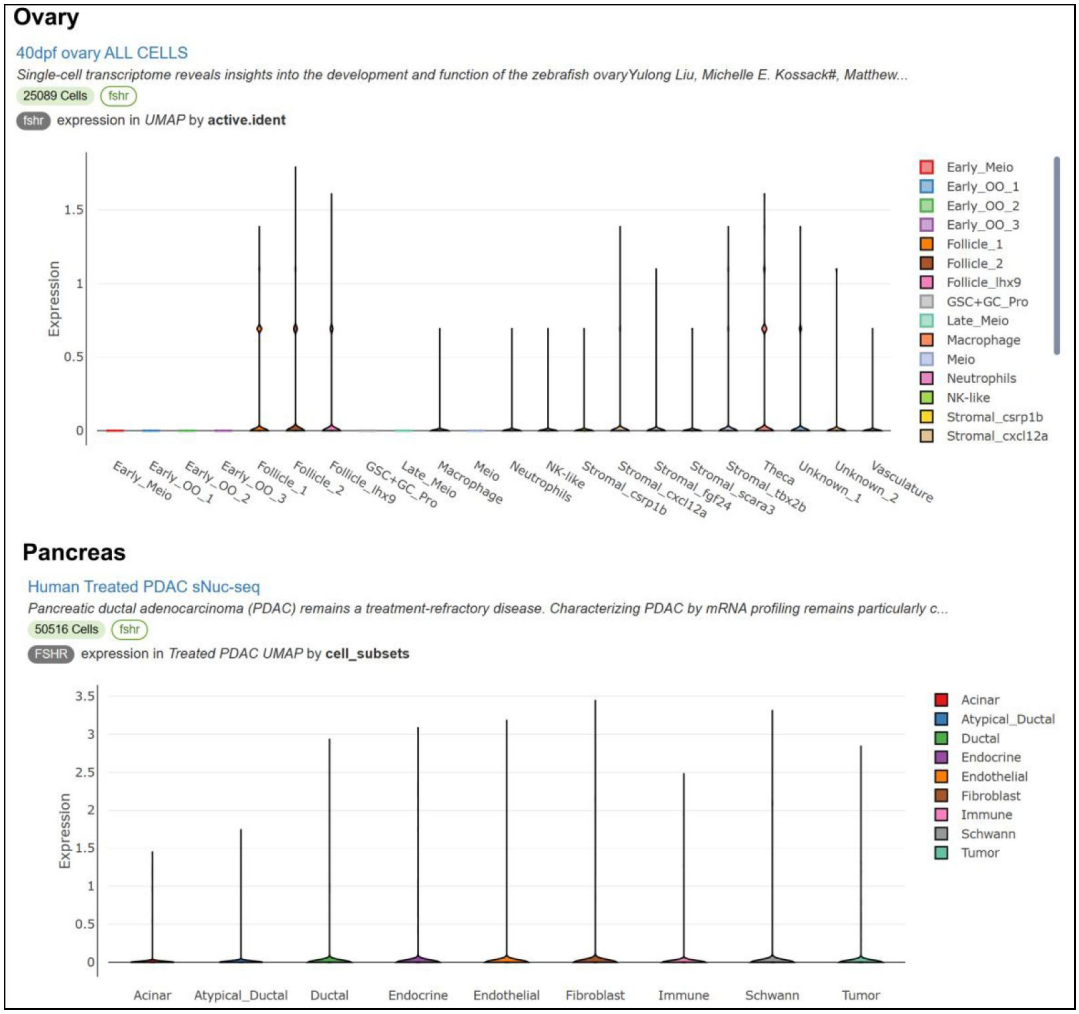

(7) Heart and vascular system

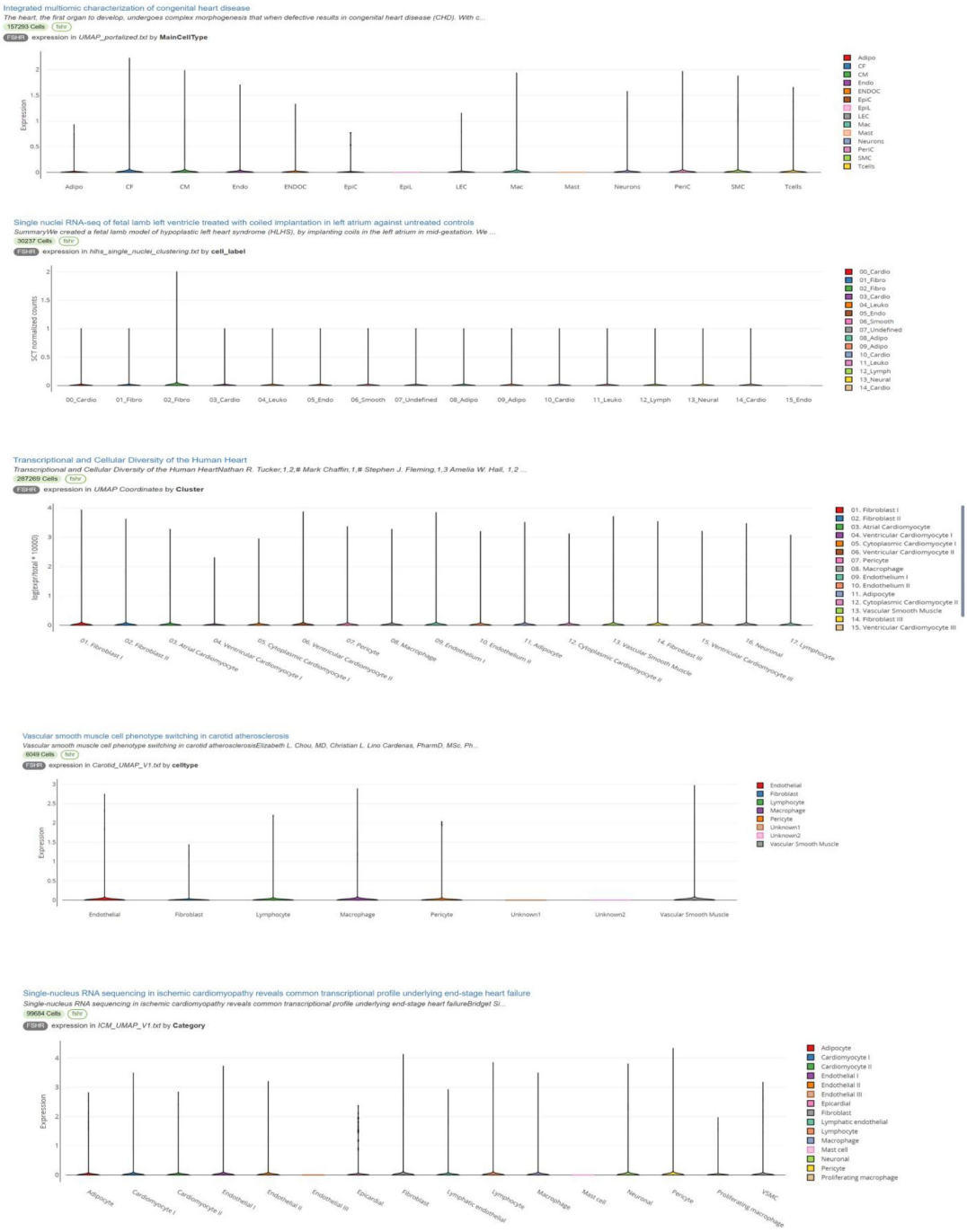

5. FSHR/Fshr expression in Leydig cells of human and mouse males from Chan Zuckerberg CELLxGENE Discover

(1) Human male: *https://cellxgene.cziscience.com/e/535e9336-2d8d-43c3-944d-bcbebe20df8a.cxg/*.

(2) Mouse male: *https://cellxgene.cziscience.com/e/a13bda79-9134-46c9-9ed1-a2858be9aafe.cxg/*.

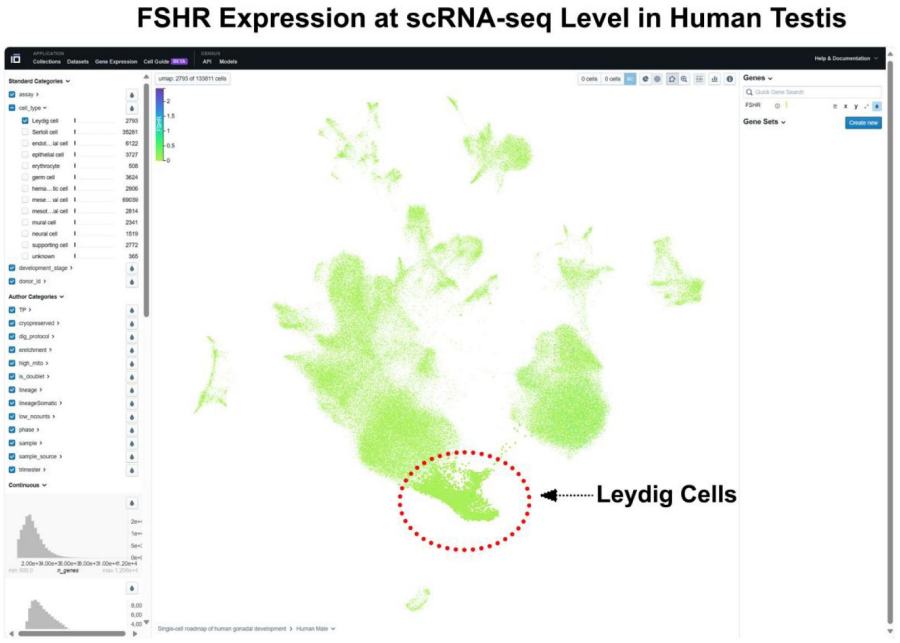

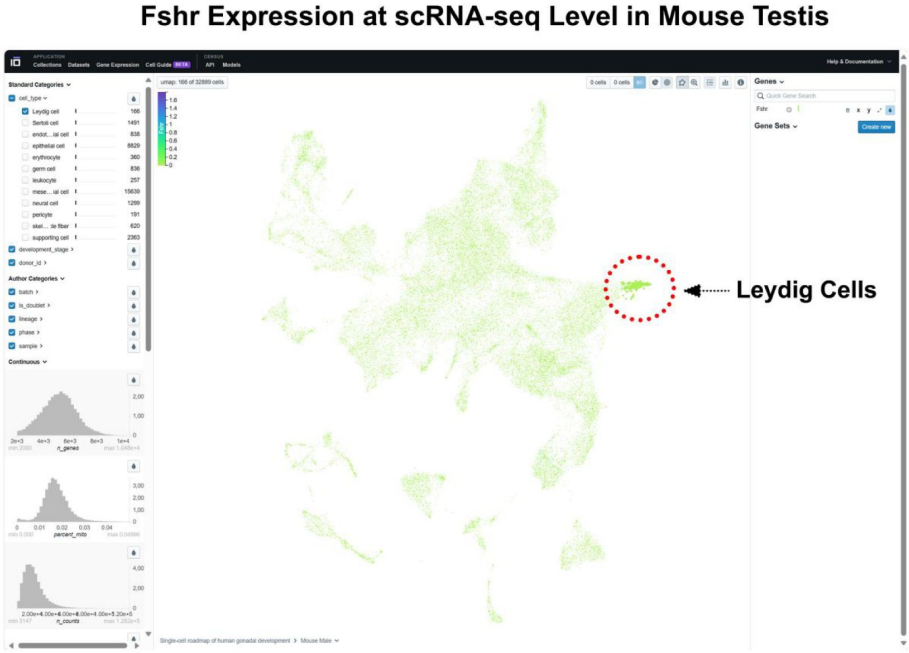

(3) FSHR in human organs: (*https://cellxgene.cziscience.com/gene-expression*)

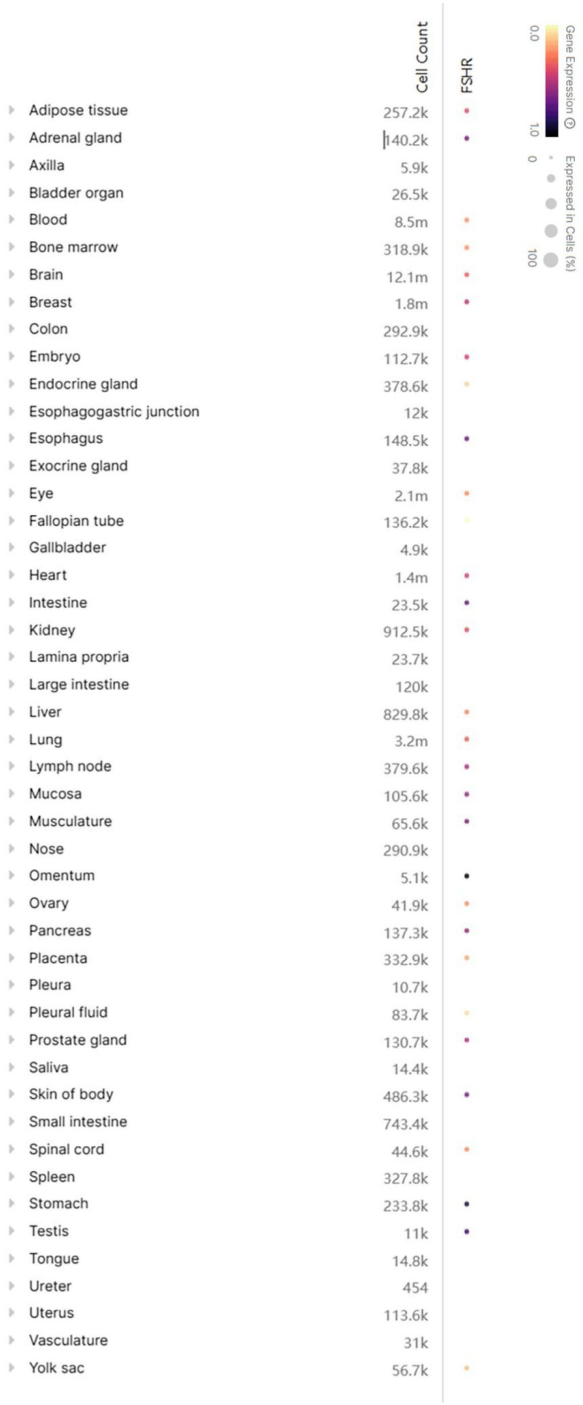
Cell Count
FSHR
Gene Expression
0.0
1.0
0
Expressed in Cells (%)
100
Adipose tissue 257.2k
Adrenal gland 140.2k
Axilla 5.9k
Bladder organ 26.5k
Blood 8.5m
Bone marrow 318.9k
Brain 12.1m
Breast 1.8m
Colon 292.9k
Embryo 112.7k
Endocrine gland 378.6k
Esophagogastric junction 12k
Esophagus 148.5k
Exocrine gland 37.8k
Eye 2.1m
Fallopian tube 136.2k
Gallbladder 4.9k
Heart 1.4m
Intestine 23.5k
Kidney 912.5k
Lamina propria 23.7k
Large intestine 120k
Liver 829.8k
Lung 3.2m
Lymph node 379.6k
Mucosa 105.6k
Musculature 65.6k
Nose 290.9k
Omentum 5.1k
Ovary 41.9k
Pancreas 137.3k
Placenta 332.9k
Pleura 10.7k
Pleural fluid 83.7k
Prostate gland 130.7k
Saliva 14.4k
Skin of body 486.3k
Small intestine 743.4k
Spinal cord 44.6k
Spleen 327.8k
Stomach 233.8k
Testis 11k
Tongue 14.8k
Ureter 454
Uterus 113.6k
Vasculature 31k
Yolk sac 56.7k

References

1. Simoni M, Gromoll J, Nieschlag E (1997) **The follicle-stimulating hormone receptor: biochemistry, molecular biology, physiology, and pathophysiology** *Endocr Rev* **18**:739–73 https://doi.org/10.1210/edrv.18.6.0320

2. Chrusciel M, Ponikwicka-Tyszko D, Wolczynski S, Huhtaniemi I, Rahman NA (2019) **Extragonadal FSHR Expression and Function-Is It Real?** *Front Endocrinol (Lausanne* **10** https://doi.org/10.3389/fendo.2019.00032

3. Asatiani K, Gromoll J, Eckardstein SV, Zitzmann M, Nieschlag E, Simoni M (2002) **Distribution and function of FSH receptor genetic variants in normal men** *Andrologia* **34**:172–6 https://doi.org/10.1046/j.1439-0272.2002.00493.x

4. Minegishi T, Nakamura K, Takakura Y, Ibuki Y, Igarashi M, Minegish T (1991) **Cloning and sequencing of human FSH receptor cDNA** *Biochem Biophys Res Commun* **175**:1125–30 https://doi.org/10.1016/0006-291x(91)91682-3

5. Stilley JAW, Segaloff DL (2018) **Deletion of fetoplacental Fshr inhibits fetal vessel angiogenesis in the mouse placenta** *Mol Cell Endocrinol* **476**:79–83 https://doi.org/10.1016/j.mce.2018.04.011

6. Robinson LJ, Tourkova I, Wang Y, et al. (2010) **FSH-receptor isoforms and FSH- dependent gene transcription in human monocytes and osteoclasts** *Biochem Biophys Res Commun* **394**:12–7 https://doi.org/10.1016/j.bbrc.2010.02.112

7. Stilley JA, Christensen DE, Dahlem KB, et al. (2014) **FSH receptor (FSHR) expression in human extragonadal reproductive tissues and the developing placenta, and the impact of its deletion on pregnancy in mice** *Biol Reprod* **91** https://doi.org/10.1095/biolreprod.114.118562

8. Sacchi S, Sena P, Degli Esposti C, Lui J, La Marca A (2018) **Evidence for expression and functionality of FSH and LH/hCG receptors in human endometrium** *J Assist Reprod Genet* **35**:1703–1712 https://doi.org/10.1007/s10815-018-1248-8

9. Papadimitriou K, Kountourakis P, Kottorou AE, et al. (2016) **Follicle-Stimulating Hormone Receptor (FSHR): A Promising Tool in Oncology?** *Mol Diagn Ther* **20**:523–530 https://doi.org/10.1007/s40291-016-0218-z

10. Bhartiya D, Patel H (2021) **An overview of FSH-FSHR biology and explaining the existing conundrums** *J Ovarian Res* **14** https://doi.org/10.1186/s13048-021-00880-3

11. Sun L, Peng Y, Sharrow AC, et al. (2006) **FSH directly regulates bone mass** *Cell* **125**:247–60 https://doi.org/10.1016/j.cell.2006.01.051

12. Liu P, Ji Y, Yuen T, et al. (2017) **Blocking FSH induces thermogenic adipose tissue and reduces body fat** *Nature* **546**:107–112 https://doi.org/10.1038/nature22342

13. Xiong J, Kang SS, Wang Z, et al. (2022) **FSH blockade improves cognition in mice with Alzheimer's disease** *Nature* **603**:470–476 https://doi.org/10.1038/s41586-022-04463-0

14. Ghinea N (2018) **Vascular Endothelial FSH Receptor, a Target of Interest for Cancer Therapy** *Endocrinology* **159**:3268–3274 https://doi.org/10.1210/en.2018-00466

15. Kumar TR (2014) **Extragonadal FSH receptor: is it real?** *Biol Reprod* **91** https://doi.org/10.1095/biolreprod.114.124222

16. Tedjawirja VN, Hooijer GKJ, Savci-Heijink CD, Kovac K, Balm R, de Waard V (2023) **Inadequate detection of the FSHR complicates future research on extragonadal FSHR localization** *Front Endocrinol (Lausanne* **14** https://doi.org/10.3389/fendo.2023.1095031

17. Kumar TR (2018) **Extragonadal Actions of FSH: A Critical Need for Novel Genetic Models** *Endocrinology* **159**:2–8 https://doi.org/10.1210/en.2017-03118

18. Chudakov DM, Lukyanov S, Lukyanov KA (2005) **Fluorescent proteins as a toolkit for in vivo imaging** *Trends Biotechnol* **23**:605–13 https://doi.org/10.1016/j.tibtech.2005.10.005

19. Cheng L, Fu J, Tsukamoto A, Hawley RG (1996) **Use of green fluorescent protein variants to monitor gene transfer and expression in mammalian cells** *Nat Biotechnol* **14**:606–9 https://doi.org/10.1038/nbt0596-606

20. Huhtaniemi IT, Eskola V, Pakarinen P, Matikainen T, Sprengel R (1992) **The murine luteinizing hormone and follicle-stimulating hormone receptor genes: transcription initiation sites, putative promoter sequences and promoter activity** *Mol Cell Endocrinol* **88**:55–66 https://doi.org/10.1016/0303-7207(92)90009-u

21. Chai W, Hao W, Liu J, et al. (2023) **Visualizing Cathepsin K-Cre Expression at the Single- Cell Level with GFP Reporters** *JBMR Plus* **7** https://doi.org/10.1002/jbm4.10706

22. Young AP, Jackson DJ, Wyeth RC (2020) **A technical review and guide to RNA fluorescence in situ hybridization** *PeerJ* **8** https://doi.org/10.7717/peerj.8806

23. Zhu X, Ricci-Tam C, Hager ER, Sgro AE (2023) **Self-cleaving peptides for expression of multiple genes in Dictyostelium discoideum** *PLoS One* **18** https://doi.org/10.1371/journal.pone.0281211

24. Trichas G, Begbie J, Srinivas S (2008) **Use of the viral 2A peptide for bicistronic expression in transgenic mice** *BMC Biol. Sep* **6** https://doi.org/10.1186/1741-7007-6-40

25. Luke GA, Ryan MD (2018) **Using the 2A Protein Coexpression System: Multicistronic 2A Vectors Expressing Gene(s) of Interest and Reporter Proteins** *Methods Mol Biol* :31–48 https://doi.org/10.1007/978-1-4939-7724-6_3

26. Miyauchi H, Ohta H, Nagaoka S, et al. (2017) **Bone morphogenetic protein and retinoic acid synergistically specify female germ-cell fate in mice** *EMBO J* **36**:3100–3119 https://doi.org/10.15252/embj.201796875

27. Heinrich A, Potter SJ, Guo L, Ratner N, DeFalco T (2020) **Distinct Roles for Rac1 in Sertoli Cell Function during Testicular Development and Spermatogenesis** *Cell Rep* **31** https://doi.org/10.1016/j.celrep.2020.03.077

28. Dai XN, Liu S, Shao L, et al. (2014) **Expression of the SET protein in testes of mice at different developmental stages** *Asian J Androl. Sep* **16**:689–93 https://doi.org/10.4103/1008-682X.129937

29. Levsky JM, Singer RH (2003) **Fluorescence in situ hybridization: past, present and future** *J Cell Sci* **116**:2833–8 https://doi.org/10.1242/jcs.00633

30. Mather JP (1980) **Establishment and characterization of two distinct mouse testicular epithelial cell lines** *Biol Reprod* **23**:243–52 https://doi.org/10.1095/biolreprod23.1.243

31. Karsenty G (2017) **Update on the Biology of Osteocalcin** *Endocr Pract* **23**:1270–1274 https://doi.org/10.4158/EP171966.RA

32. Lindunger A, MacKay CA, Ek-Rylander B, Andersson G, Marks SC (1990) **Histochemistry and biochemistry of tartrate-resistant acid phosphatase (TRAP) and tartrate-resistant acid adenosine triphosphatase (TrATPase) in bone, bone marrow and spleen: implications for osteoclast ontogeny** *Bone Miner* **10**:109–19 https://doi.org/10.1016/0169-6009(90)90086-u

33. Chan CK, Seo EY, Chen JY, et al. (2015) **Identification and specification of the mouse skeletal stem cell** *Cell* **160**:285–98 https://doi.org/10.1016/j.cell.2014.12.002

34. Kuroda R, Matsumoto T, Kawakami Y, Fukui T, Mifune Y, Kurosaka M (2014) **Clinical impact of circulating CD34-positive cells on bone regeneration and healing** *Tissue Eng Part B Rev* **20**:190–9 https://doi.org/10.1089/ten.TEB.2013.0511

35. Handgretinger R, Gordon PR, Leimig T, et al. (2003) **Biology and plasticity of CD133+ hematopoietic stem cells** *Ann N Y Acad Sci* **996**:141–51 https://doi.org/10.1111/j.1749-6632.2003.tb03242.x

36. Handgretinger R, Kuci S (2013) **CD133-Positive Hematopoietic Stem Cells: From Biology to Medicine** *Adv Exp Med Biol* **777**:99–111 https://doi.org/10.1007/978-1-4614-5894-4_7

37. Pozzobon M, Piccoli M, Ditadi A, et al. (2009) **Mesenchymal stromal cells can be derived from bone marrow CD133+ cells: implications for therapy** *Stem Cells Dev* **18**:497–510 https://doi.org/10.1089/scd.2008.0003

38. Guo X, Sunil C, Adeyanju O, et al. (2022) **PD-L1 mediates lung fibroblast to myofibroblast transition through Smad3 and beta-catenin signaling pathways** *Sci Rep* **12** https://doi.org/10.1038/s41598-022-07044-3

39. Wang S, Zhu Q, Liang G, et al. (2021) **Cannabinoid receptor 1 signaling in hepatocytes and stellate cells does not contribute to NAFLD** *J Clin Invest* **131** https://doi.org/10.1172/JCI152242

40. Ismail JA, Poppa V, Kemper LE, et al. (2003) **Immunohistologic labeling of murine endothelium** *Cardiovasc Pathol. Mar* **12**:82–90 https://doi.org/10.1016/s1054-8807(02)00166-7

41. Simms BA, Zamponi GW (2014) **Neuronal voltage-gated calcium channels: structure, function, and dysfunction** *Neuron* **82**:24–45 https://doi.org/10.1016/j.neuron.2014.03.016

42. Springer TA (1994) **Traffic signals for lymphocyte recirculation and leukocyte emigration: the multistep paradigm** *Cell* **76**:301–14 https://doi.org/10.1016/0092-8674(94)90337-9

43. Chatenoud L, Bluestone JA (2007) **CD3-specific antibodies: a portal to the treatment of autoimmunity** *Nat Rev Immunol* **7**:622–32 https://doi.org/10.1038/nri2134

44. Bai H, Liu L, An K, et al. (2020) **CRISPR/Cas9-mediated precise genome modification by a long ssDNA template in zebrafish** *BMC Genomics* **21** https://doi.org/10.1186/s12864-020-6493-4

45. Matz MV, Fradkov AF, Labas YA, et al. (1999) **Fluorescent proteins from nonbioluminescent Anthozoa species** *Nat Biotechnol* **17**:969–73 https://doi.org/10.1038/13657

46. Zhu J, Jankovic D, Oler AJ, et al. (2012) **The transcription factor T-bet is induced by multiple pathways and prevents an endogenous Th2 cell program during Th1 cell responses** *Immunity* **37**:660–73 https://doi.org/10.1016/j.immuni.2012.09.007

47. Pippin JW, Sparks MA, Glenn ST, et al. (2013) **Cells of renin lineage are progenitors of podocytes and parietal epithelial cells in experimental glomerular disease** *Am J Pathol* **183**:542–57 https://doi.org/10.1016/j.ajpath.2013.04.024

48. Pippin JW, Glenn ST, Krofft RD, et al. (2014) **Cells of renin lineage take on a podocyte phenotype in aging nephropathy** *Am J Physiol Renal Physiol* **306**:F1198–209 https://doi.org/10.1152/ajprenal.00699.2013

49. Buller NV, Rosekrans SL, Metcalfe C, et al. (2015) **Stromal Indian hedgehog signaling is required for intestinal adenoma formation in mice** *Gastroenterology* **148**:170–180 https://doi.org/10.1053/j.gastro.2014.10.006

50. Dewas C, Chen X, Honda T, et al. (2015) **TSLP expression: analysis with a ZsGreen TSLP reporter mouse** *J Immunol* **194**:1372–80 https://doi.org/10.4049/jimmunol.1400519

51. Nazareth L, Lineburg KE, Chuah MI, et al. (2015) **Olfactory ensheathing cells are the main phagocytic cells that remove axon debris during early development of the olfactory system** *J Comp Neurol* **523**:479–94 https://doi.org/10.1002/cne.23694

52. Xiao L, McCann JV, Dudley AC (2015) **Isolation and Culture Expansion of Tumor-specific Endothelial Cells** *J Vis Exp* **105** https://doi.org/10.3791/53072

53. Kaverina NV, Eng DG, Schneider RR, Pippin JW, Shankland SJ (2016) **Partial podocyte replenishment in experimental FSGS derives from nonpodocyte sources** *Am J Physiol Renal Physiol* **310**:F1397–413 https://doi.org/10.1152/ajprenal.00369.2015

54. Saito K, He Y, Yan X, et al. (2016) **Visualizing estrogen receptor-alpha-expressing neurons using a new ERalpha-ZsGreen reporter mouse line** *Metabolism* **65**:522–32 https://doi.org/10.1016/j.metabol.2015.12.011

55. Fougere M, van der Zouwen CI, Boutin J, Ryczko D (2021) **Heterogeneous expression of dopaminergic markers and Vglut2 in mouse mesodiencephalic dopaminergic nuclei A8-A13** *J Comp Neurol* **529**:1273–1292 https://doi.org/10.1002/cne.25020

56. Wang Y, Wang F, Wang R, Zhao P, Xia Q (2015) **2A self-cleaving peptide-based multi- gene expression system in the silkworm Bombyx mori** *Sci Rep* **5** https://doi.org/10.1038/srep16273

57. Kim JH, Lee SR, Li LH, et al. (2011) **High cleavage efficiency of a 2A peptide derived from porcine teschovirus-1 in human cell lines, zebrafish and mice** *PLoS One* **6** https://doi.org/10.1371/journal.pone.0018556

58. Garcia-Lopez A, Bogerd J, Granneman JC, et al. (2009) **Leydig cells express follicle-stimulating hormone receptors in African catfish** *Endocrinology* **150**:357–65 https://doi.org/10.1210/en.2008-0447

59. Levavi-Sivan B, Bogerd J, Mananos EL, Gomez A, Lareyre JJ (2010) **Perspectives on fish gonadotropins and their receptors** *Gen Comp Endocrinol* **165**:412–37 https://doi.org/10.1016/j.ygcen.2009.07.019

60. Garcia-Lopez A, de Jonge H, Nobrega RH, et al. (2010) **Studies in zebrafish reveal unusual cellular expression patterns of gonadotropin receptor messenger ribonucleic acids in the testis and unexpected functional differentiation of the gonadotropins** *Endocrinology* **151**:2349–60 https://doi.org/10.1210/en.2009-1227

61. Burow S, Mizrahi N, Maugars G, et al. (2020) **Characterization of gonadotropin receptors Fshr and Lhr in Japanese medaka** *Oryzias latipes. Gen Comp Endocrinol* **285** https://doi.org/10.1016/j.ygcen.2019.113276

62. Chauvigne F, Verdura S, Mazon MJ, et al. (2012) **Follicle-stimulating hormone and luteinizing hormone mediate the androgenic pathway in Leydig cells of an evolutionary advanced teleost** *Biol Reprod* **87** https://doi.org/10.1095/biolreprod.112.100784

63. Ohta T, Miyake H, Miura C, Kamei H, Aida K, Miura T (2007) **Follicle-stimulating hormone induces spermatogenesis mediated by androgen production in Japanese eel, Anguilla japonica** *Biol Reprod* **77**:970–7 https://doi.org/10.1095/biolreprod.107.062299

64. An K, Yao B, Kang Y, et al. (2022) **Seasonal Expression of Gonadotropin Genes in the Pituitary and Testes of Male Plateau Zokor (Eospalax baileyi)** *Animals* **12** https://doi.org/10.3390/ani12060725

65. Kasimanickam VR, Kasimanickam RK (2022) **Sertoli, Leydig, and Spermatogonial Cells' Specific Gene and Protein Expressions as Dog Testes Evolve from Immature into Mature States** *Animals* **12** https://doi.org/10.3390/ani12030271

66. Bonci EA, Buiga R, Badan M, et al. (2018) **Follicle-stimulating hormone receptors: A comparison of commercially-available monoclonal and polyclonal antibodies as immunohistochemical markers for cancer research** *J BUON. Nov* **23**:1912–1921

67. Baker PJ, Pakarinen P, Huhtaniemi IT, et al. (2003) **Failure of normal Leydig cell development in follicle-stimulating hormone (FSH) receptor-deficient mice, but not FSHbeta-deficient mice: role for constitutive FSH receptor activity** *Endocrinology* **144**:138–45 https://doi.org/10.1210/en.2002-220637

68. Su J, Song Y, Yang Y, et al. (2023) **Study on the changes of LHR, FSHR and AR with the development of testis cells in Hu sheep** *Anim Reprod Sci* **256** https://doi.org/10.1016/j.anireprosci.2023.107306

69. Zhu LL, Blair H, Cao J, et al. (2012) **Blocking antibody to the beta-subunit of FSH prevents bone loss by inhibiting bone resorption and stimulating bone synthesis** *Proc Natl Acad Sci U S A* **109**:14574–9 https://doi.org/10.1073/pnas.1212806109

70. Zhu LL, Tourkova I, Yuen T, et al. (2012) **Blocking FSH action attenuates osteoclastogenesis** *Biochem Biophys Res Commun* **422**:54–8 https://doi.org/10.1016/j.bbrc.2012.04.104

71. Abudureyimu A, Cai Y, Huo S, et al. (2018) **Expression and localization of follicle- stimulating hormone receptor in the yak uterus during different stages of the oestrous cycle** *Reprod Domest Anim* **53**:1539–1545 https://doi.org/10.1111/rda.13313

72. Liu XM, Chan HC, Ding GL, et al. (2015) **FSH regulates fat accumulation and redistribution in aging through the Galphai/Ca(2+)/CREB pathway** *Aging Cell* **14**:409–20 https://doi.org/10.1111/acel.12331

73. Cheng Y, Zhu H, Ren J, et al. (2023) **Follicle-stimulating hormone orchestrates glucose-stimulated insulin secretion of pancreatic islets** *Nat Commun* **14** https://doi.org/10.1038/s41467-023-42801-6

74. Wada T, Becskei A (2017) **Impact of Methods on the Measurement of mRNA Turnover** *Int J Mol Sci* **18** https://doi.org/10.3390/ijms18122723

Editors

Reviewing Editor
Dolores Shoback
University of California, San Francisco, San Francisco, United States of America

Senior Editor
Yamini Dalal
National Cancer Institute, Bethesda, United States of America

Reviewer #1 (Public Review):

The manuscript by Hong-Qian Chen and collaborators describes the development of a mouse model that co-expresses a fluorescent protein ZsGreen marker in gene fusion with the Fshr gene.

The authors are correct in that there is a lack of reliable antibodies against many of the GPCR family members. The approach is novel and interesting, with a potential to help understand the expression pattern of gonadotropin receptors. There has been a very long debate about the expression of gonadotropin receptors in other tissues other than gonads. While their expression of the Fshr in some of those tissues has been detected by a variety of methods, their physiological, or pathophysiological, function(s) remain elusive.

The authors in this manuscript assume that the expression of ZsGren and the Fshr are equal. While this is correct genetically (transcription->translation) it does not go hand in hand to other posttranslational processes.

One of the shocking observations in this manuscript is the expression of Fshr in Leydig cells. Other observations are in the osteoblasts and endothelial cells as well as epithelial cells in different organs. The expression of ZsGreen in these tissues seems high and one shall start questioning if there are other mechanisms at play here.

First, the turnover of fluorescent proteins is long, longer than 48h, which means that they accumulate at a different speed than the endogenous Fshr. This means that ZsGreen will accumulate in time while the Fshr receptor might be degraded almost immediately. This correlated with mRNA expression (by the authors) but does not with the results of other studies in single-cell sequencing (see below).

Then, the expression of ZsGreen in Leydig cells seems much higher than in Sertoli cells, this is "disturbing" to put it mildly. This is visible in both, the ZsGreen expression and the FISH assay (Fig 2 B-D).

The expression in WAT and BAT is also questionable as the expression of ZsGreen is high everywhere. What makes it difficult to actually believe that the images are truly informative? For example, the stainings of the aorta show the ZsGreen expression where elastin and collagen fibres are - these are not "cells" and therefore are not expressing ZsGreen.

FISH expression (for Fshr) in WT mice is missing.

Also, the tissue sections were stained with the IgG only (neg control) but in practice both the KI and the WT tissues should be stained with the primary and secondary antibodies.

The only control that I could think of to truly get a sense of this would be a tagged receptor (N-terminal) that could then be analysed by immunohistochemistry.

The authors also claim:
To functionally prove the presence of Fshr in osteoblasts/osteocytes, we also deleted Fshr in osteocytes using an inducible model. The conditional knockout of Fshr triggered a much more profound increase in bone mass and decrease in fat mass than blockade by Fsh antibodies (unpublished data)

This would be a good control for all their images. I think it is necessary to make the large claim of extragonadal expression, as well as intragonadal such as Leydig cells.

Claiming that the under-developed Leydig cells in FSHR KO animals is due to a direct effect of the FSHR, and not via a cross-talk between Sertoli and Leydig cells, is too much of a claim. It might be speculated to some degree but as written at the moment is suggests this is "proven".

We also do not know if this Fshr expressed is a spliced form that would also result in the expression of ZsGreen but in a non-functional Fshr, or whether the Fshr is immediately degraded after expression. The insertion of the ZsGreen might have disturbed the epigenetics, transcription or biosynthesis of the mRNA regulation.

The authors should go through single-cell data of WT mice to show the existence of the Fshr transcript(s). For example here:
https://www.nature.com/articles/sdata2018192

Comments after revision:

The response by the authors does not seem sufficient or adequate, by any length, for what one would expect for a work having such a large claim as the expression of the Fshr in multiple cell types and organs. It is not the fact that Fshr might be expressed extragonadally or even by other cells in the gonads, but the surprising images where virtually every cell in the provided tissues, and not only cells but structures, glows green.

It is not possible to know, as a reviewer, whether the excitation intensity and exposure for all images is equal. We believe that they cannot be, as control organs such as fat, testes, ovaries, and vasculature have a natural fluorescence background.

Leydig cells cannot simply express more Fshr than Sertoli cells, that would go against what we have known for >50 years in physiology. While it is scientific to question 'old' data, to make extraordinary claims there is a need for "extraordinary evidence". There is very low expression in Sertoli cells (Fig 2) while Leydig cells and spermatozoa glow vividly.

Moreover, even the tails of spermatozoa glow! This is not cytoplasm and cannot contain a soluble fluorescent protein.

The controls should be shown side-by-side to the experimental images. It would be a lot more credible if the WT and the KI tissues were placed on the same slide, with images taken from them side by side not only for ZsGreen but antibody immunofluorescence staining.

Moreover, I noticed that the entire manuscript is based on a single founder mouse, which is not acceptable as an error - either multiple integrations other than in the correct locus or genetic instability created by the KI integration would result in promiscuous expression. The founder mouse is not well enough characterised as it is only performed by Southern blots and PCR, while additional integrations cannot be detected by such. Other methods should be used such as FISH or even whole genome sequencing. Yet, several lines should be used to ensure no other effects exist.

In Fig 5, the section of aorta shows low staining in the elastin/collagen fibres, while there is clearly in Suppl Data 2. In the same figure, the 2nd lung images show green fluorescence in the mucosa (centre) which should not be as there is no cells there.

The additional single-cell data does not truly support their claims, in the sense that while some of the data might go in line e.g. Leydig cells showing as high expression as "tubules", there are many other cell types that show no expression such as hepatocytes and skeletal muscle, where the authors claim to have high expression of Fshr. Moreover, in the datasets presented organs like "ovary" have almost no Fshr expression, which should question the validity of such.

The authors use an Fshr antibody without enough validation. The Fshr KO animals should be used for this. In fact, one of the very first statements in the manuscript is that antibodies against GPCRs in general, and gonadotropin receptors more specifically, are unreliable. The fact that controls show the same pattern as transgenic animals questions the validity, as no single acceptable antibody against FSHR recognises Leydig cells.

The detection of Fshr in e.g. adipocytes of B6 mice is as questionable as many other claims of gonadotropin receptors in extragonadal tissues, which has been questioned a number of times by many researchers.

One question we should ask is, is there any tissue on these mice that does not 'express' (Fshr)-ZsGreen? Because from what I see every single tissue analysed has 'Fshr". Which might be the problem why it is so difficult to find.

Some images seem to be duplicated such as in Fig 2C where the first row and the 3rd row seem to be the same image.

https://doi.org/10.7554/eLife.93413.2.sa1

Author response:

The following is the authors' response to the original reviews.

We would like to thank you very much for reviewing our manuscript and express our sincere appreciation for the valuable and thoughtful comments that led us to significantly improve the manuscript on Fshr-ZsGreen reporter mice. We have seriously taken your comments to make a major revision of the manuscript, and here is a summary of the revision:

(1) New data on Fshr expression are input to the revised Manuscript:

a. Fshr expression in the testis and adipose tissues (WAT and BAT) of B6 mice;

b. Fshr expression in the testis of B6 by RNA-smFISH;

c. Comparison of Fshr expression in the testis and ovary between Fshr-ZsGreen and B8 mice by ddRT-PCR to prove Fshr expression without interruptions by insertion of P2A-ZsGreen vector;

d. Reduction of Fshr expression in osteocytes within the femoral sections from DMP1-CreERT2:Fshrfl/fl mice;

e. Fshr expression in an established Leydig cell line-TM3 by immunofluorescence and ddRT-PCR, also show Fshr located in the nuclei of TM3 cells;

f. Fshr expression at scRNA-seq level from 5 public single cell portals as Supplementary Data 3 to support our findings of the widespread expression pattern of Fshr, particularly in Leydig cells.

(2) Re-organization of Figure 2 with a new legend.

(3) A new paragraph is added to the Discussion Section of the revised MS to explain the function of P2A peptide in generation of GFP reporter mice and why Fshr express is not interrupted by the P2A-ZsGreen insertion in Fshr-ZsGreen reporter.

(4) Deletion of Figure 1-D-c, as it is not necessary.

(5) Replace of Figure 8-A (the left panel) with a reduced exposure time image.

(6) Amended parts of the revised MS are labeled in red.

A point by point response to the Reviewers' comments:

> ***Reviewer 1:***
>
> *One of the shocking observations in this manuscript is the expression of FSHR in Leydig cells. Other observations are in the osteoblasts and endothelial cells as well as epithelial cells in different organs. The expression of ZsGreen in these tissues seems high and one shall start questioning if there are other mechanisms at play here.*
>
> *First, the turnover of fluorescent proteins is long, longer than 48h, which means that they accumulate at a different speed than the endogenous FSHR This means that ZsGreen will accumulate in time while the FSHR receptor might be degraded almost immediately. This correlated with mRNA expression (by the authors) but does not with the results of other studies in single-cell sequencing (see below).*
>
> *The expression of ZsGreen in Leydig cells seems much higher than in Sertoli cells, this is "disturbing" to put it mildly. This is visible in both the ZsGreen expression and the FISH assay (Figure 2 B-D).*

Thank you for this valuable comments. We added new data on Fshr expression to prove the presence of Fshr in Leydig cells in B6 detected by immunofluorescence staining, RNA-smFISH and ddRT-PCR, as well as in TM3 cells-isolated Leydig cells from a male mice in the revise MS (Fig 2E, F and G), that demonstrate no interruptions of normal Fshr expression by insertion of P2A-ZsGreen vector into a locus located between exon10 and stop code. We use ZsGreen as an indicator for active Fshr promoter status, rather than a method to measure Fshr expression, which is done by ddRT-PCR. These data are shown in Figure 2G of the revised MS

In addition, we provide scRNA-seq based evidence on Fshr expression in human Leydig cells from two single cell portals (DISCO and BioGPS) as shown in Supplementary Data 3 in the revised MS. We also cited a recent report on scRNA-seq analysis of Fshr expression in Hu

sheep in the revised MS as Reference 65 (PMID: 37541020) 1, which also clearly showed Fshr expression in Leydig cells at single cell level in Hu Sheep.

We believe that the lack of Fshr expression in some single cell databases may be due to the degradation of Fshr transcript in cells during the process of single cell populations. In our laboratory, we spent more than 6 months to optimize methods and reagents to perverse mRNA integrity more than 8 for RAN-seq.

> *The expression in WAT and BAT is also questionable as the expression of ZsGreen is high everywhere. That makes it difficult to believe that the images are truly informative. For example, the stainings of aorta show the ZsGreen expression where elastin and collagen fibres are - these are not "cells" and therefore are not expressing ZsGreen.*
>
> *FISH expression (for FSHR) in WT mice is missing.*
>
> *Also, the tissue sections were stained with the IgG only (neg control) but in practice both the KI and the WT tissues should be stained with the primary and secondary antibodies. The only control that I could think of to truly get a sense of this would be a tagged receptor (N-terminal) that could then be analysed by immunohistochemistry.*

Reply 2 and 3: Thank you for these comments. New data on Fshr expression in WAT and BAT of B6 mice by immunofluorescence staining and in the testis of B6 mice by immunofluorescence staining and RNA-smFISH are added to the revised MS (Fig.2D and E, and Fig. 4G), showing similar patterns to that of Fshr-ZsGreen mice. Furthermore, we provide more evidences as Supplementary Data 3 on Fshr expression obtained from 4 public single cell portables, showing FSHR expression in a widespread organs and tissues (including different fractions of adipose cells) of human, mice and rat at single cell levels. Please also check Fshr expression pattern in adipose tissues by immunostaining for Fshr in previous reports (Fig. 3a of PMID: 28538730 and Fig. 2 of PMID: 25754247) 2 3, which showed a similar expression pattern to our finding. These data should address your concerns on Fshr expression in WAT and BAT and other organs/tissues.

Regard of “For example, the stainings of aorta show the ZsGreen expression where elastin and collagen fibres are - these are not "cells" and therefore are not expressing ZsGreen.” We believe that you referred to the image of the aorta in Supplementary Data2. However, Please take a look at the images of the aorta in Figure 5-C, which shows positively stained the layer of ‘elastin and collagen fibres’ for EMCN and a-SMA colocalized with Fshr expression with stained DAPI at a 1000X magnification, indicating endothelial cells and the cellular membrane presented in this layer, not just ‘elastin and collagen’.

> *The authors also claim:*
>
> *To functionally prove the presence of FSHR in osteoblasts/osteocytes, we also deleted FSHR in osteocytes using an inducible model. The conditional knockout of FSHR triggered a much more profound increase in bone mass and decrease in fat mass than blockade by FSHR antibodies (unpublished data).*
>
> *This would be a good control for all their images. I think it is necessary to make the large claim of extragonadal expression, as well as intragonadal such as Leydig cells.*

Thank you for this very encouraging comment. As you suggested, we did add a result of reduced Fshr expression in osteocytes from DMP1-CreERT2+:Fshrfl/fl mice treated with tamoxifen to the revise MS, as shown in Figure 3D, demonstrating Fshr present in osteocytes and the specificity of Fshr antibody. Furthermore, we incorporated your advice on making ‘ large claim of extrogonadal and intragonadal expression of Fshr’ into the revised MS in red.

> *Claiming that the under-developed Leydig cells in FSHR KO animals are due to a direct effect of the FSHR, and not via a cross-talk between Sertoli and Leydig cells, is too much of a claim. It might be speculated to some degree but as written at the moment it suggests this is "proven".*

Thank you for pointing out this incorrect claim and we apologized for it. In the revised MS, we deleted this claim.

> *We also do not know if this FSHR expressed is a spliced form that would also result in the expression of ZsGreen but in a non-functional FSHR, or whether the FSHR is immediately degraded after expression. The insertion of the ZsGreen might have disturbed the epigenetics, transcription, or biosynthesis of the mRNA regulation.*

Thanks for this comment. In the revised MS, we added a new section to explain the function of P2A peptide in generation of a GFP reporter by sgRNA-guilded site specific knockin of P2A ZsGreen vector through CRISPRA/cas9 and provided a new result on comparison of Fshr expression in the testes and ovaries from Fshr-ZsGreen and B6 mice, showing equivalent Fshr expression between Fshr-ZsGreen and B6 mice (Figure 2G), which indicates no interruptions of Fshr expression by the insertion of P2A vector.

> *The authors should go through single-cell data of WT mice to show the existence of the FSHR transcript(s).*
> *For example here:*
> *https://www.nature.com/articles/sdata2018192*

Thank you so much for the valuable comment. Yes, we took you critical advice to check Fshr expression through 4 single cell portals, including DISCO, GTEx, BioGPS and Human single cell portal, and present the collected data as Supplementary Data 3 in the revised MS, that strongly support our findings of the wider Fshr expression. Particularly, Fshr expression in Leydig cells is proved by scRNA-seq studies of human cells from DISCO and BioGPS, as well as a recent study in Hu sheep (PMID: 37541020) 1 and we cited it in the revised MS.

> ***Reviewer 2:***
>
> *Is the FSHR expression pattern affected by the knockin mice (no side-by-side comparison between wt and GSGreen mice, using in situ hybridization and ddRTPCR, at least in the gonads, is provided)?*

Thanks for the comment. In the revised MS, we provided a set of new data on Fshr expression in the testis, ovary, WAT and BAT of B6 mice by immunofluorescence staining and by RNA-smFISH for Fshr expression, showing similar expression patterns. Additionally, we also performed ddRT-PCT to compare Fshr expression in the testes and ovaries between Fshr-ZsGreen and B6 mice, demonstrating equivalent expression of Fshr expression between Fshr-ZsGreen and B6 mice. Interestingly, we also observed an significantly higher Fshr expression in the testis than that in the ovary (more than 30 folds).

> *Is the splicing pattern of the FSHR affected in the knockin compared to wt mice, at least in the gonads?*

Thanks for the question. Please see our reply to the Reviewer 1 for the function of P2A peptide used for generation of GFP reporters. Although we didn't directly assess the splicing pattern, we provide a result of comparison of Fshr expression in Figure 2F in the revised MS,

indirectly showing no changes of the splicing pattern. We will assess the splicing pattern of Fshr in the future that has been neglected in the field.

> *Are there any additional off-target insertions of GSGreen in these mice?" and "Are similar results observed in separate founder mice?*

Thanks for the questions. As we describe it in the method section in detail in the MS, Fshr-ZsGreen reporter was produced by the a site-specific long ssDNA recombination of the P2A-ZsGreen targeting vector to the locus between Exon10 and stop code by CRIPRA/cas9, which was guided by site-specific single guide RNA (sgRNA). We showed the results of Southern blot, DNA sequencing and site-specific PCR, proving the site-specific insertion of P2A-ZsGreen as shown in Figure 1. Because of the site-specific recombination, professionally, only one funder line is required for the study and there are no additional off-target insertions.

> *How long is GSGreen half-life? Could a very long half-life be a major reason for the extremely large expression pattern observed?*

Thanks for the question. The half life of ZsGreen, also called ZsGreen1, is at least 26 h in mammalian cells or slightly longer due to its tetrameric structure, in contrast with the monomeric configuration of other well-known fluorescent proteins (PMID: 17510373) 4. The rationale for using this GFP protein is that ZsGreen is an exceptionally bright green fluorescent protein, which is up to 4X brighter than EGFP—and is ideally suited for whole-cell labelling, promoter-reporter studies, considering of the higher turnover and rapid degradation of Fshr transcript. In this study, we used ZsGreen as a monitor or an indicator of the active Fshr endogenous promoter, rather than a means for measuring the promoter activity. Therefore, regardless of its accumulation or not, ZsGreen driven by Fshr promoter, indicates the presence of active Fshr promoter in the defined cells. In stead, we used ddRT-PCR to measure Fshr expression degrees in this study. In addition, we also provide single cell sequence-based evidence from 4 public single cell portables to support our findings of the wide Fshr expression. Please see Supplementary Data 3 in the revised MS.

References:

(1) Su J, Song Y, Yang Y, et al. Study on the changes of LHR, FSHR and AR with the development of testis cells in Hu sheep. *Anim Reprod Sci*. Sep 2023;256:107306. doi:10.1016/j.anireprosci.2023.107306

(2) Liu P, Ji Y, Yuen T, et al. Blocking FSH induces thermogenic adipose tissue and reduces body fat. *Nature*. Jun 1 2017;546(7656):107-112. doi:10.1038/nature22342

(3) Liu XM, Chan HC, Ding GL, et al. FSH regulates fat accumulation and redistribution in aging through the Galphai/Ca(2+)/CREB pathway. *Aging Cell*. Jun 2015;14(3):409-20. doi:10.1111/acel.12331

(4) Bell P, Vandenberghe LH, Wu D, Johnston J, Limberis M, Wilson JM. A comparative analysis of novel fluorescent proteins as reporters for gene transfer studies. *J Histochem Cytochem*. Sep 2007;55(9):931-9. doi:10.1369/jhc.7A7180.2007

https://doi.org/10.7554/eLife.93413.2.sa0